8-11-2017 11:00 AM

Experimental and Simulation Studies of an oxygen concentration system using pressure/vacuum swing adsorption technique: system miniaturization and prototype design

Mingfei Pan, *The University of Western Ontario*

Supervisor: Sohrab Rohani, *The University of Western Ontario*

A thesis submitted in partial fulfillment of the requirements for the Master of Engineering Science degree in Chemical and Biochemical Engineering

Abstract

The miniaturization of a pressure swing adsorption (PSA) oxygen concentrator is of prime significance for portable applications. This work presents a simplified pressure/vacuum swing adsorption (PVSA) cycle with a concentrator prototype design using a deep evacuation step (-0.82 barg) instead of desorption with purge flow to improve the efficiency of oxygen production process and miniaturize the size of the concentrator. The output of the oxygen concentrator is a 50-90 vol.% enriched oxygen stream in a continuous adsorption and desorption cycle (cycle time = 75-90 s). The size of the adsorption column is 3 cm in diameter and 20 cm in length. A Li^+ exchanged 13X zeolite is used as the adsorbent to selectively adsorb nitrogen from air. A dynamic model of pressure and vacuum swing adsorption units is developed to study the pressurization and depressurization process of the adsorption column. The describing equations are solved using COMSOL Multiphysics Chemical Engineering module. The output flow rate and oxygen concentration results from the simulation model are compared with the experimental data. Velocity and concentration profiles are obtained to study the adsorption process and optimize the operational parameters.

Keywords

zeolite, microporous adsorption, bidisperison dynamic model, portable oxygen concentrator, COMSOL Multiphysics, respiration monitoring

Co-Authorship Statement

Chapter 4

Article title: Application of nanosized zeolite molecular sieves for medical oxygen concentration
Authors: Mingfei Pan, Hecham M. Omar and Sohrab Rohani
Article status: Published in Nanomaterials
Mingfei Pan performed the experiment, developed the model, ran the simulations and wrote the manuscript. Hecham Omar helped with data analysis and writing of the manuscript. The work was supervised by Prof. Sohrab Rohani. The draft of the manuscript was reviewed, revised and submitted by Prof. Rohani.

Acknowledgments

I would like to acknowledge the guidance provided by Professor Sohrab Rohani. Professor Rohani provided valuable advice and vast knowledge in many areas. His constant encouragement allowed me to exceed my own expectations.

I would like to acknowledge all of my colleagues and members from my lab, for their advice and help when needed. I would specifically like to show appreciation to Dr. Ali Alizadeh and Dr. Hossein Kazemian who worked closely with me and provided valuable advice. I would like to thank Yuanyi Wu for providing knowledge of microcontroller programming used in my work.

I would like to acknowledge my parents, Qin Pan and Wenyang Xu for pushing me towards pursuing my Master's Degree, for never losing faith and for their unbounded support.

In conclusion, I recognize that this research would not have been possible without the financial assistance of Natural Sciences and Engineering Research Council of Canada (NSERC), Ontario Centres of Excellence (OCE), the Department of Chemical and Biochemical Engineering at the University of Western Ontario, and express my gratitude to those agencies.

Table of Contents

List of Tables

List of Figures

List of Abbreviations

BET Brunauer–Emmett–Teller theory

BJH Barrett-Joyner-Halenda

COPD chronic obstructive pulmonary disease

FEA finite element method

LPM liter per minute

OSA obstructive sleep apnea

POC portable oxygen concentrator

PSA pressure swing adsorption

PVSA pressure vacuum swing adsorption

VSA vacuum swing adsorption

RH relative humidity

TGA thermogravimetric analysis

XRD X-ray Diffraction

List of Appendices

Chapter 1

1.Introduction

Pressure swing adsorption(PSA) process is a novel gas separation method for medical and metallurgical applications. The PSA process works by introducing a feed gas mixture to the inlet of the adsorption column filled with adsorbent. After a short adsorption time, a concentrated gas stream is obtained from the outlet of the adsorption column. For the same adsorbate, the equilibrium gas adsorption capacity of adsorbent increases with the rising pressure. The basic principle for gas separation is the selective adsorption of gas mixtures onto the microporous surface of the adsorbents under high-pressure condition. During the adsorption process, high portion of the strong adsorbate and low portion of the weak adsorbate are adsorbed by the adsorbent inside the adsorption column which leads to a concentrated outflow of weak adsorbate as the product gas stream. With the appropriate pressure swing range, the gas separation process could achieve a stable circulation for continuous production between high-pressure adsorption and low-pressure desorption. The adsorbent for PSA are typically porous material with different adsorption functions like carbon molecular sieves for nitrogen concentration, activated alumina for gas drying and 5A/13X zeolites for oxygen concentration [1-3].

1.1 Background

Oxygen as the third largest artificial commodity chemical is widely used in many medical applications as a treatment to the pulmonary diseases. The enriched oxygen supplement is important to maintain the blood oxygen level which is significant to the cell metabolism of people. The main sorts of concentrated oxygen source are summarized as: liquid tank, compressed cylinder and oxygen concentrator. Liquid tank is widely used as the hospital oxygen storage and requires vacuum insulated evaporator to release as a product gas. The volume of the compressed oxygen cylinder varies from liters to cubic meters which could be used as the mobile oxygen generator for on-site use. Compared to the compressed oxygen

cylinders that requires replacement in days, the oxygen concentrator generates a continuous product flow and the lifespan of the adsorbents are usually over a month. Patients with respiration problems like cystic pulmonary fibrosis and asthma require long term oxygen therapy which promotes the development of the continuous oxygen generation system. The novel design of the light weight portable oxygen concentrator provides the convenience of carryon oxygen supplement for household and outdoor use.

1.1.1 Air separation methods: cryogenic distillation, membrane separation and PSA process

Gas component like nitrogen and oxygen/argon can be separated from room air by separation plant for various applications. There are four common air separation methods known as cryogenic distillation, temperature swing adsorption (TSA), membrane separation and pressure swing adsorption (PSA). Cryogenic distillation is developed as the most efficient but energy intensive way to separate gas mixtures based on the different boiling points of the components [4,5]. High purity gas can be obtained by distilling the liquefied gas for the production of cylinder gas tank. Temperature swing adsorption is also sort of thermal separation processes consisting of two steps: room temperature adsorption and high temperature desorption based on the equilibrium adsorption capacity of adsorbent at different temperature [6-8]. By heating the saturated adsorption column, strong adsorbate and contaminants like vapor and carbon dioxide could be desorbed from the adsorbent for the complete reactivation. The performance of adsorption column in temperature swing adsorption is outstanding with a long lifespan while the adsorption cycle time is long due to the gas-solid heat transfer rate. Compared to the cryogenic distillation and temperature swing adsorption, pressure driven operations like membrane separation and pressure swing adsorption have the advantage of lowering production scales and energy cost. Membrane separation is designed based on the different permeation rates of gas mixtures passing through the permeable membrane materials. By introducing compressed feed gas to the membrane fibers, components that pass through the membrane are released back to the atmosphere while the retained component is stored and delivered as the concentrate for terminal use [9-13]. The

main drawback of the membrane separation is the maintenance costs of sensitive membrane fibers especially in harsh environment compared to the PSA process using zeolite adsorbents. The adsorption mechanism of PSA process is the selective adsorption of gas mixtures onto the zeolite surface under high pressure. The saturated adsorbents could be regenerated by lowering the pressure. By switching the high-pressure adsorption step and low-pressure desorption step, a continuous concentrated gas production could be achieved. The adsorbents for air separation are porous zeolites known as molecular sieves with a relatively long lifespan and stable adsorption performance compared to membrane fibers which means the maintenance costs are low.

1.1.2 Adsorption and desorption stages for PSA cycles

The PSA apparatus usually consists of two adsorbent columns undergoing adsorption and desorption alternatively for the continuous production of enriched gas. In the adsorption stages, the adsorbent column is first pressurized with high-pressure gas flow then output the enriched product gas at a super-atmospheric pressure. In the desorption stages, the adsorbed gas species are released by lowering the pressure to atmospheric/vacuum pressure generating a regenerated adsorbent column for next adsorption cycle.

The pressure swing adsorption process was patented by Finlayson and Sharp (GB Patent 365092) describing an air separation process with pressurization adsorption and depressurization desorption steps [14]. In 1958, two different pressure swing adsorption units were patented: one by Skarstrom using fractional product purge flow for desorption step at atmospheric pressure and the other by Montgareuil and Domine using pressure vacuum adsorption (PVSA) step [15,16]. Both the Skarstrom and Montgareuil/Domine cycle have been successfully used in the industrial oxygen production plant as an alternative to the cryogenic distillation plant due to the flexible plant scale and lower power consumption. Based on the development of the zeolite adsorbent for PSA process, the performance of the cyclic oxygen production is stable and outstanding with a low maintenance cost.

1.2 Limitations for conventional PSA process

Due to the growing demand of oxygen supply for the individual medical care, the miniaturization of oxygen concentrator unit is necessary to the design and manufacturing of mobile oxygen concentrator. The main technical issue concerning the development of mobile PSA processes is the poor nitrogen/oxygen selectivity during the adsorption steps which makes the adsorption column bulky. The challenge could be summarized as maintaining the productivity of adsorption cycles during the system miniaturization process. In this way, the characterization of novel zeolite adsorbent designed for high performance PSA oxygen production cycle is significant for the adsorption process using small adsorption column. In addition to the zeolite characteristic study, specifying the operational parameters of PSA cycle like pressure swing range, adsorption/desorption stage time and inflow/outflow temperature are also important for the understanding of separation kinetics. Therefore, one of the main objectives of this dissertation research is to figure out the appropriate adsorption cycle for portable oxygen concentrator apparatus and investigate the commercial zeolite samples for the best adsorption performance.

1.3 Objective

The objectives of this thesis work are:

(a) To develop a miniature PVSA oxygen concentrator with the appropriate zeolite and operational parameters with an intermittent oxygen product flow

(b) To develop a mathematical model that defines the transport phenomena and adsorption kinetics for the internal gas adsorption analysis of the zeolite column

(c) To develop a novel breath monitoring and gas supply method to deliver the concentrated oxygen to the patients

1.4 Motivation

Air pollution is becoming a worldwide problem particularly in heavily populated cities like Beijing, Los Angeles, Mexico City. Air pollution leads to acute and chronic respiratory problems that are becoming a growing concern from both global and individual levels. Wearing disposal face masks has become a popular method to get some protection from exposure to pollutants. However, for people with poor autonomous respiration ability like chronic obstructive pulmonary disease patients, it is hard to breathe through disposal face masks. As a result, there is a growing need to address the health and quality of life through a light-weight and portable oxygen concentrator. The portable oxygen concentrator is typically coupled with a continuous pressure airway therapy (CPAP) mask to help open the airway to deliver the enriched oxygen which improves the respiratory capacity and increases fraction of inspired oxygen. The development of the portable oxygen concentrator is mainly focused on the characterization of the zeolites and adsorption cycle modification for the enhanced performance and reduced size and weight

1.5 Thesis outline

Chapter one presents a brief introduction to the techniques and materials used to achieve the objectives outlined in Section 1.3. Chapter one also provides the motivations of the work presented in this thesis.

Chapter two presents a literature review that covers various scales of oxygen production application using pressure swing adsorption, the kinetics of competitive adsorption of nitrogen and oxygen with the physical properties of the active cation sites on the zeolite microporous surface area and the strategies for productivity improvement of PSA process. In additions, the modelling methodology of computational fluid dynamics simulation using finite elements method (FEM) to describe the gas transport inside the porous media area is also illustrated in this review chapter.

Chapter three presents the study of zeolite samples characterization with three main analysis methods: (i) TGA analysis; (ii) BET analysis; (iii) XRD analysis. The geometry design issues of the zeolite column is also summarized in this chapter based on the experimental adsorption tests with commercial zeolite samples.

Chapter four presents a dynamic model that describes transport phenomena of the column pressurization and gas mixture adsorption inside the zeolite particles. The model equations in the gas flow interface describe the flow in the column open voids and porous media area. The model equations in the species transport interface describe the convection, diffusion and adsorption inside the column.

Chapter five presents experimental data of flowrate, oxygen concentration and outlet pressure at the column end during the adsorption/desorption cycle tests with the outcomes from the simulation models. Miniaturization and optimization strategies of PSA oxygen concentration apparatus are also summarized for the continuous oxygen production process.

Chapter six presents the hardware development for the concentrator prototype design. Circuit of the controlling system with the microcontroller programs are illustrated with the prototype tests.

Chapter seven provides the conclusion of the overall work with the potential direction for the future research.

Reference

[1] Ivanova, Svetlana, and Robert Lewis. "Producing Nitrogen via Pressure Swing Adsorption." Chemical Engineering Progress 108.6 (2012): 38-42.

[2] Sethia, Govind, et al. "Sorption of methane, nitrogen, oxygen, and argon in ZSM-5 with different SiO2/Al2O3 ratios: Grand canonical monte carlo simulation and volumetric measurements." Industrial & Engineering Chemistry Research 49.5 (2010): 2353-2362.

[3] Siriwardane, Ranjani V., et al. "Adsorption of CO2 on molecular sieves and activated carbon." Energy & Fuels 15.2 (2001): 279-284.

[4] Kansha, Yasuki, et al. "A novel cryogenic air separation process based on self-heat recuperation." Separation and Purification Technology 77.3 (2011): 389-396.

[5] Agrawal, Rakesh, Donn Michael Herron, and Jung Soo Choe. "Process for distillation of multicomponent fluid and production of an argon-enriched stream from a cryogenic air separation process." U.S. Patent No. 6,240,744. 5 Jun. 2001.

[6] Mason, Jarad A., et al. "Evaluating metal–organic frameworks for post-combustion carbon dioxide capture via temperature swing adsorption." Energy & Environmental Science 4.8 (2011): 3030-3040.

[7] Kalbassi, Mohammed Ali, Rodney John Allam, and Timothy Christopher Golden. "Temperature swing adsorption." U.S. Patent No. 5,846,295. 8 Dec. 1998.

[8] Wurzbacher, Jan Andre, Christoph Gebald, and Aldo Steinfeld. "Separation of CO2 from air by temperature-vacuum swing adsorption using diamine-functionalized silica gel." Energy & Environmental Science 4.9 (2011): 3584-3592.

[9] Burdyny, Thomas, and Henning Struchtrup. "Hybrid membrane/cryogenic separation of oxygen from air for use in the oxy-fuel process." Energy 35.5 (2010): 1884-1897.

[10] Adams, Ryan, et al. "Metal organic framework mixed matrix membranes for gas separations." Microporous and Mesoporous Materials 131.1 (2010): 13-20.

[11] Baker, Richard W. "Future directions of membrane gas separation technology." Industrial & Engineering Chemistry Research 41.6 (2002): 1393-1411.

[12] Robeson, Lloyd M. "Polymer membranes for gas separation." Current Opinion in Solid State and Materials Science 4.6 (1999): 549-552.

[13] Hashim, S. S., A. R. Mohamed, and S. Bhatia. "Oxygen separation from air using ceramic-based membrane technology for sustainable fuel production and power generation." Renewable and Sustainable Energy Reviews 15.2 (2011): 1284-1293.

[14] Finlayson, D., and A. J. Sharp. "Improvements in or Relating to the Treatment of Gaseous Mixtures for the Purpose of Separating them into their Components or Enriching them with Respect to one or more of their Components." GB Patent 365 (1932): 1932.

[15] Skarstrom, Charles W. "Method and apparatus for fractionating gaseous mixtures by adsorption." U.S. Patent No. 2,944,627. 12 Jul. 1960.

[16] Daniel, Domine, and Montgareuil Pierre Guerin De. "Process for separating a binary gaseous mixture by adsorption." U.S. Patent No. 3,155,468. 3 Nov. 1964.

Chapter 2

2. Literature Review

This review is aimed at various scales of oxygen production application using pressure swing adsorption. The kinetics of competitive adsorption of nitrogen and oxygen with the physical properties of the active cation sites on the zeolite microporous surface area are also reviewed to give a comprehensive explanation to the dynamic adsorption process as a novel air separation method. In additions, the modelling methodology of computational fluid dynamics simulation using finite elements method (FEM) to describe the gas transport inside the porous media area is also illustrated in this review chapter.

2.1 Application of pressure swing adsorption for oxygen production

2.1.1 Industrial PSA oxygen plant

In 1975, the first industrial medical oxygen concentrator was patented by Bendix Corp [1]. The industrial oxygen concentrator consists of two adsorption columns, several solenoid valves, an continuous gas supply and backpressure regulators shown in Fig.2.1. The concentrator operation consists of four steps. In step 1, a compressed flow is introduced to column 1 through valve 2 while column 2 is connected to column 1 through valve 5 to transfer the remaining high-pressure product gas. In step 2, the pressure inside column 1 reaches the working pressure with enriched oxygen flowing out through the backpressure regulator to the surge tank. Meanwhile the column 2 is connected to the ambient to regenerate the zeolite and the valve 5 is closed. In step 3 and step 4, the adsorption and desorption positions of column 1 and 2 are reversed to regenerate the saturated column 1 and pressurize the regenerated column 2. By switching the valve sequence (step 1→4→1), a continuous enriched oxygen stream can be obtained from the surge tank. Due to shortage of commercial electricity, the PSA concentrator is also used in wastewater treatment and steelmaking process for on-site oxygen production.

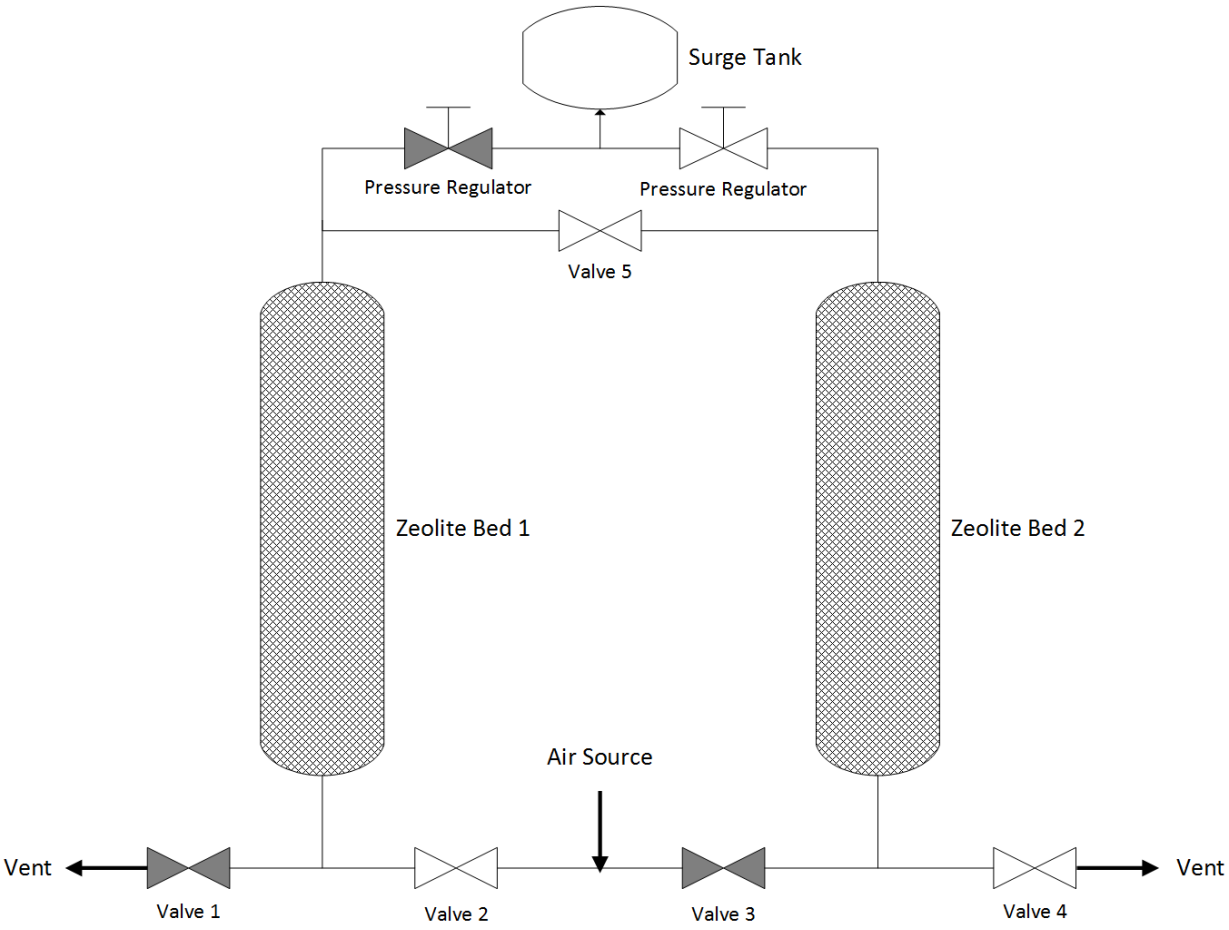

Figure 2.1 Schematics of medical oxygen concentrator

2.1.2 Mobile PSA plant for on-site medical use

For medical oxygen supply, the volume fractions of oxygen should be over 88 vol.%. Conventional adsorption column for oxygen concentrator is bulky and heavy due to the low selectivity and nitrogen capacity of zeolite. With the development of zeolite surface modification technique and ion exchanged methods, the new types of zeolite (LiX and CaX) for oxygen concentration have been commercialized since 1980 [2-4]. With the desiccant column for air source pre-treatment to remove CO_2 and vapor, a stable oxygen output and relatively long lifespan of the adsorption column is achieved by the novel LiX and CaX zeolite. The size of the adsorption column is decreased significantly for the mobility of the oxygen

concentrator. Figure 2.2 shows a patent search of "medical oxygen concentrator, PSA" from 1980 to 2015. An overwhelming number of oxygen concentration applications were patented every year and still several new patents appeared in the last decades. The PSA process for oxygen concentration is becoming a mature and applicable technique in the hospital oxygen supply market and widely used for on-site oxygen treatment.

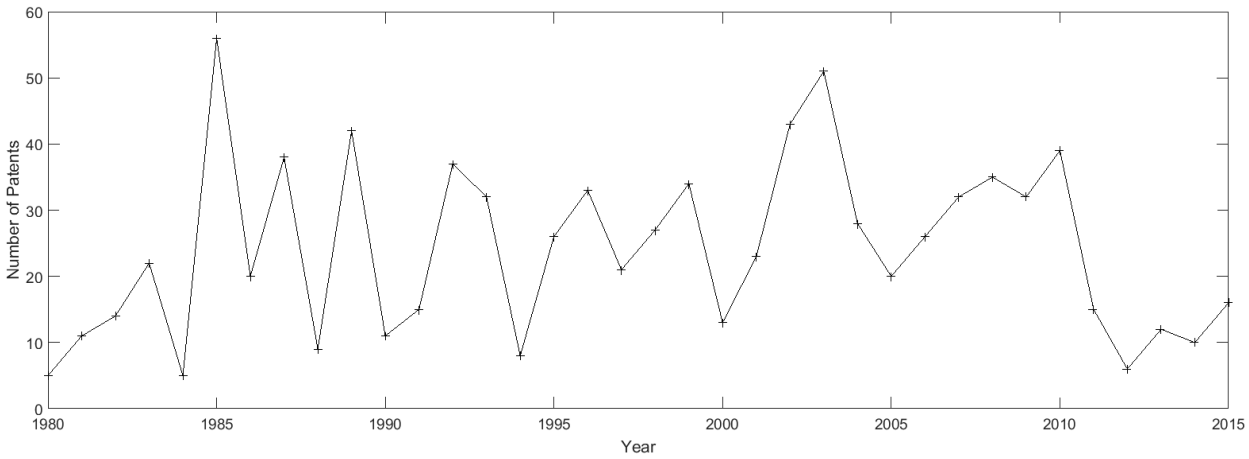

Figure 2.2 Result of patent search for 1980-2015

2.1.3 Portable oxygen concentrator

Due to the poor air quality in modern cities, more people are suffering from chronic obstructive pulmonary disease (COPD), obstructive sleep apnea (OSA) and other respiratory diseases. There is a growing need to increase the fraction of inspired oxygen for these patients through the output oxygen flow of the portable oxygen concentrator. The most important issue for the development of portable oxygen concentrator is the size and productivity of the adsorption column. Bed size factor (BSF) is suggested as the criterion corresponding the column size to the oxygen productivity for the PSA apparatus design [5]:

$$\text{BSF} = \frac{lbs\ of\ adsorbent}{tons\ of\ O_2\ in\ product/cycle} \text{ x } \frac{day}{cycle}$$

The unit of BSF is (lb/$TPDO_2$), where lb is the weight of the adsorbent and $TPDO_2$ represents tons of pure oxygen per day.

For the portable PSA system design, the BSF number is used to evaluate the performance of the adsorption column. Lower BSF means higher productivity for the same adsorption column for the zeolite selection and operational parameters fitting. The selection of the pressure swing range is based on the adsorption equilibrium isotherms for nitrogen and oxygen onto zeolite surface. There are three different PSA processes for different pressure swing ranges from vacuum to high-pressure (super-atmospheric pressure) conditions, namely, pressure swing adsorption (PSA), vacuum swing adsorption (VSA) and pressure vacuum adsorption (PVSA). For the same pressure swing range, the nitrogen capacity ($\Delta q/\Delta P$) of VSA and PVSA processes are higher than that of the PSA process shown in Fig.2.3. For the conventional PSA process, increasing the productivity of the adsorption column could only be completed by increasing the adsorption pressure due to the system miniaturization requirement of the portable PSA oxygen concentrator to maintain the column volume. However, higher adsorption pressure means higher power consumptions for the air compressor while the temperature of the inflow from the compressor would increase with the flow pressure which decreases the nitrogen capacity of the zeolite adsorbents. Considering the size of the air compressor, PVSA cycle is more widely used in the portable oxygen concentration systems. According to the literature research, evacuation desorption is important for the ion-exchanged zeolite LiX to achieve the complete regeneration in each adsorption. The vacuum condition in the desorption step provides the driving force to release the adsorbed nitrogen from the saturated adsorbent and enhances the mass transfer rate from the microporous area to the column void. Plenty of portable oxygen concentrator were patented using PVSA system providing enriched oxygen product flow varying from 50 vol.% to 90 vol.% since 1990 and coupled with oxygen delivery apparatus for the treatment of respiratory diseases.

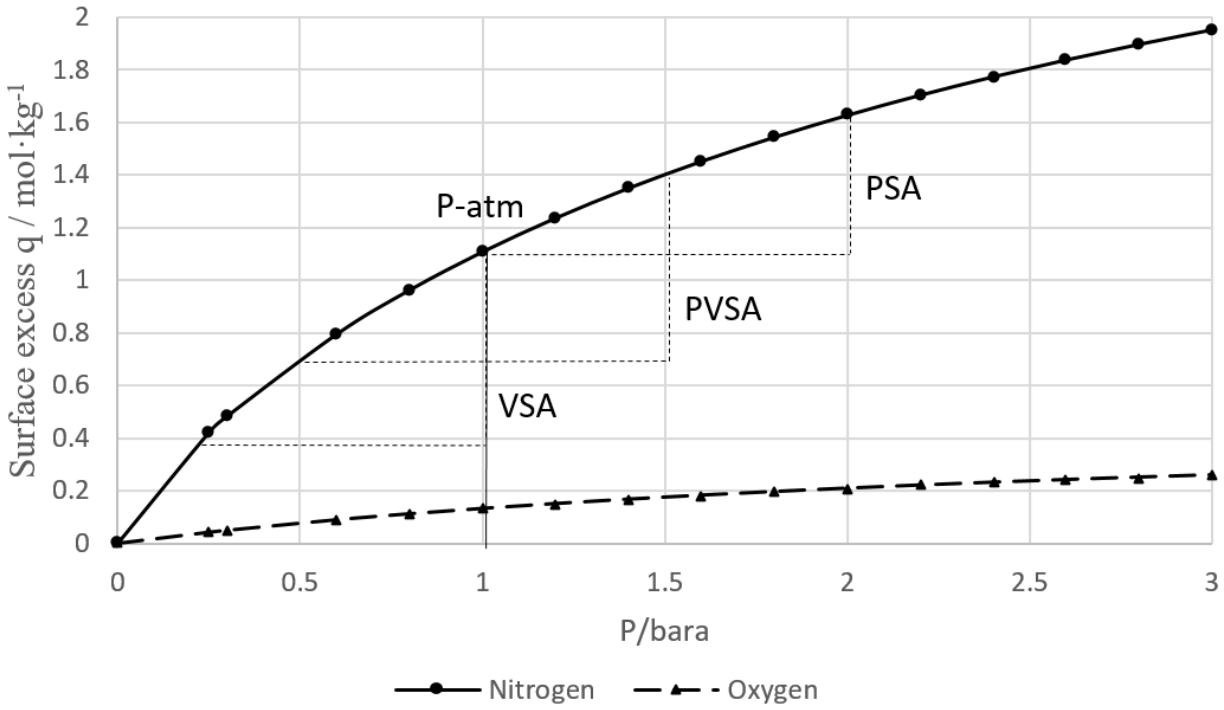

Figure 2.3 Adsorption equilibrium isotherms for nitrogen and oxygen onto zeolite LiX at 20˚C [6]

2.2 Adsorption kinetics of zeolite adsorbent

2.2.1 Langmuir Adsorption model

The Langmuir adsorption model demonstrates isothermal adsorption phenomena of an ideal gas on the surface of the adsorbent. Most of the monolayer adsorption models deal with pure component adsorption process. However, the applications of pressure swing adsorption systems deal with gas mixtures. Therefore, adsorption equilibria involving competition between different molecules is necessary for the adsorption process study as well as for the design purposes. The assumptions made by Langmuir in the treatment of pure component systems are also applicable to multicomponent systems, that each molecule occupying only one site, no mobility on the surface, and constant heat of adsorption. The surface capacity constant of nitrogen and oxygen molecules are the same due to the similar molecular kinetic diameter.

The kinetics approaches are used to a modified Langmuir adsorption model for a binary gas system.

The surface coverage of the zeolite surface is defined as:

$$\theta_T = \theta_1 + \theta_2 \quad (1)$$

where θ_T is the total surface coverage, θ_1 is the fractional coverage of N_2 molecular and θ_2 is the fractional coverage of O_2 coverage. (subscript 1,2 represents N_2 and O_2 respectively).

The rate of adsorption of the species i onto the solid surface is:

$$R_a = k_{a,i} * P_i * (1 - \theta_T) \quad (2)$$

where $k_{a,i}$ is the adsorption rate constant of species i, mol/(kg·s·bar); P_i is the partial pressure of species i, Pa; (1-θ_T) is the fraction of the vacant sites on the surface; i=1,2.

The rate of desorption of the species i is proportional to its fractional loading:

$$R_d = k_{d,i} * \theta_i \quad (3)$$

where $k_{d,i}$ is the desorption rate constant of species i, mol/(kg*s); θ_i is the fractional coverage of species i.

At equilibrium, the rate of adsorption of the species i is equal to the rate of desorption of that species shown in Fig.2.4:

$$R_a = R_d \quad (4)$$

$$k_{a,i} * P_i * (1 - \theta_T) = k_{d,i} * \theta_i \quad (5)$$

$$b_i * P_i * (1 - \theta_T) = \theta_i \quad (6)$$

where b_i is the affinity constant of species I defined as $k_{a,i}/k_{d,i}$, bar^{-1}.

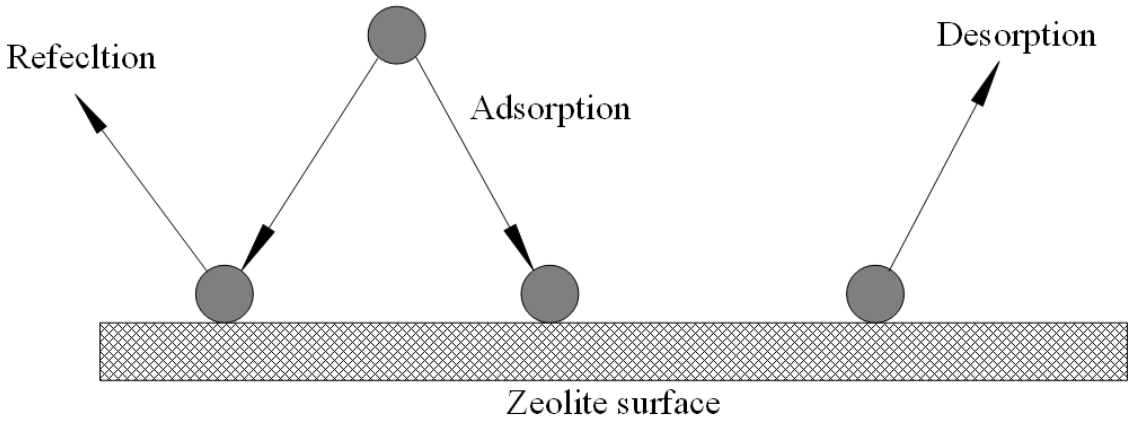

Figure 2.4 Schematics of adsorption and desorption phenomenon on the zeolite surface

Here, the equilibrium total surface coverage at pressure P ($P=P_1+P_2$) is solved as:

$$\theta_T = \frac{b_1P_1+b_2P_2}{1+b_1P_1+b_2P_2} \quad (7)$$

The fraction of the species i is:

$$\theta_i = \frac{b_iP_i}{1+\sum_{j=1}^{2} b_jP_j} \quad (8)$$

or written in terms of molar concentration:

$$\frac{q_i^*}{q_{s,i}} = \frac{b_iP_i}{1+\sum_{j=1}^{2} b_jP_j} \quad (9)$$

where q_i^* is the molar concentration of equilibrium adsorbed species i, mol/(kg adsorbent); $q_{s,i}$ is the constant of maximum capacity of species i, usually given by empirical approaches, mol/(kg adsorbent);

Table 2.1 shows the adsorption isotherm constant of LiX zeolite from UOP Oxysiv series [6].

Table 2.1 Adsorption constant of LiX zeolite

Parameter	Magnitude	Unit
zeolite type	LiX	-
Diameter	0.4	mm
$q_{S,N2}$	3.091	mol/kg
$q_{S,O2}$	3.091	mol/kg
b_{N2}	0.1006	bar^{-1}
b_{O2}	0.0367	bar^{-1}
Temperature	293.15	K

The equilibrium surface coverage is solved in Table 2.2 for pure component gas system and binary gas system (nitrogen-oxygen pair). Compared to pure gas adsorption, equilibrium adsorbed concentration of oxygen decreases by 19% due to the appearance of nitrogen. The competitive occupation of gas mixture onto the zeolite surface leads to selective adsorption of PSA process.

Table 2.2 Adsorption equilibrium data of pure component and binary gas system

Gas type	Partial pressure(abs)/ bar	Pure gas equilibrium coverage, $\theta_{e,p}$	Binary gas equilibrium coverage, $\theta_{e,b}$	Pure gas equilibrium adsorbed concentration, mol/kg	Binary gas equilibrium adsorbed concentration, mol/kg
N_2	2.34	0.191	0.187	0.589	0.578
O_2	0.66	0.024	0.019	0.073	0.059

Where $\theta_{e,p}$ is the pure gas equilibrium coverage, $\theta_{e,b}$ is the binary gas equilibrium coverage

2.2.2 Bidispersion model for mass transfer from column void to zeolite microporous surface

Langmuir adsorption model describes the adsorption equilibrium of gas component onto the adsorbent surface. However, the pressure swing adsorption is a dynamic process with mass transportation and gas-solid adsorption inside the adsorption column. For the fast cycling pressure swing adsorption, monitoring the concentration inside the adsorption column is not applicable due to the difficulty of the gas detection. A dynamic adsorption model is required to evaluate the column dynamic data for the adsorption system design. The adsorption model is validated with the inlet and outlet data (gas concentration, velocity and temperature) of the adsorption column. The linear driving force (LDF) model is widely used in the analysis of the fixed bed adsorption process as an effective approximation to describe the diffusion of gas onto the adsorbent surface [7]. A lumped rate constant is used in the diffusion equations:

$$\frac{dq_i}{dt} = k_i(q_i^* - q_i) \quad (10)$$

q_i, q_i^* are the molar concentration of adsorbed and equilibrium adsorbed species i, respectively, mol/(kg adsorbent); k_i is the diffusion rate constant of species i.

The commercial zeolite particles are produced by sticking microparticles (zeolite powder) with binder. The structure of the zeolite particles is shown in Fig.2.5. In the pressure swing process, the high-pressure flow will first disperse from the column void to the macropore area inside the zeolite particles represented by the macropore dispersion equations. The gas adsorption usually happens at the micropore surface of the zeolite microparticles which is simulated by the adsorption mass transfer equations in the model describing the intraparticle dispersion. Based on the mass transfer kinetics of the commercial zeolites, the dispersion model describing the PSA process is named bidispersion model which presents a more accurate model describing the flow resistance caused by the adsorption process compared to the simple LDF approximation [8,9].

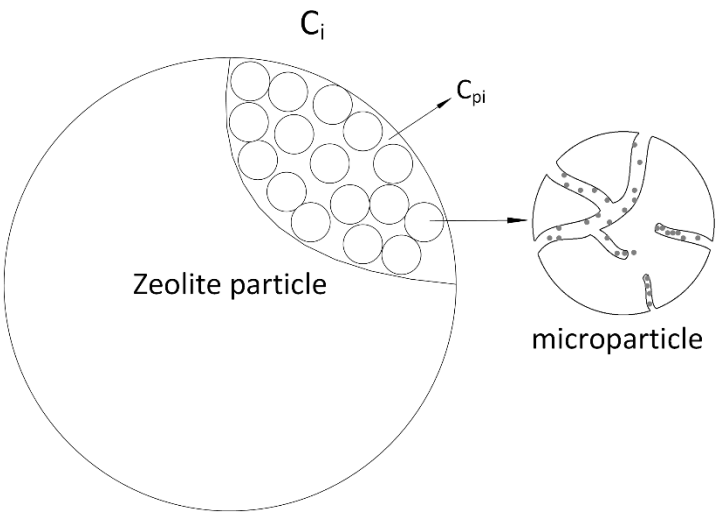

Figure 2.5 Schematics of the zeolite particle structure

The macropore dispersion is described by the first order dispersion equations

$$\varepsilon_p \frac{\partial c_{pi}}{\partial t} + \rho_p \frac{\partial q_i}{\partial t} = k_i (c_i - c_{pi}) \quad (11)$$

Where ε_p is the particle voidage [-], ρ_p is the particle density [kg/m^3], k_i is the macropore mass transfer rate of nitrogen and oxygen from column void into zeolite macropore area [1/s], c_i and c_{pi} are the column gas concentration and particle concentration of nitrogen and oxygen, respectively [mol/m^3].

The micropore dispersion is described by the second order dispersion equations with the adsorption equilibria.

$$\frac{\partial q_i}{\partial t} = k_{pi} (q_i^* - q_i) \quad (12)$$

Where k_{pi} is the micropore mass transfer rate of nitrogen and oxygen [1/s], q_i^* and q_i are the equilibrium and actual adsorbed species to the zeolite, respectively [mol/kg].

2.3 Zeolite adsorbents for pressure swing adsorption process

2.3.1 Zeolite for PSA oxygen concentration

The most common commercial adsorbent used in the PSA process is the 5A and 13X zeolite working based on the selective adsorption of nitrogen from air source to produce a concentrated oxygen stream [10]. Zeolites are crystalline molecular sieves with large surface area due to their porous structure shown in Fig.2.6 [11-13]. Adsorption of nitrogen and oxygen molecules usually happens at the micropore area in the PSA process. For the selection of the zeolite for PSA applications, the pore size distribution of the zeolite is one of the important factors to measure the nitrogen capacity of the single adsorbent particle. A typical pore distribution is illustrated in Fig.2.7 by BJH desorption cumulative pore area. Pores on the surface of zeolite 13X are well-defined micropores (<2 nm in diameter) and mesopores (2-50 nm in diameter) with only negligible macropores (>50 nm in diameter).

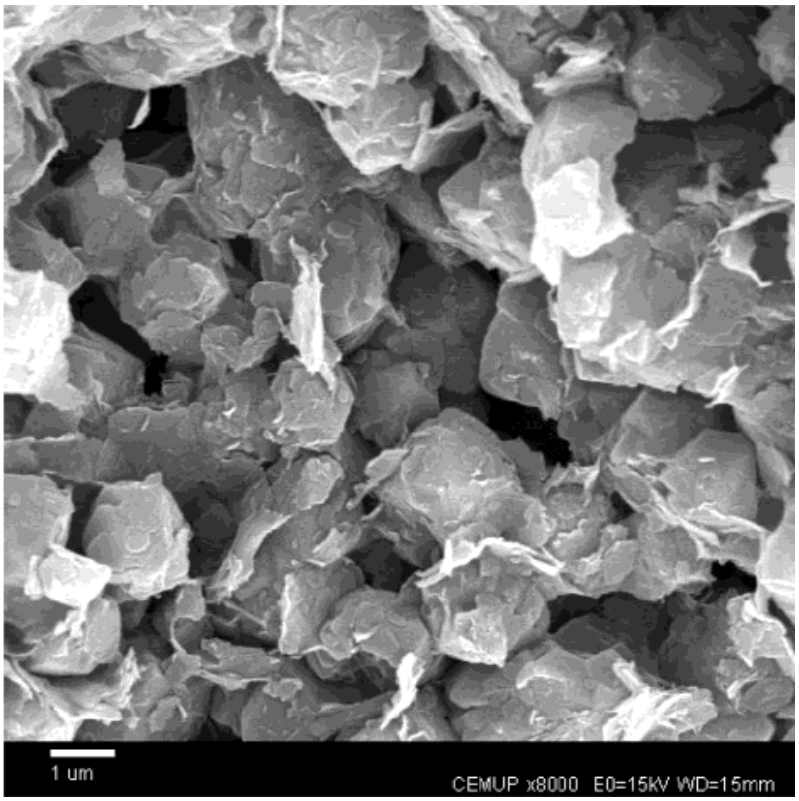

Figure 2.6 A SEM image of the 13X zeolite (figure reprinted with permission from reference [12])

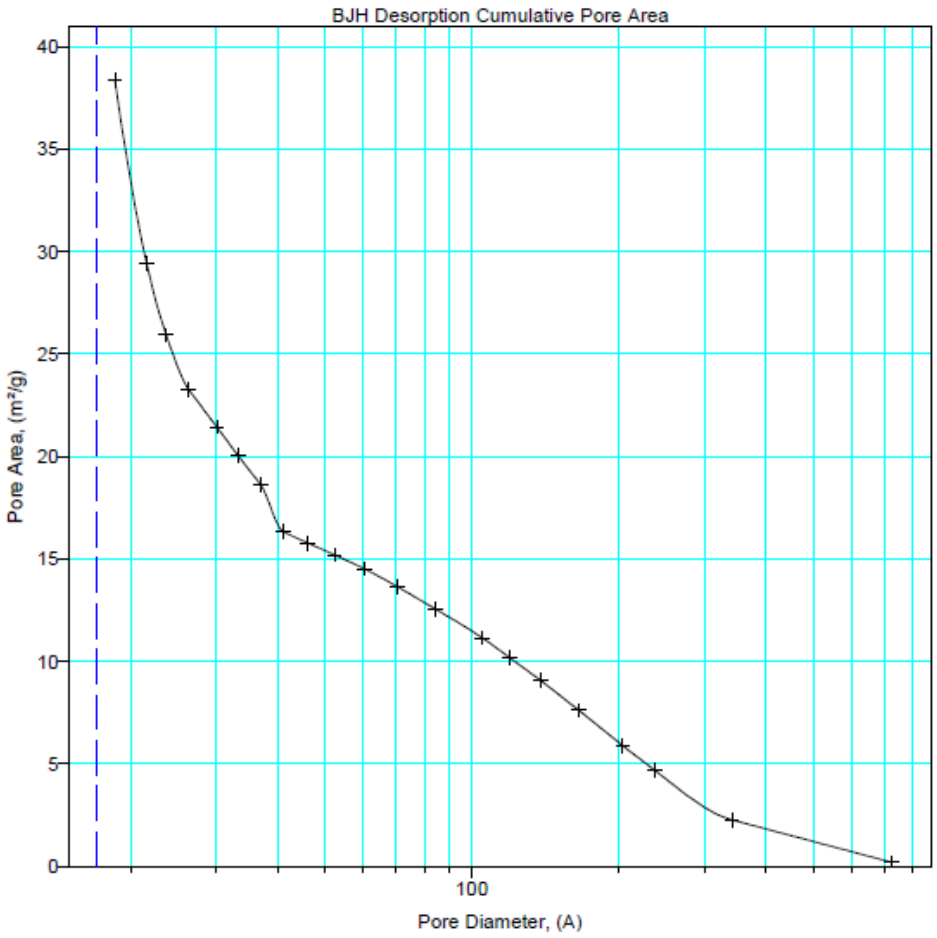

Figure 2.7 The BJH desorption cumulative pore distribution of zeolite 13X

The basic structural units of zeolite adsorbents are silica tetrahedron (SiO_2) and alumina tetrahedron (AlO_2) [14-17]. These primary structures can be arranged for the formation of the secondary sub-building units (SBUs) in the form of square and hexagon. Different combinations in space of these secondary SBUs lead to tertiary sub-building units by chemical bonds between Si and Al (Si-O-Al) sharing an oxygen atom. Eventually the zeolite crystalline structures are made up of by the arrangement of the tertiary units in a triaxial cavity construction [18-20].

The general formula of zeolite is given by [21]**:**

$$M_{x/n}[(AlO_2)_x(SiO_2)_y] \cdot zH_2O$$

where M represents the different types of cations that are attached to the zeolite framework. The affinity of zeolite for air component is determined by the location and types of cations that appear in the zeolite framework [22-24]. Another leading factor is lower Si:Al ratio (y:x) which can enhance the hydrophilicity of zeolite with negative charged surface to attract molecules with high quadrupole moment [25-27]. The molecule quadrupole moment is the parameters which shows the effective shape of the ellipsoid of molecule charge distribution. A non-zero quadrupole moment illustrates that the molecule charge distribution is not spherically symmetric. In air, the quadrupole moment of CO_2 and H_2O is much stronger than that of N_2 due to their polarity. This property can be harnessed to adsorb CO_2 and H_2O from an air stream preferentially as the air source is introduced to a modern PSA oxygen concentrator system using microporous zeolite. The selectivity for zeolite adsorbents to adsorb nitrogen compared to oxygen is due to the interaction between electrostatic field of the cationic zeolite and the quadrupole moment of the nitrogen and oxygen [28-30]. Higher quadrupole moment of air components leads to a stronger adsorption on the zeolite surface area shown in Table 2.3. The appropriate cations as well as the Si:Al ratio (y:x) are the dominant factors for the preferential adsorption of nitrogen.

Table 2.3 Adsorption characteristics of major air component [31]

Adsorbate	Kinetic Diameter (Å)	Quadrupole (Q/e, $Å^2$)
CO_2	3.30	0.65
N_2	3.64	0.27
O_2	3.46	<0.09

2.3.2 Li^+ exchanged zeolite for enhanced separation performance

Productivity of PSA oxygen concentration system highly depends on the characteristics of zeolite adsorbent. The type of cations attached to the zeolite framework is the most vital factor

to the surface charge of the zeolite pore area. Conventional zeolite 13X with Na^+ attached to the framework was proven to be the appropriate zeolite type to separate oxygen from air compared to other zeolites (A type and P type). However, the productivity of 13X zeolite is relatively low due to the poor nitrogen capacity. In order to the get the enhanced performance of zeolite adsorption, ion exchange technology was presented for the zeolite surface modification. The ion exchange of commercial 13X zeolite (NaX form) is first carried out 6 times with NH_4Cl solution at T=360-365 K for 24 h. Then NH_4X form zeolite is exchanged 3 times with 1M LiCl solution and 6 M LiCl at 365 K for 24 h, respectively [32]. The Li^+ exchanged zeolites with low silica portion exhibit greater bonding energy between the cation framework and the nitrogen than that of oxygen. High Li^+ cations concentration attached to the zeolite lattice, significantly improves the nitrogen loading capacity at 1 bar and 298 K as illustrated in Fig.2.8 [33]. The PSA and VSA oxygen cycle based on these types of ion exchanged zeolites, dramatically reduce the column size and enhance productivity which is vital for the development of portable oxygen concentrator.

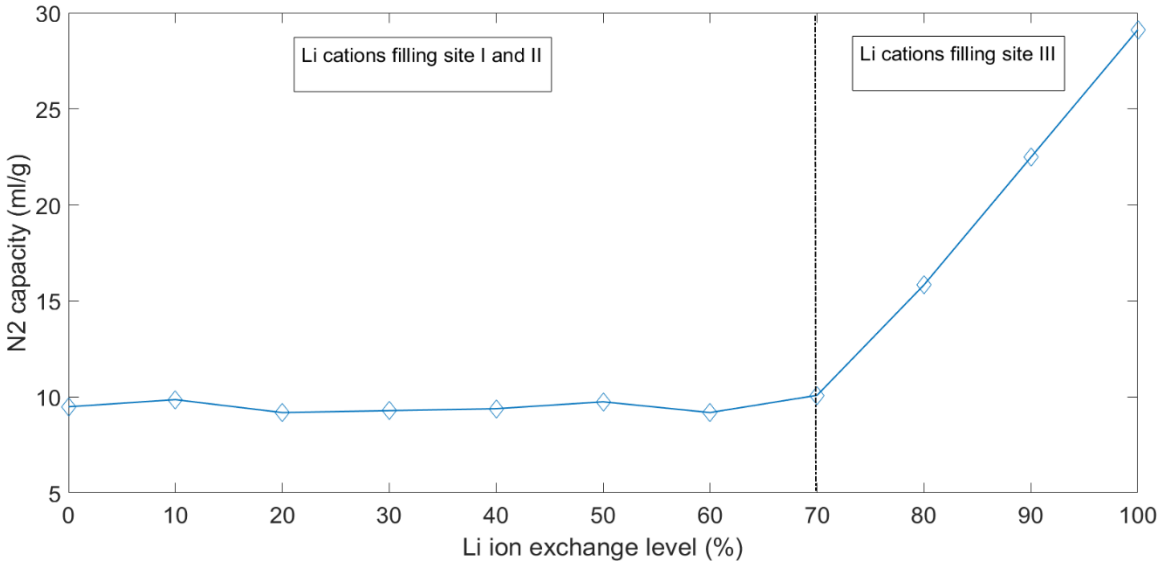

Figure 2.8 The N_2 loading capacity on LiX and CaX zeolite at 1 bar, 298 K[33]

2.4 Strategies for productivity improvement of PSA process

2.4.1 Influence of extra-framework Li+ cations

X type zeolites with low Silica to Alumina ratio and higher Li^+ exchanged portion exhibit best nitrogen capacity and relatively high N_2 to O_2 selectivity for air separation process. The adsorption performance of ion-exchanged zeolites shows a high correlation with the amount of extra-framework cations attached to the negative charged zeolite surface. Characterization of the adsorption sites of zeolites are of prime importance to the zeolite surface modification. As shown in Fig.2.9, the Li cations in the faujasite-type framework of zeolite X are located in sites type I (inside the sodalite cage), type II (inside the supercage) and type III (near the four-ring window of the supercage) [34].

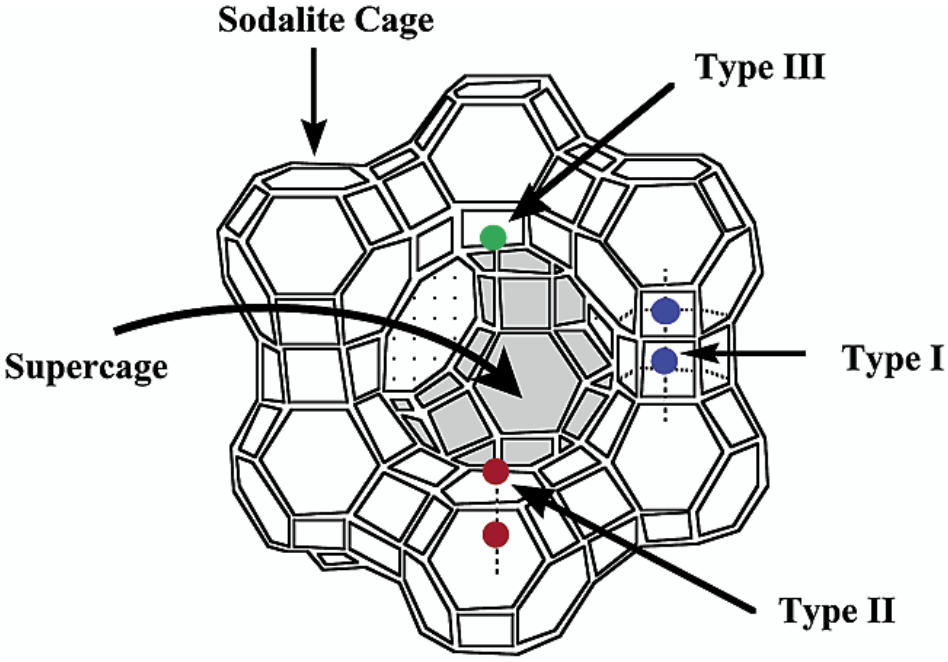

Figure 2.9 Structure of the faujasite-type zeolite X with cation sites Types I, II, and III [34]

The sites of Li^+ in the X type zeolite framework were characterized using neutron diffraction and ^6Li and ^7Li MAS NMR spectroscopy [35,36]. The Li cations in type I sites are spatially blocked by the sodalite cage and double six-ring while the Li cations in type II sites are shielded by the super-cage framework. The Li cations in type III sites close to the four-ring window of supercage are partially mobilizable which is capable of providing a higher electrostatic interaction with nitrogen molecules. The ^7Li MAS NMR spectra investigation of low silica zeolite LiX (Si/Al ratio 1:1) before and after nitrogen adsorption reported by Feuerstein indicated that only the peaks of type III cations sites shifted after nitrogen which is in agreement with the prediction that nitrogen adsorption happens at type III cation sites. The result of NMR spectra study also explains the phenomena that the nitrogen capacity increases after 70% Li^+ exchange level for the preparation of LiX zeolite [37]. The cation sites of type I and type II are first occupied by Li^+ to form an immobile structure during the ion exchange process which have no effect on the adsorption performance for the zeolite surface modification.

2.4.2 Column strategy for different level of oxygen enrichment

Due to the electrostatic field of mobilized cations in type III sites, polar components like vapor and carbon dioxide would first occupied the effective adsorption surface area of zeolite during the PSA process. For the theoretical analysis of zeolite adsorption performance, dry cylinder gas is typically used as the gas source. However, for the commercial oxygen concentrator using room air as the gas source, H_2O and CO_2 in the air are the inevitable and undesired adsorbates. The correlation of nitrogen capacity and residual water in the framework of Li-LSX (low silica X zeolite) is illustrated in Fig.2.10. The nitrogen capacity of Li-LSX zeolite decreases drastically by 90% from 18 molec/uc to 2 molec/uc with only 30 molec/uc residual water which simulates the condition that the zeolite is contaminated by the vapor in air. Conventional vacuum desorption cannot fully desorb the H_2O and CO_2 molecules which gradually decreases the zeolite capacity under the cyclic operation of adsorption and desorption steps [38]. In this way, the pre-treatment process is required to protect the adsorption column from contaminants in the air. In industrial scale PSA plant, an activated alumina pre-

treatment column is usually installed before the adsorption column using temperature swing process for effectively gas drying. However, for the adsorption column of portable oxygen concentrator, a thin layer of activated alumina is added before the zeolite layer as a desiccant to prevent zeolite deactivation. The main role of the desiccant layer is to perform PSA gas drying process simultaneously with oxygen concentration process. The volume ratio of the desiccant to whole column was 0.15-0.20 using ambient air source (0.04 vol.% CO_2 and 0.4-0.8 vol.% moisture) [39].

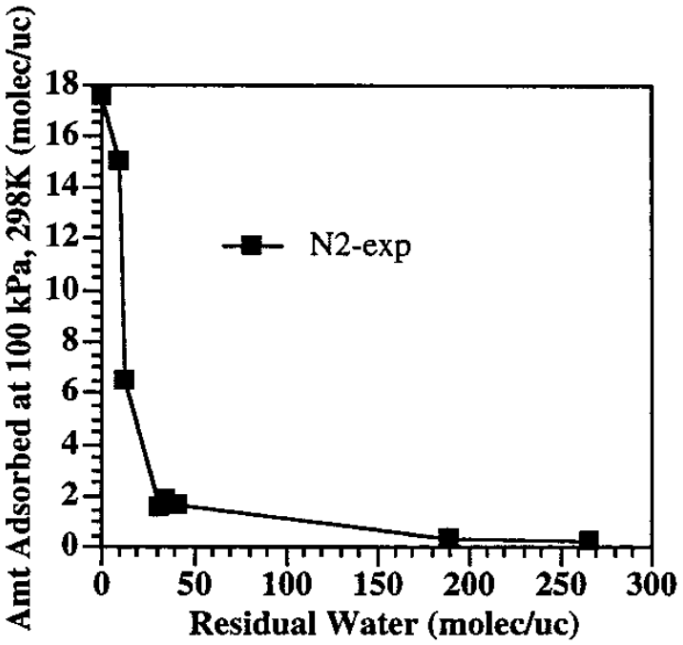

Figure 2.10 Amount of nitrogen absorbed at 100 kPa and 298 K versus residual water in Li-LSX (figure reprinted with permission from reference [38])

The conventional oxygen concentration using PSA process is limited by 95% due to the argon in the air. The selectivity of argon to oxygen for the zeolite 5A, 13X and LiX is close to 1:1 which means the output oxygen product is the enriched mixture of oxygen and argon. Recently, a silver-exchanged titanosilicate was investigated as an argon selective adsorbent for the production of high purity oxygen [40]. The single component adsorption isotherms are shown in Fig.2.11 with the argon to oxygen selectivity around 1.25:1. The production of high

purity oxygen requires a 95%/5% oxygen/argon inflow which represents the highest output oxygen concentration level using LiX zeolite. A column strategy for high purity oxygen concentration process is illustrated in Fig.2.12 with a desiccant layer and two adsorbent layers. The air source first flows through the desiccant layer and LiX zeolite layer to generate a dry oxygen product flow with the concentration of 95 vol.% then passes the silver-exchanged titanosilicate layer for the high purity production.

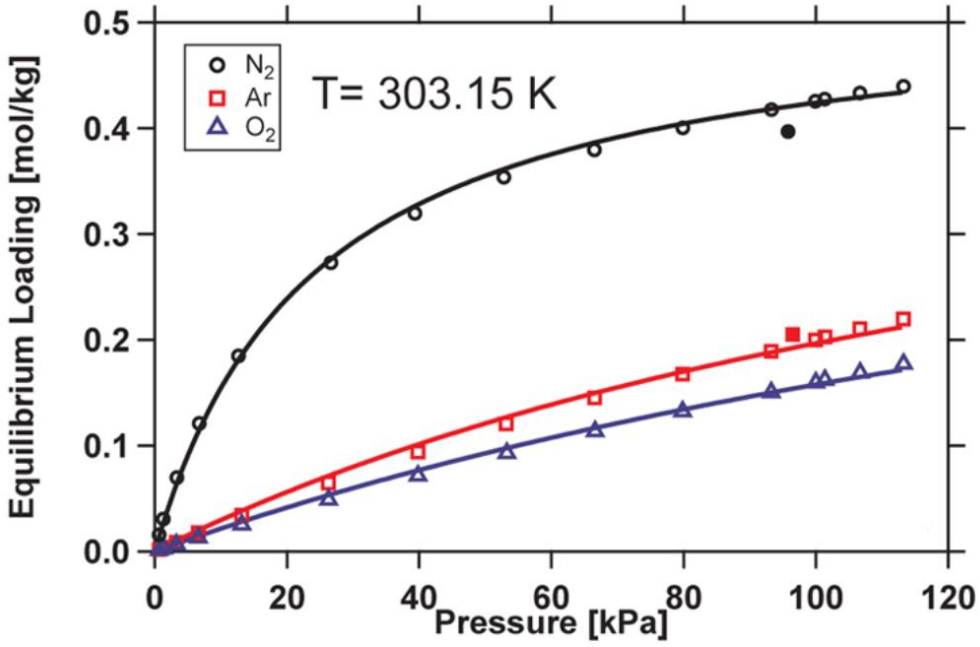

Figure 2.11 Single component adsorption isotherm of N_2 , O_2 and Ar on Ag-ETS-10 extrudates (figure reprinted with permission from reference [40])

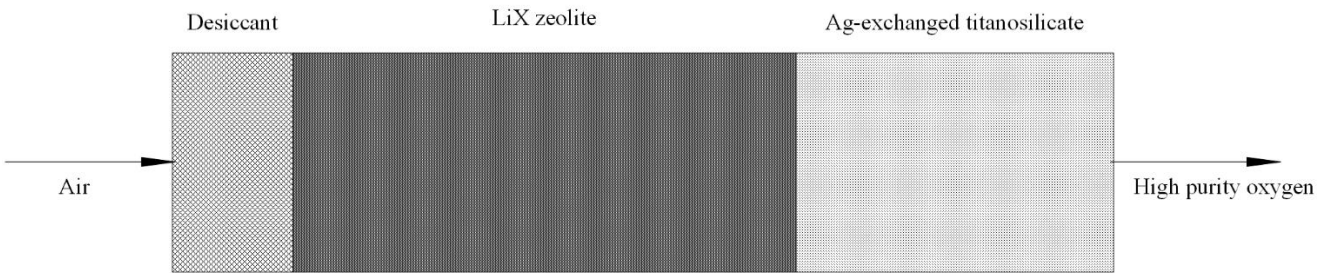

Figure 2.12 Schematics of adsorption column with desiccant layer and adsorbent layers

2.4.3 Rapid pressure swing adsorption (RPSA) process for small particle zeolite bed

Rapid pressure swing adsorption is the process developed for the portable oxygen concentrator design using fast cycling adsorption-desorption switch. It works for the condition that high purity is not necessary for the terminal use. The productivity (O_2 flowrate/weight of adsorbent) of the conventional PSA cycle is limited by the pressurization time and the desorption efficiency. The pressurization time depends on the pressure drop during the axial gas transportation and adsorption inside the zeolite. Applying shallow column (length < diameter) instead of the narrow column is one of the effective method to increase the cross-sectional area for gas flow. The schematics of the shallow adsorption column is illustrated in Fig.2.13. The inlet gas distributor is added to generate an adequate gas-solid contact for the adsorption step. The rapid PSA process was summarized by Rao with two main steps: a) super-atmospheric gas pass through the shallow adsorption bed with an enriched oxygen product flowing out; b) countercurrent desorption when the adsorption bed is not fully saturated [41-44]. The adsorbent column switches from adsorption step to desorption step when portion of the column is still filled with enriched oxygen. The remained less concentrated product gas in the column void is utilized as the purge gas in the countercurrent desorption step to enhance the desorption efficiency. Fast cycling of the RPSA process increases the productivity of adsorption column while avoids the temperature rising caused by the adsorption heat to maintain an stable production cycle. However, the manufacturing and installation of the shallow zeolite column is complicated and expensive for the miniature oxygen concentration system.

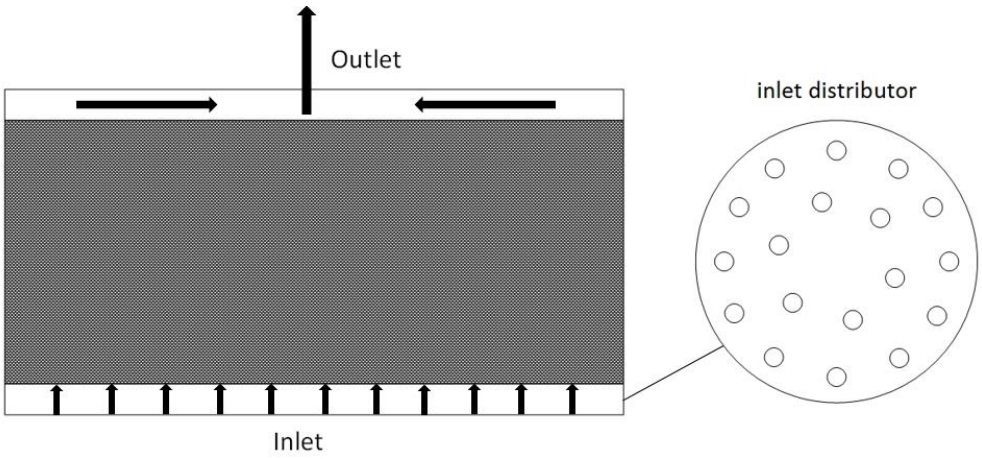

Figure 2.13 Schematic of shallow bed with inlet gas distributor

2.5 Modelling Methodology

2.5.1 Methodology

COMSOL Multiphysics was used in this project as the equation-based simulation software platform providing numerical methods of velocity and concentration solutions of adsorption process. The simulation model of PSA process was built based on the transportation and balance laws of solid-gas systems with two interfaces: the Free and Porous Media Flow Interface and the Transport of Diluted Species in Porous Media Interface. The Free and Porous Media Flow Interface includes a set of Navier-Stokes equations which describes the flow in column voids and a set of Brinkman equations which describes the flow in the internal voids of porous media [45]. The velocity and pressure are solved in the flow interface as the dominant transport factors of free flow in column voids and porous media flow in zeolite voids. The Transport of Diluted Species in Porous Media Interface deals with the gas species (N_2 and O_2) transported by conversion and dispersion with adsorption model equations discussed in chapter 1.2. The concentration of nitrogen and oxygen are solved in the mass balance equations in the species transport interface coupled with the velocity profile from the flow interface.

2.5.2 Finite element method

The models built to describe the engineering physics are usually a set of partial differential equations (PDEs). For the complicated mathematical models, it is difficult to get the solutions using analytical methods. On the contrary, an approximation model with algebraic equations is typically applied to represent the original model using discretization methods shown in Fig.2.14. The entire model geometry is divided into numerous small elements interconnected at points called nodes. In this way, the models are solved by substituting boundary conditions into the algebraic model equations of each elements which generates the approximation numerical solutions instead of the exact ones. The accuracy of the approximate solutions depends on the properties of the elements (number, shape and area).

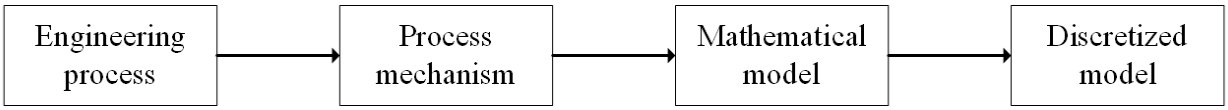

Figure 2.14 Flowchart for summarizing the strategy of model approximation

The 2D geometry meshing of the adsorption column is shown in Fig.2.15. The equations are solved in a 2D axisymmetric geometry model to save the computation cost while the 3D simulation results are generated from the revolved 2D plot. Due to shape of the adsorption column, rectangular mesh type was selected to represent the axial transport of the inflow and the boundary wall condition. Each element has four nodes to generate approximation solutions while the results inside the elements are obtained by averaging the solutions of nodes spatially.

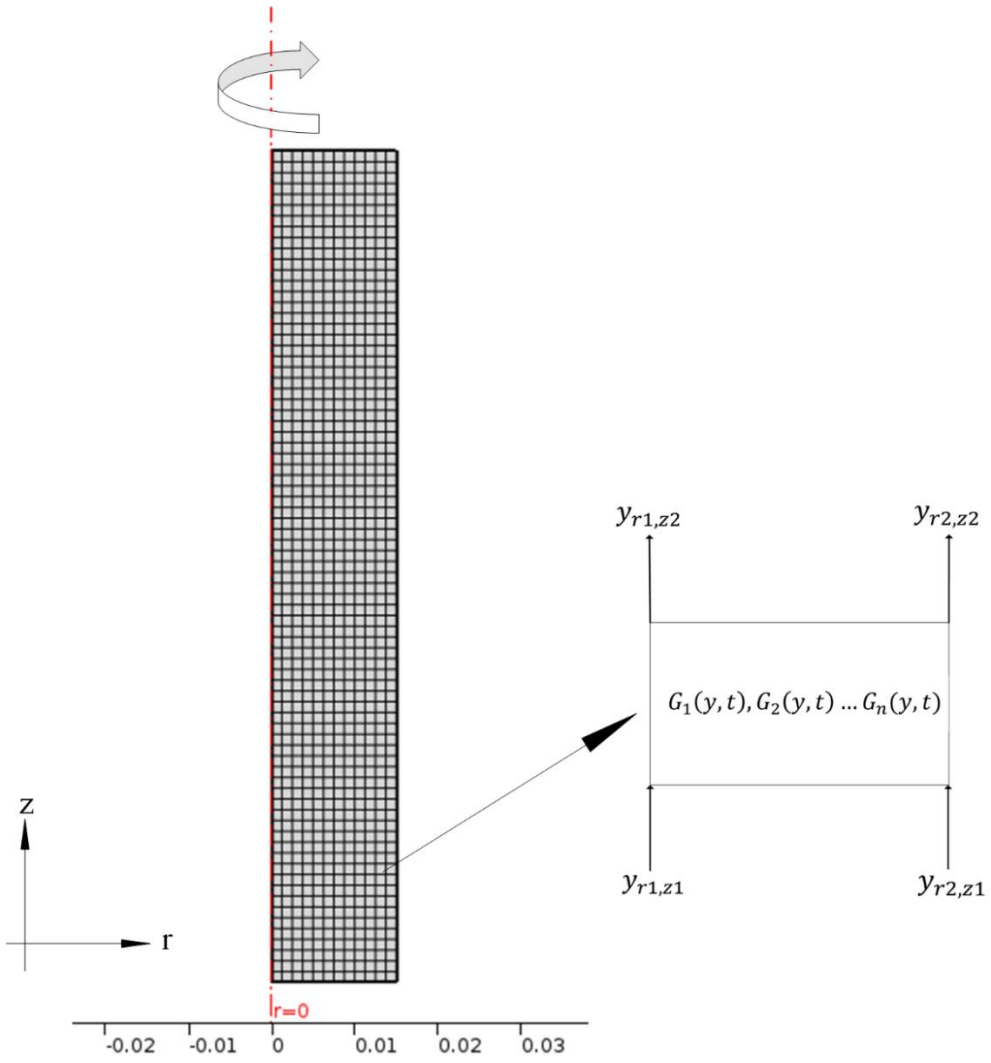

Figure 2.15 Schematics of the adsorption column meshing using finite element method

Reference

[1] Johnson, Robert L., and William P. Myers. "Respiratory support system." U.S. Patent No. 3,880,616. 29 Apr. 1975.

[2] Watson, Charles F., Roger D. Whitley, and Michael L. Meyer. "Multiple zeolite adsorbent layers in oxygen separation." U.S. Patent No. 5,529,610. 25 Jun. 1996.

[3] Sircar, Shivaji, and William Emil Waldron. "Oxygen production by adsorption." U.S. Patent No. 6,468,328. 22 Oct. 2002.

[4] Sircar, S., M. B. Rao, and T. C. Golden. "Fractionation of air by zeolites." Studies in surface science and catalysis 120 (1999): 395-423.

[5] Chai, Siew Wah, Mayuresh V. Kothare, and Shivaji Sircar. "Rapid pressure swing adsorption for reduction of bed size factor of a medical oxygen concentrator." Industrial & Engineering Chemistry Research 50.14 (2011): 8703-8710.

[6] Santos, J. C., F. D. Magalhaes, and A. Mendes. "Contamination of zeolites used in oxygen production by PSA: effects of water and carbon dioxide." Industrial & Engineering Chemistry Research 47.16 (2008): 6197-6203.

[7] Alpay, E., and D. M. Scott. "The linear driving force model for fast-cycle adsorption and desorption in a spherical particle." Chemical Engineering Science 47.2 (1992): 499-502.

[8] Azevedo, Diana CS, and Alírio E. Rodrigues. "Bilinear driving force approximation in the modeling of a simulated moving bed using bidisperse adsorbents." Industrial & engineering chemistry research 38.9 (1999): 3519-3529.

[9] Mendes, Adélio MM, Carlos AV Costa, and Alírio E. Rodrigues. "PSA simulation using particle complex models." Separation and purification technology 24.1 (2001): 1-11.

[10] Brandani, S., Hufton, J., & Ruthven, D. (1995). Self-diffusion of propane and propylene in 5A and 13X zeolite crystals studied by the tracer ZLC method. Zeolites, 15(7), 624-631.

[11] Ruthven, D. M., & Xu, Z. (1993). Diffusion of oxygen and nitrogen in 5A zeolite crystals and commercial 5A pellets. Chemical engineering science, 48(18), 3307-3312.

[12] Cavenati, S., Grande, C. A., & Rodrigues, A. E. (2004). Adsorption equilibrium of methane, carbon dioxide, and nitrogen on zeolite 13X at high pressures. Journal of Chemical & Engineering Data, 49(4), 1095-1101.

[13] Da Silva, F. A., & Rodrigues, A. E. (1999). Adsorption equilibria and kinetics for propylene and propane over 13X and 4A zeolite pellets. Industrial & engineering chemistry research, 38(5), 2051-2057.

[14] Broussard, L., & Shoemaker, D. (1960). The structures of synthetic molecular sieves. Journal of the American Chemical Society, 82(5), 1041-1051.

[15] Deng, H., Yi, H., Tang, X., Yu, Q., Ning, P., & Yang, L. (2012). Adsorption equilibrium for sulfur dioxide, nitric oxide, carbon dioxide, nitrogen on 13X and 5A zeolites. Chemical engineering journal, 188, 77-85.

[16] Selbin, J., & Mason, R. B. (1961). Preparation of gallium-containing molecular sieves. Journal of Inorganic and Nuclear Chemistry, 20(3), 222-228.

[17] Loughlin, K. F., Hasanain, M. A., & Abdul-Rehman, H. B. (1990). Quaternary, ternary, binary, and pure component sorption on zeolites. 2. Light alkanes on Linde 5A and 13X zeolites at moderate to high pressures. Industrial & engineering chemistry research, 29(7), 1535-1546.

[18] Kanazirev, V. I., & Latus, D. G. (2003). U.S. Patent No. 6,638,340. Washington, DC: U.S. Patent and Trademark Office.

[19] Plank, C. J., & Rosinski, E. J. (1976). U.S. Patent No. 3,939,058. Washington, DC: U.S. Patent and Trademark Office.

[20] Plank, C. J., Rosinski, E. J., & Hawthorne, W. P. (1964). Acidic crystalline aluminosilicates. New superactive, superselective cracking catalysts. Industrial & Engineering Chemistry Product Research and Development, 3(3), 165-169.

[21] Yang, R. T. (2003). Adsorbents: fundamentals and applications. John Wiley & Sons.

[22] Hutson, N. D., Rege, S. U., & Yang, R. T. (1999). Mixed cation zeolites: LixAgy- X as a superior adsorbent for air separation. AIChE journal, 45(4), 724-734.

[23] Mondale, K. D., Carland, R. M., & Aplan, F. F. (1995). The comparative ion exchange capacities of natural sedimentary and synthetic zeolites. Minerals Engineering, 8(4), 535-548.

[24] Gal, I. J., & Radovanov, P. (1975). Ion-exchange equilibria of synthetic 13X zeolite with Ni 2+, Co 2+, Zn 2+ and Cd 2+ ions. Journal of the Chemical Society, Faraday Transactions 1: Physical Chemistry in Condensed Phases, 71, 1671-1677.

[25] Mintova, S., Valtchev, V., Onfroy, T., Marichal, C., Knözinger, H., & Bein, T. (2006). Variation of the Si/Al ratio in nanosized zeolite Beta crystals. Microporous and mesoporous materials, 90(1), 237-245.

[26] Calleja, G., Pau, J., & Calles, J. A. (1998). Pure and multicomponent adsorption equilibrium of carbon dioxide, ethylene, and propane on ZSM-5 zeolites with different Si/Al ratios. Journal of Chemical & Engineering Data, 43(6), 994-1003.

[27] De Lucas, Antonio, et al. "Synthesis of 13X zeolite from calcined kaolins and sodium silicate for use in detergents." Industrial & engineering chemistry research 31.9 (1992): 2134-2140.

[28] Delgado, J. A., Uguina, M. A., Gómez, J. M., & Ortega, L. (2006). Adsorption equilibrium of carbon dioxide, methane and nitrogen onto Na-and H-mordenite at high pressures. Separation and purification technology, 48(3), 223-228.

[29] Mulgundmath, V. P., Tezel, F. H., Saatcioglu, T., & Golden, T. C. (2012). Adsorption and separation of CO2/N2 and CO2/CH4 by 13X zeolite. The Canadian Journal of Chemical Engineering, 90(3), 730-738.

[30] Habgood, H. W. (1964). Adsorptive and gas chromatographic properties of various cationic forms of zeolite X. Canadian Journal of Chemistry, 42(10), 2340-2350.

[31] Drain, L. E. "Permanent electric quadrupole moments of molecules and heats of adsorption." Transactions of the Faraday Society 49 (1953): 650-654.

[32] Feuerstein, M., and R. F. Lobo. "Characterization of Li cations in zeolite LiX by solid-state NMR spectroscopy and neutron diffraction." Chemistry of materials 10.8 (1998): 2197-2204.

[33] Ackley, Mark William, et al. "PSA apparatus and process using adsorbent mixtures." U.S. Patent No. 6,027,548. 22 Feb. 2000.

[34] Shailaja, J., et al. "Alkali ion-controlled excited-state ordering of acetophenones included in zeolites: Emission, solid-state NMR, and computational studies." The Journal of Physical Chemistry A 107.18 (2003): 3187-3198.

[35] Plevert, J., et al. "Structure of dehydrated zeolite Li− LSX by neutron diffraction: evidence for a low-temperature orthorhombic faujasite." The Journal of Physical Chemistry B 101.49 (1997): 10340-10346.

[36] Feuerstein, M., and R. F. Lobo. "Characterization of Li cations in zeolite LiX by solid-state NMR spectroscopy and neutron diffraction." Chemistry of materials 10.8 (1998): 2197-2204.

[37] Feuerstein, M., R. J. Accardi, and R. F. Lobo. "Adsorption of nitrogen and oxygen in the zeolites LiA and LiX investigated by 6Li and 7Li MAS NMR spectroscopy." The Journal of Physical Chemistry B 104.44 (2000): 10282-10287.

[38] Santos, J. C., F. D. Magalhaes, and A. Mendes. "Contamination of zeolites used in oxygen production by PSA: effects of water and carbon dioxide." Industrial & Engineering Chemistry Research 47.16 (2008): 6197-6203.

[39] Chai, Siew Wah, Mayuresh V. Kothare, and Shivaji Sircar. "Rapid pressure swing adsorption for reduction of bed size factor of a medical oxygen concentrator." Industrial & Engineering Chemistry Research 50.14 (2011): 8703-8710.

[40] Hosseinzadeh Hejazi, Sayed Alireza, et al. "Dynamic Column Breakthrough and Process Studies of High-Purity Oxygen Production Using Silver-Exchanged Titanosilicates." Industrial & Engineering Chemistry Research 55.20 (2016): 5993-6005.

[41] Rao, V. R., Kothare, M. V., & Sircar, S. (2014). Numerical simulation of rapid pressurization and depressurization of a zeolite column using nitrogen. Adsorption, 20(1), 53-60.

[42] Huang, W. C., & Chou, C. T. (2003). Comparison of radial-and axial-flow rapid pressure swing adsorption processes. Industrial & engineering chemistry research, 42(9), 1998-2006.

[43] Rao, V. R., Kothare, M. V., & Sircar, S. (2014). Novel design and performance of a medical oxygen concentrator using a rapid pressure swing adsorption concept. AIChE Journal, 60(9), 3330-3335.

[44] Rao, V. Rama, S. Farooq, and W. B. Krantz. "Design of a two- step pulsed pressure-swing adsorption- based oxygen concentrator." AIChE journal 56.2 (2010): 354-370.

[45] COMSOL, 2016. COMSOL Documentation. www.comsol.com.

Chapter 3

3. Study of zeolite characterization and adsorption column design

3.1 Zeolite Characterization

For the pressure swing adsorption process, the selection of the adsorbent is of great importance to the separation efficiency. Zeolite 5A and 13X as the commercial molecular sieves are proven to be the appropriate adsorbent types for the oxygen concentration process. The nitrogen capacity and adsorption/desorption performance of zeolite samples could be investigated through instrument analysis and adsorption test under the PVSA cycle. Design issues of the adsorption column and the operational parameters of the PVSA cycle were summarized in this chapter based on the results of zeolite characterization and adsorption performance in a swing cycle.

3.1.1 TGA analysis

Characterization of different zeolite samples is a vital procedure for the design of the adsorption process. The desorption of zeolite with nitrogen is measured by thermal gravimetric analysis (TGA). TGA is a method that measures the mass of a sample as it is heated at a constant heating rate in a defined atmosphere. Figure 3.1 (a) and (b) show the TGA weight loss curve of zeolite UOP 5A and UOP 13X with N_2 as the support gas at constant heating rate 10℃/min from 25℃to 600℃[1]. The sorbates desorbed from the zeolite are mainly nitrogen and vapor with a small amount of oxygen and carbon dioxide. The weight loss of zeolite UOP 5A and 13X is 7.18% and 10.80% respectively which means the adsorption capacity of 13X zeolite is higher than that of 5A with air as the gas source. According to the weight loss curve of zeolite 5A and 13X, the zeolite sample could be fully regenerated in an oven at 500℃, however, in a continuously nitrogen flow environment to avoid the reversed adsorption of vapor during the cooling of the sample. The zeolitic molecular sieve for oxygen

concentration is a recyclable adsorbent and reactivation cost is acceptable. Figure 3.2 shows the TGA weight loss curve of fresh, used (after adsorption test) 13X-Beijing-DF from Beijing Dongfang Technology with N_2 as the support gas at constant heating rate 10℃/min from 25℃ to 600℃[2]. A higher weight loss of used zeolite 13X was detected compared to fresh one which could be explained by the remained vapor inside the zeolite after the pressure swing adsorption test with room air. The desiccant is of great importance to the lifespan of adsorption column as a pre-treatment media to provide dry air for the oxygen concentration process.

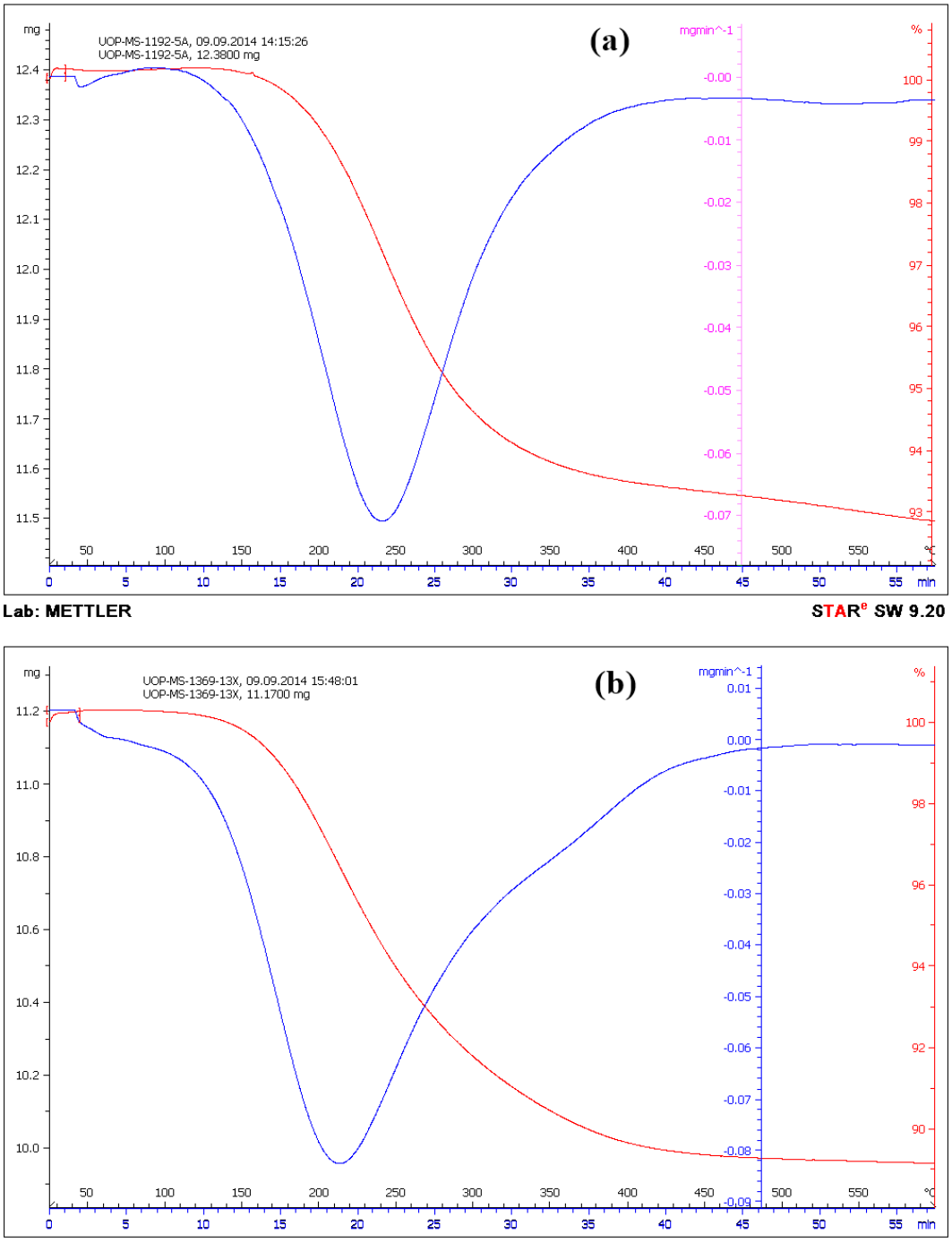

Figure 3.1 TGA weight loss curve of zeolite (a) UOP 5A (b) UOP 13X with N_2 support gas at constant heating rate 10℃/min

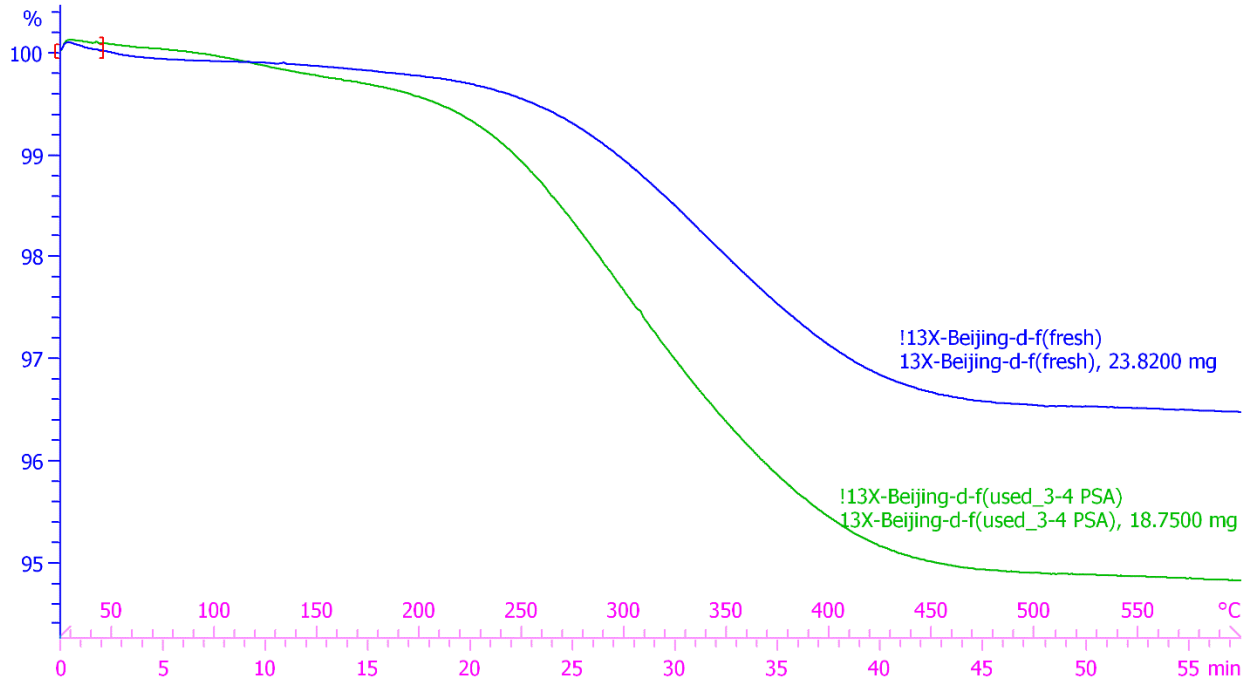

Figure 3.2 TGA weight loss curve of fresh, used and regenerated zeolite 13X-Beijing-DF with N_2 support gas at constant heating rate 10℃/min

3.1.2 BET analysis

Brunauer-Emmett-Teller (BET) Surface Area Analysis evaluates the surface area of a specific material by nitrogen multilayer adsorption measurement as a function of relative pressure. Barrett-Joyner-Halenda (BJH) analysis are utilized to characterise the pore area and volume with the size distribution through nitrogen adsorption and desorption techniques. Table 3.1 illustrates the BET analysis results of zeolite JLOX-LiX-101 from JianLong Chemical and 13X-BJ-DF [3]. The BET surface area, Langmuir area and micropore area of Li exchanged 13X zeolite JLOX-101 are higher than those of 13X zeolite BJ-DF due to zeolite modification using ion exchanged technique. Portion of micropore volume to the total adsorption pore volume is summarized (78.6%-JLOX-101 and 76.1%-13X-BJ-DF) as a prove to the

assumption of adsorption model that the adsorption happens at the microporous area and mesoporous area of the zeolite. The micropore volume of zeolite JLOX-101 is higher than that of zeolite 13X-BJ-DF. The adsorption average pore diameter of zeolite JLOX-101 and 13X-BJ-DF are 21.26 Å and 22.36 Å, respectively, which is in agreement with the microporous adsorption theory of zeolite. The BJH Adsorption Cumulative Pore area distribution of JLOX-101 is shown in Fig.3.3. The nitrogen occupies most of the microporous surface area (pore diameter <2 nm) and small part of the mesoporous surface area (pore diameter 2~50 nm).

Table 3.1 BET adsorption results of JLOX-101 and 13X-BJ-DF

Zeolite	**JLOX-101**	**13X-BJ-DF**
BET surface area (m^2/g)	574.77	522.93
Langmuir area (m^2/g)	760.01	690.53
Micropore area (m^2/g)	515.39	477.04
Single Point Adsorption Total Pore Volume (cm^3/g)	0.30	0.29
Micropore Volume (cm^3/g)	0.24	0.22
Adsorption Average Pore Diameter (Å)	21.26	22.36

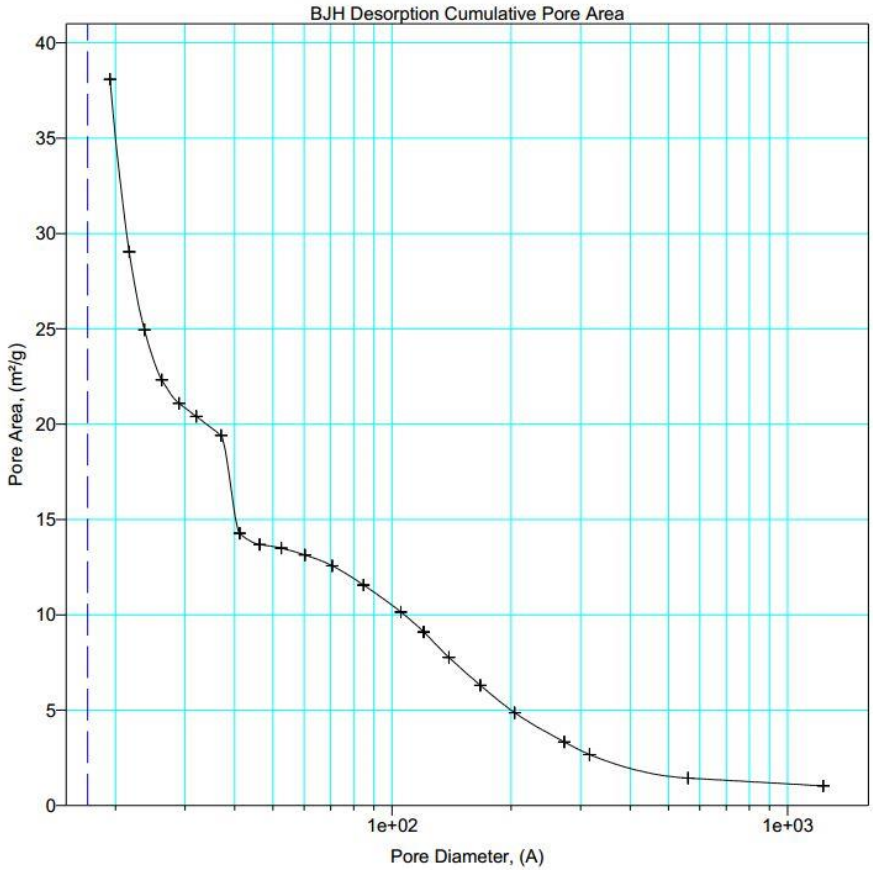

Figure 3.3 BJH Adsorption Cumulative Pore Area distribution of JLOX-101

3.1.3 XRD analysis

The structure and phase purity of the zeolites were confirmed by X-ray powder diffraction (XRD). Figure 3.4 exhibits the powder XRD patterns of zeolite JLOX-101 with two types of sample zeolite 13X from UOP and Beijing-DF. The PXRD spectra of the collected solid forms were obtained on a 2500 diffractometer (D/MAX, Rigaku, Japan) with a Cu Kα radiation source (λ = 1.5406 Å) at 100 mA and 40 kV. The samples were recorded at a scanning rate of 5° per minute over a 2θ range of 5–40°.The XRD peak position and shape of zeolite JLOX101-LiX are essentially the same as those of zeolite 13X which means zeolite JLOX101-LiX still maintains the intrinsic crystalline structure of zeolite 13X after Li^+ ion-exchange method.

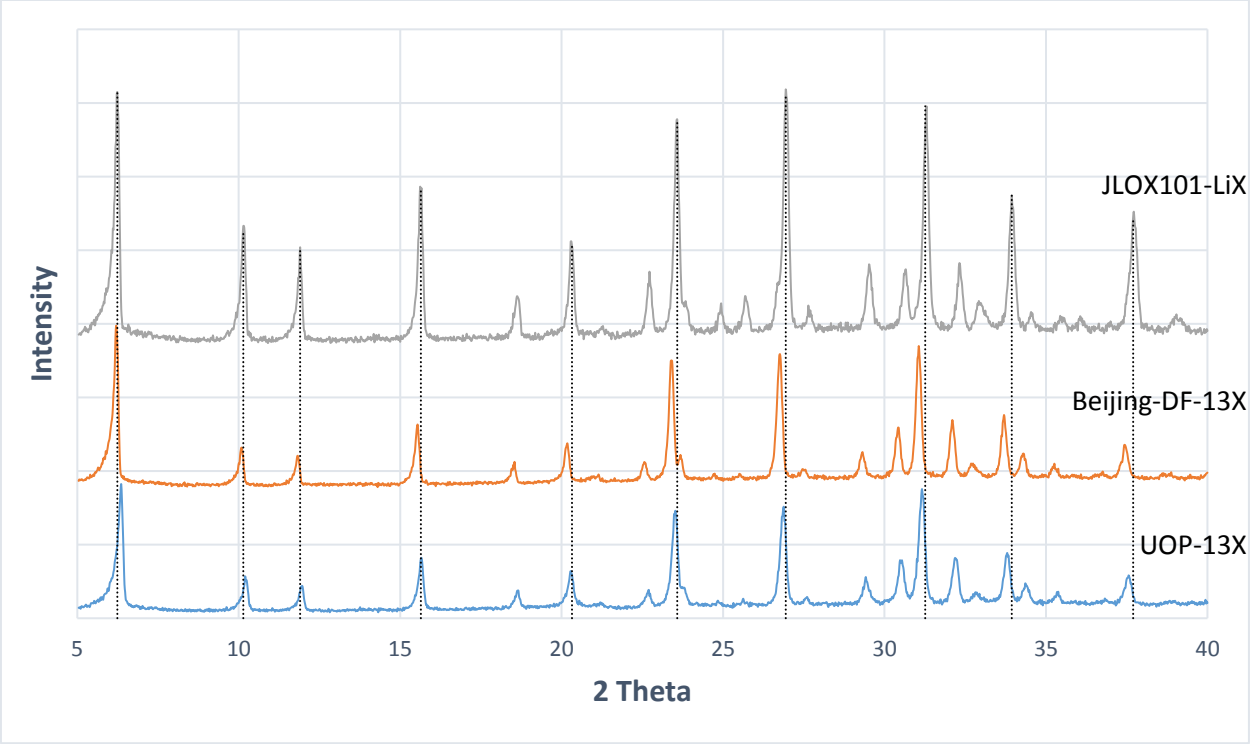

Figure 3.4 XRD patterns of three different types of zeolites: UOP-13X, Beijing-DF-13X and JLOX101-LiX

3.2 Zeolite column design with adsorption performance test

The adsorption performance of different zeolite samples could also be tested in a cylinder to perform pressure vacuum swing cycle. The setup that was used to test the zeolite adsorption performance is illustrated in Fig.3.5. The flowrate of the air was adjusted to 2 L/min by the mass flow controller and the adsorption pressure was adjusted to 2 barg by the pressure relief valve (back pressure regulator) through the bypass (V4). The oxygen volume concentration is recorded by the oxygen analyzer GB300 (Teledyne Technologies, ON, Canada) and the sampling rate is 1HZ [4]. The zeolite samples were filled in a glass column of 3.2cm in diameter and 11cm in length shown in Fig.3.6. The adsorption performance of different zeolite samples

is summarized in Table 3.2. The oxygen peak vol.% and duration time for concentration over 30 vol.% were measured among 5 zeolite samples to get the best adsorbent: JLOX-LiX-101.

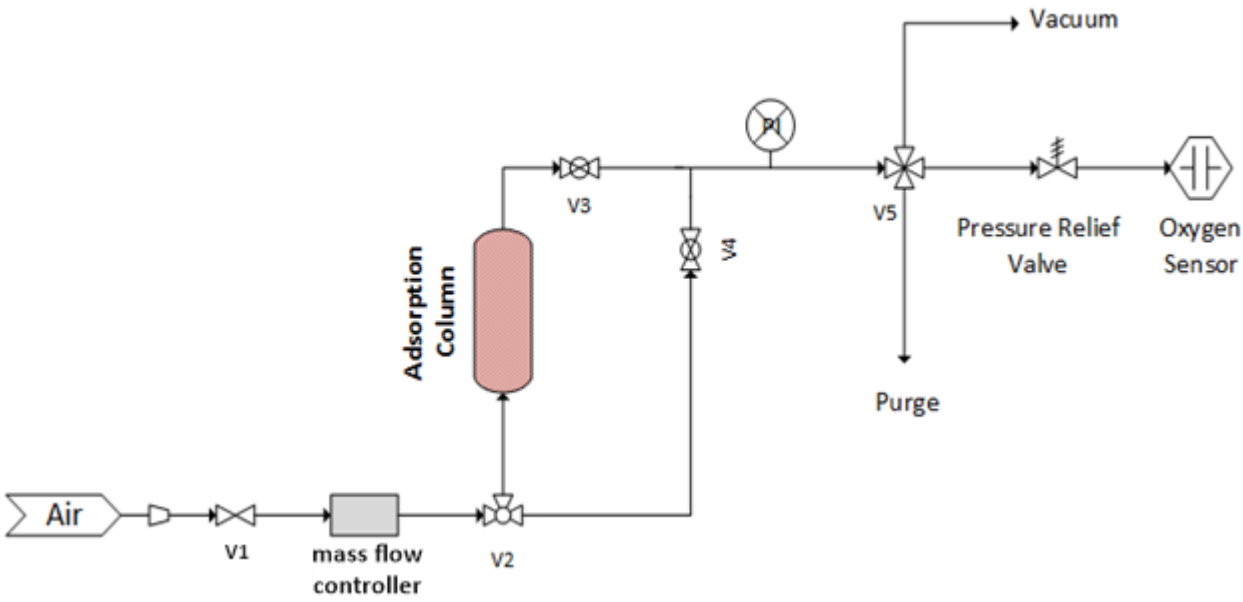

Figure 3.5 Schematics of experimental setup for zeolite performance test (V1,V2,V3,V4,V5 is the sequence of rotatory valves)

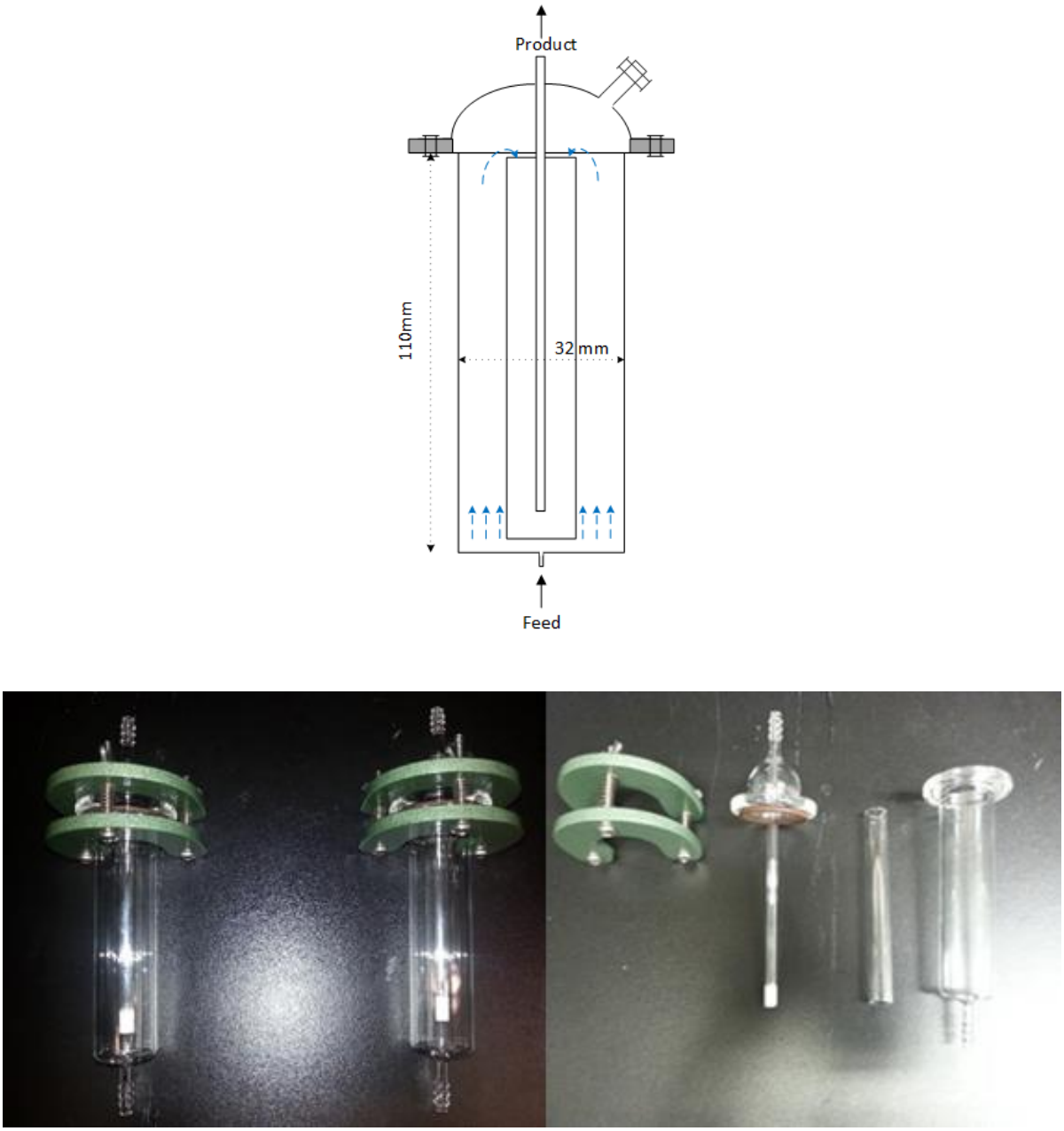

Figure 3.6 Schematic diagram (top) and the photographs (bottom) of the first glass-made adsorption column

Table 3.2 Preliminary adsorption results of different type of adsorbents

Adsorbent	**Max Concentration of O_2 (vol.%)**	**Δt (30% - 30% O_2)/s**
13x-φ0.5-0.8mm-Jiuzhou	26	-
5A-φ1.6-2.5mm-Jiuzhou	33	3.6
13X-φ2.0mm-UOP	37	9.2
13x-φ0.85-1.15mm- Beijing-DF	38	9.5
JLOX-LiX 101-φ 0.4-0.8mm-Jianlong Chemical	45	12.3

The design issue of the glass column is to provide long mass transfer area for adsorption through a double-layer gas way using the glass tube inside the column. However, the adsorption results revealed that the zeolite filling was not compact enough to provide adequate gas-solid contact for the adsorption and there is channeling inside the column. Several modifications were added to the adsorption column shown in Fig.3.7 with distributors inside. The effect of column length was evaluated to ensure the importance of long mass transfer area to get better adsorption performance. The results of adsorption performance by increasing the effective zeolite length are shown in Fig.3.8. The oxygen concentration increases considerably with the column length however along with an increasing time for pressurization. Further consideration is required to decrease the pressurizing time to improve the adsorption efficiency and productivity.

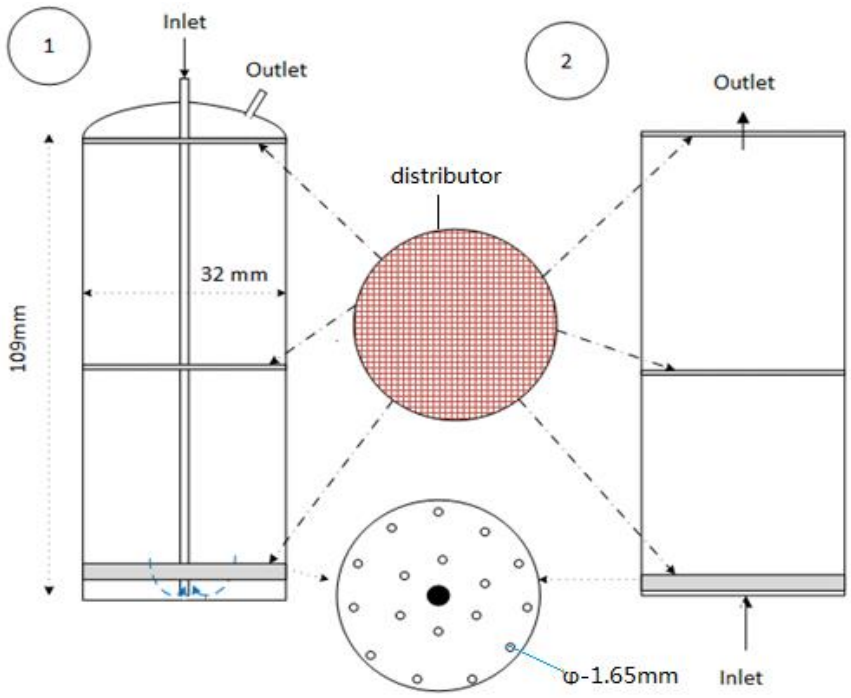

Figure 3.7 Schematic diagram of the modified adsorption column with gas distributors

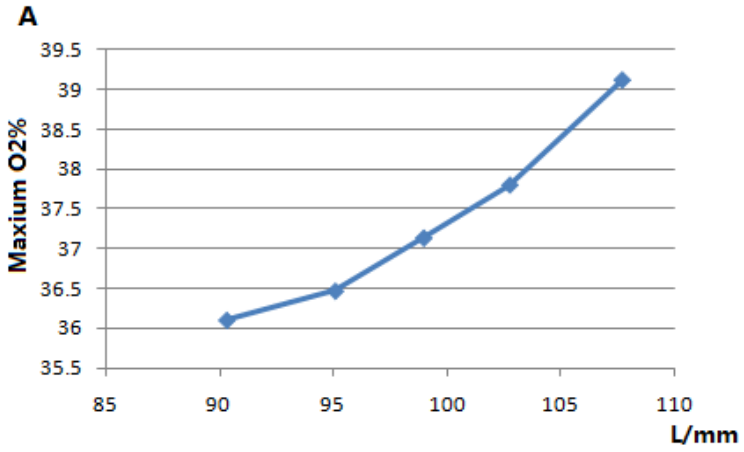

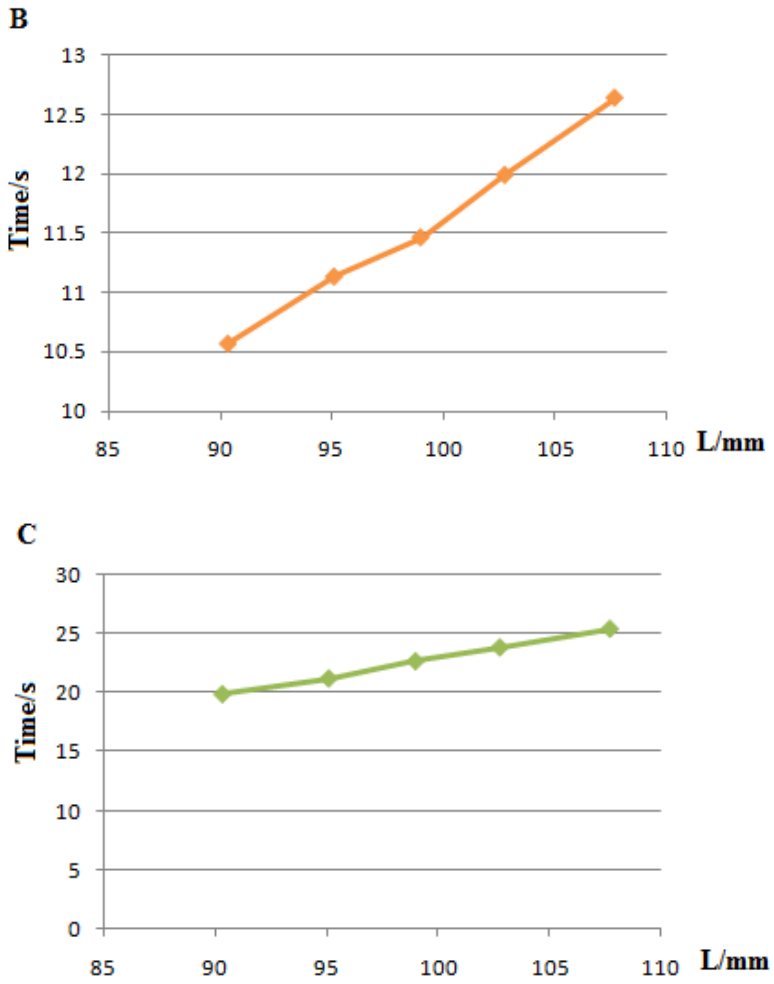

Figure 3.8 A) maximum purity at different column length, B) duration time (30 vol.% to 30 vol.%) at different column length, C) time to reach 2 barg (experimental pressure)

Considering that the adsorption process is an exothermic process, the thermal conductivity of the column should be taken into account to avoid a significant temperature rising during the adsorption step. The aluminum was selected to be the column material due to the high thermal conductivity for the cooling of zeolite particles and low density for lightweight design of oxygen concentrator. The thermal conductivity of aluminum (205 W/m/K) is 256 times higher than that of glass (0.8 W/m/K).

In order to understand the influence of the adsorption pressure, a set of adsorption tests were carried out at three different pressures in the modified aluminum adsorption column under a constant flow rate at room temperature. Adsorption tests were performed in a pressure vacuum swing adsorption (PVSA) process using supply gas and vacuum in the lab. The results are summarized in Table 3.3, Table 3.4, Table 3.5 and the shape of the output concentration curve are shown in Fig.3.9. Compared to the results at 1 barg, adsorption performance at 2 barg is better with higher concentration and longer duration time. However, increasing adsorption pressure from 2 barg to 3 barg couldn't improve the adsorption performance significantly with similar concentration peak and the duration time is only 1.5s longer. Considering the long pressurization time and higher hardware cost for high pressure adsorption, pressure around 2 barg are preferred for the adsorption process design of the portable oxygen concentrator.

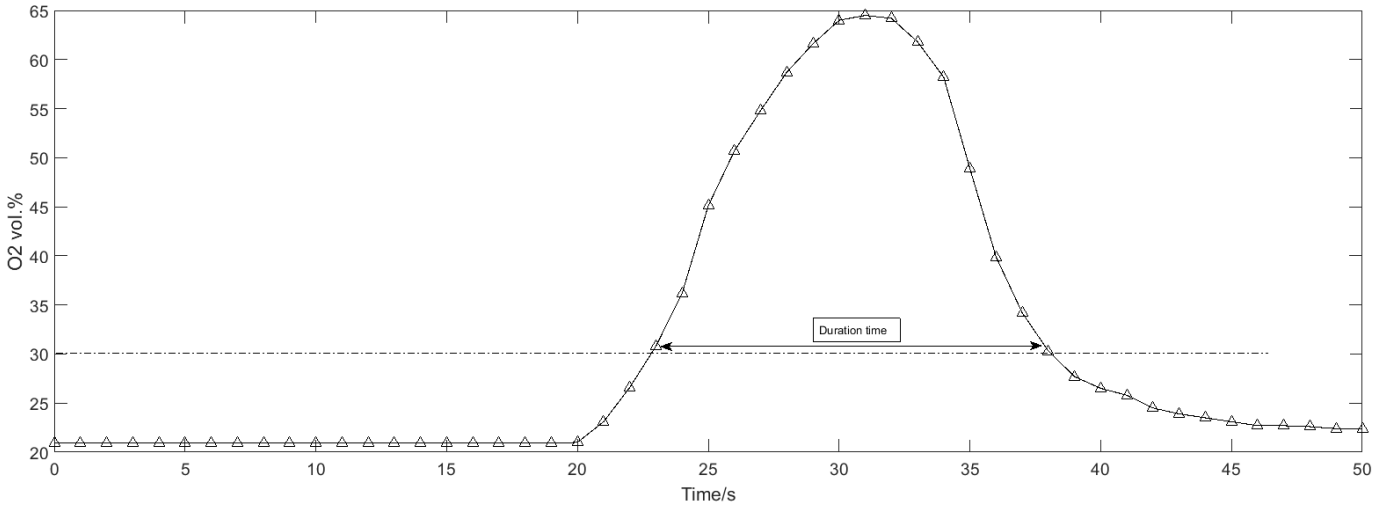

Figure 3.9 Output curve of the adsorption test under 2 barg

Table 3.3 Adsorption test on the aluminum column at 1 barg, flowrate 1.9 LPM

No. Exp.	Max Concentration of O_2 (vol.%)	Δt (30% - 30% O_2) (s)
1	54.00	11.90
2	53.00	18.14
3	60.90	14.62
4	63.40	13.40
5	61.20	13.55
6	55.50	11.15
7	54.80	10.87
Average	57.54	13.38

Table 3.4 Adsorption test on the aluminum column at 2 barg, flowrate 1.9 LPM

No. Exp.	Max Concentration of O2 (vol.%)	Δt (30% - 30% O2) (s)
1	63.80	15.84
2	63.70	15.00
3	65.90	16.12
4	61.50	14.81
5	64.30	16.01
6	59.80	13.37
7	64.80	14.78
Average	63.40	15.13

Table 3.5 Adsorption test on the aluminum column at 3 barg, flowrate 1.9 LPM

No. Exp.	Max Concentration of O2 (vol.%)	Δt (30% - 30% O2) (s)
1	60.90	16.24
2	64.90	18.02
3	64.90	17.06
4	63.20	17.68
5	60.20	15.65
6	65.00	17.68
7	65.20	15.31
Average	63.47	16.81

3.3 Geometry design of the adsorption column

The adsorption column should be sealed completely with only inlet and outlet connected to the tubing to avoid the leakage. However, based on the results of zeolite characterization, the zeolite is recyclable through the temperature swing methods. In order to replace the zeolite in the adsorption column, the inlet of the column is designed as a cap sealed with an O-ring gasket and fixed by several screws shown in Fig.3.10 to ensure a compact zeolite loading inside the cylinder. Gas distributor is installed at the inlet to generate a uniform gas distribution inside the column. Desiccant layer could be placed before the zeolite and held by very fine round metal mesh.

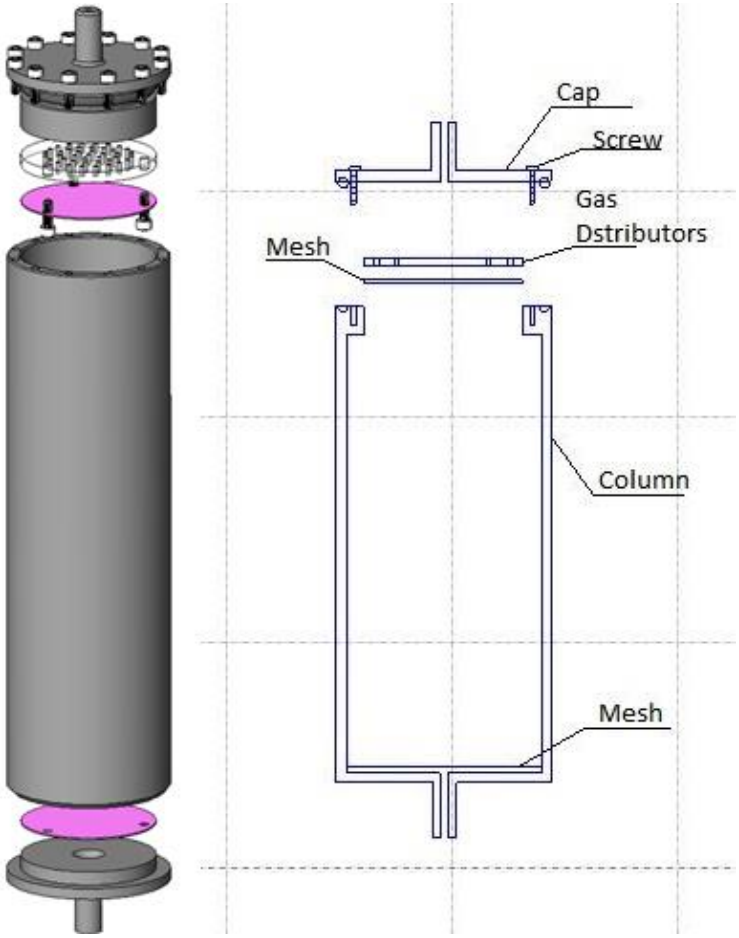

Figure 3.10 Schematics of zeolite column design

3.4 Conclusions and summary

Based on the zeolite characterization and adsorption test, several design issues could be summarized. LiX zeolite JLOX-101 is selected as the best zeolite among the commercial zeolite samples and would be used for the preparation of the oxygen concentrators. Adsorption pressure is set to be 2 barg due to the outstanding adsorption performance with relatively fast pressurization speed. The overpressure resistant for the air compressor and solenoid valves could be around 2 barg which benefits the hardware selection and concentrator miniaturization. The material of the adsorption column is selected to be

aluminum due to the high thermal conductivity for zeolite cooling and low density to ensure the lightweight of the adsorption column.

Reference

[1] MOLSIV 13X APG. (2010). UOP Adsorbents. Honeywell UOP, Des Plaines, Illinois, United States.

[2] Zeolite 13X. (2014). Beijing Dongfang Guansen Technology Co., Ltd., Beijing, China.

[3] Molecular sieve JLOX-101. (2016). LUOYANG JIANLONG CHEMICAL, Yanshi, Henan, China.

[4] GB300 oxygen analyzer. (2016). Teledyne Technologies International Corp., Waterloo, ON, Canada.

Chapter 4

4. Mathematical Model for Pressure/Vacuum swing adsorption process

4.1 Introduction

Transport phenomena equations were developed in a 3-dimensional dynamic mathematical model that describes the competitive adsorption of air components for the oxygen concentration. The model equations were solved using the finite element method (FEM) with the modules in a commercial computational fluid dynamics (CFD) software COMSOL Multiphysics ®. The adsorption parameters are fitted using the Sips adsorption model of LiX zeolite reported in the literature. The inlet flowrate is a function of pressure fitted with the experimental data. The pressure inside the column is determined by the inlet flowrate from the initial vacuum condition to the pre-set adsorption pressure. The outlet backpressure regulator is also simulated by the global equation function in the COMSOL Multiphsics as a boundary condition. This model provides a framework to understand how N_2 and O_2 is adsorbed inside the column and type of flow permeating along the column. Figure 4.1 shows a flow diagram that outlines the steps used for the model development.

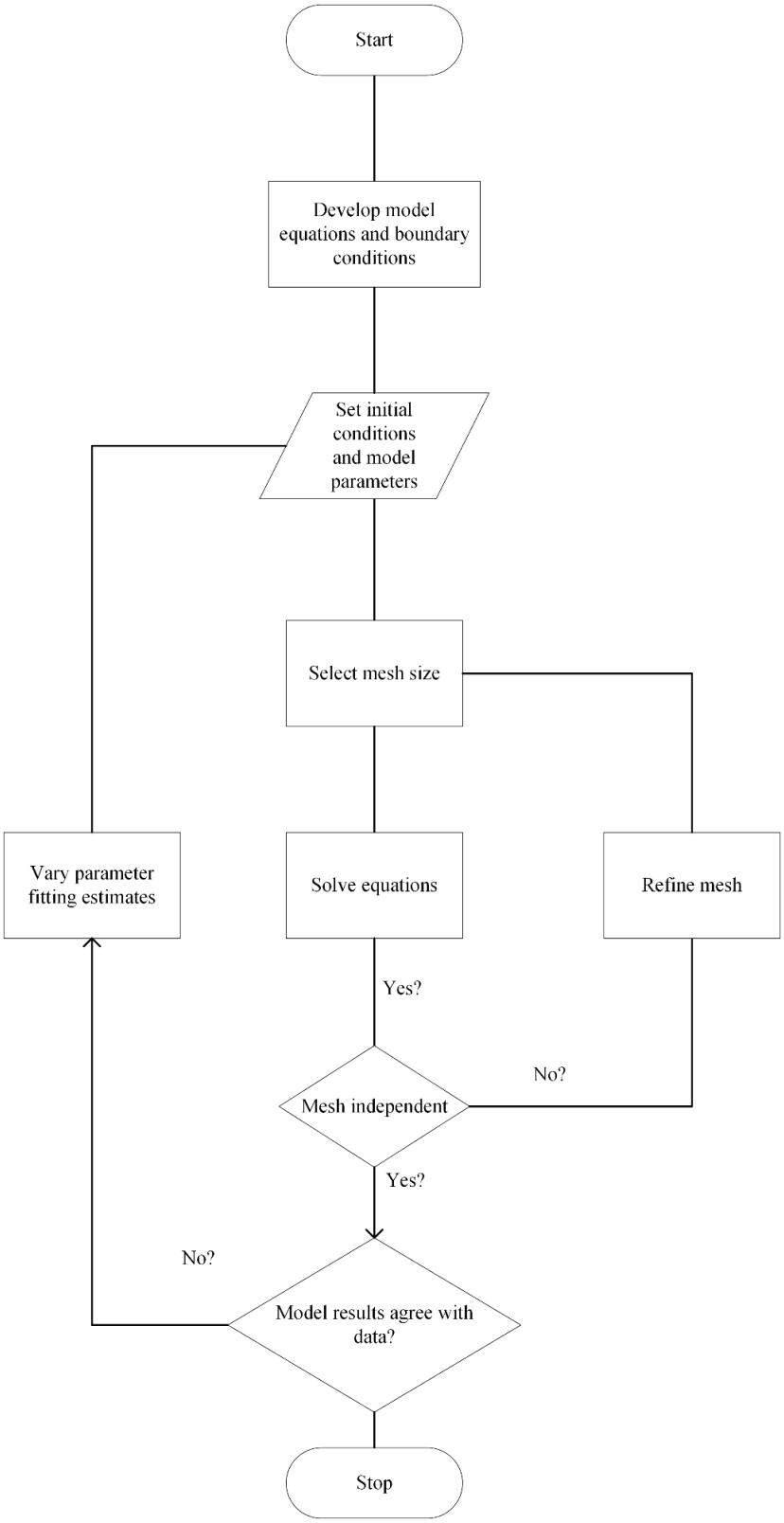

Figure 4.1 Flowchart showing model formulation steps

Due to the cylindrical geometry of the adsorption column, a 2-dimensional axi-symmetrical approximation was used to decrease the computational cost. The following assumptions were made in the model equations:

a) The air source is assumed to be a binary ideal gas with 79% N_2 and 21% O_2.
b) Uniform bed voidage and particle diameter.
c) The stabilized gas temperature at inlet and outlet is measured to be 22.5℃ and 23.8 ℃ by thermocouple, checking the temperature dependent adsorption model, the nitrogen and oxygen capacity difference (error $= \frac{|q_{i,22.5^\circ C} - q_{i,23.8^\circ C}|}{q_{i,22.5^\circ C}} \times 100\%$) at 1.79 barg is calculated to be 1.47% and 1.03%, respectively, which is negligible compared to the adsorption equilibrium equations, so the adsorption amount is assumed to be constant with the temperature.
d) Gravity effects on fluid flow are negligible.

4.2 Theory and computation technique

4.2.1 Fluid flow solution in the Free and Porous Media Flow Interface of COMSOL Multiphsics

In a porous medium, the global transport of momentum by shear stresses in the fluid is often negligible: the pore walls impede momentum transport between fluid occupying different pores. Darcy's law states that the velocity field is determined by the pressure gradient, the fluid viscosity, and the structure of the porous medium [1]:

$$\mathbf{u} = -\frac{\kappa}{\mu}\nabla p$$

In this equation, κ denotes the permeability of the porous medium [m^2], μ is the dynamic viscosity of the fluid [kg/(m·s)], p is the gauge pressure of the fluid flow [Pa], and $\mathbf{u}$ is the Darcy velocity [m/s].

The Brinkman equation extends Darcy's law to include a term that accounts for the viscous transport in the momentum balance, and it treats both the pressure and the flow velocity vector as independent variables.

The Free and Porous Media Flow Interface uses the Navier-Stokes equations to describe the flow in the column voids, and the Brinkman equations to describe the flow in the internal voids of porous media. The continuity in **u** and p implies a stress discontinuity at the interface between a free-flow domain and a porous domain. The difference corresponds to the stress absorbed by the rigid porous matrix, which is a consequence implicit in the formulations of the Navier-Stokes and Brinkman equations.

The flow in zeolite microporous area is governed by a set of the continuity equation and the momentum equation, which together form the Brinkman equations (COMSOL, 2016)[1]:

$$\frac{\partial}{\partial t}(\varepsilon_c \rho) + \nabla(\rho \mathbf{u}) = Q_{br} \quad (1)$$

$$\frac{\rho}{\varepsilon_c}\left(\frac{\partial \mathbf{u}}{\partial t} + (\mathbf{u}\cdot\nabla)\frac{\mathbf{u}}{\varepsilon_c}\right) = -\nabla p + \nabla\cdot\left\{\frac{1}{\varepsilon_c}\left[\mu(\nabla\mathbf{u} + (\nabla\mathbf{u})^T - \frac{2}{3}\mu(\nabla\cdot\mathbf{u})\mathbf{I}\right]\right\} - \left(\kappa^{-1}\mu + \frac{Q_{br}}{\varepsilon_c^2}\right)\mathbf{u} \quad (2)$$

where ρ is the density of the fluid [kg/m^3], ε_c is the column voidage [-], t is the time [s], Q_{br} is the volumetric mass source of the fluid phase [kg/m^3/s], κ denotes the permeability of the porous medium [m^2], μ is the dynamic viscosity of the fluid [kg/(m·s)], p is the gauge pressure of the fluid flow [Pa], and $\mathbf{u}$ is the Darcy velocity [m/s].

The permeability of the packed bed of spherical particles can be described by the Blake-Kozeny equation [2]:

$$\kappa = \frac{d^2}{150}\left(\frac{\varepsilon_c}{1-\varepsilon_c}\right)^2 \quad (3)$$

where d is the average diameter of zeolite particles [m].

The mass source term Q_{br} is defined as the mass deposit rate of nitrogen and oxygen inside the adsorbent to simulate the adsorption process [3].

$$Q_{br} = -\sum_{i=1}^{2} k_i M_i (c_i - c_{pi}) \quad (4)$$

where k_i is the macropore mass transfer rate of nitrogen and oxygen into zeolite particles [1/s], M_i is the molecular weight of N_2 and O_2 [kg/mol], c_i and c_{pi} are the column gas concentration and particle concentration of nitrogen and oxygen, respectively [mol/m^3] [4].

$$k_i = \frac{60 D_{i,j}^e}{K \cdot d^2} \quad (5)$$

where $D_{i,j}^e$ are the molecular diffusivity of N_2 and O_2 into the zeolite pore area [m^2/s], K is the dimensionless Henry's law constant for N_2 and O_2 [5].

The molecular gas diffusivity was defined by the Chapman-Enskog Equation [6,7]. The parameters used in the Chapman-Enskog equation are shown in Table 4.2.

$$D_{i,j}^e = \frac{5.953 \times 10^{-24}}{p \sigma_{ij}^2 \Omega_D} \sqrt{\frac{T^3}{M_i} + \frac{T^3}{M_j}} \quad (6)$$

where σ_{ij} is the average collision diameter of components i and j [m], Ω_D is the collision integral [−], M_i is the molecular mass of component i [kg/mol] and M_j is the molecular mass of component j [kg/mol].

$$\sigma_{ij} = \frac{\sigma_i + \sigma_j}{2} \quad (7)$$

where σ_i is the collision diameter of component i [m] and σ_j is the collision diameter of components j [m].

$$\Omega_D = \frac{1.060}{T_N^{0.156}} + \frac{0.193}{e^{0.476T_N}} + \frac{1.036}{e^{1.530T_N}} + \frac{1.765}{e^{3.894T_N}} \quad (8)$$

Where T_N is the standardized temperature[-].

$$T_N = \frac{T}{\sqrt{\frac{\varepsilon_i}{k_{b,i}}}\sqrt{\frac{\varepsilon_i}{k_{b,i}}}} \quad (9)$$

where ε_i is the characteristic energy of component *i* [J], ε_j is the characteristic energy of component *j* [J], $k_{b,i}$ is the Boltzman's constant of component *i* [J/K] and $k_{b,j}$ is the Boltzman's constant of component *j* [J/K].

The pressure drop is given by Ergun equation [8].

$$\frac{\partial p}{\partial z} = \frac{150\mu}{d_p^2}\frac{(1-\varepsilon_c)^2}{\varepsilon_c^2}\mathbf{u} + \frac{1.75\rho}{d_p}\frac{(1-\varepsilon_c)}{\varepsilon^3}\mathbf{u}|\mathbf{u}| \quad (10)$$

where z represents the coordinate axis of the gas flow [m].

Input flow rate F is a function of pressure fitted with experimental data

$$F(p) = 2.478 - 0.7251p \quad (11)$$

where F is the flow rate of inlet gas [L/min].

4.2.2 Gas component transportation solution in the Transport of Diluted Species in Porous Media Interface of COMSOL Multiphysics

The Transport of Diluted Species interface provides an equation-based simulation environment of chemical species transport by convection, diffusion and adsorption equations. The velocity field are derived from the results of Free and Porous Media Flow Interface while the diffusion is governed by Fick's law. The inflow is a mixture of nitrogen and oxygen while the outflow is coupled with the boundary velocity which means there is negligible outflow until the outlet opens.

The gas distribution is solved in the Transport of Diluted Species in Porous Media Interface of COMSOL Multiphysics with convection and dispersion equations [1].

$$\frac{\partial c_i}{\partial t} - \nabla(D_D \cdot \nabla c_i) + \nabla(\mathbf{u} c_i) = \frac{(1-\varepsilon_c)}{\varepsilon_c}(\varepsilon_p \frac{\partial c_{pi}}{\partial t} + \rho_p \frac{\partial q_i}{\partial t}) \quad (12)$$

The total gas mass deposit rate from column void to zeolite particles are calculated from the combination of particle concentration dispersion rate and microparticle adsorption rate.

$$\varepsilon_p \frac{\partial c_{pi}}{\partial t} + \rho_p \frac{\partial q_i}{\partial t} = k_i (c_i - c_{pi}) \quad (13)$$

$$\frac{\partial q_i}{\partial t} = k_{pi}(q_i^* - q_i) \quad (14)$$

$$q_i^* = q_i^e \frac{(b_i P \omega_i)^{1/n_i}}{1 + \sum_{j=1}^{2} (b_j P \omega_j)^{1/n_j}} \quad (15)$$

$$D_D = 0.7 D_{i,j}^e + 0.5 d_p \mathbf{u} \quad (16)$$

where k_{pi} is the micropore mass transfer rate of nitrogen and oxygen [1/s], ρ_p is the density of zeolite particle [kg/m^3], q_i^* and q_i are the equilibrium and actual adsorbed species to the

zeolite, respectively [mol/kg], ω_i is the volume fraction of N_2 and O_2 [-], q_i^e is the maximum surface excess of gas component onto zeolite pore area [mol/kg], b_i is the adsorption constant of N_2 and O_2 [1/bar], D_D is the axial dispersion coefficient [m^2/s].

$$k_{pi} = \frac{60 D_i^e}{K \cdot d_p^2} \quad (17)$$

$$D_i^e = \frac{\varepsilon_p}{\tau_p} \left(\frac{1}{\frac{1}{D_{k,i}^e} + \frac{1}{D_{i,j}^e}} \right) \quad (18)$$

where D_i^e is the effective intra particle diffusivity of N_2 and O_2 into zeolite pore area [m^2/s], $D_{k,i}^e$ is the effective Knudsen diffusivity of N_2 and O_2 into the zeolite pore area [m^2/s] [9-11], τ_p is the pore tortuosity [2].

The effective Knudsen diffusivity is given by [12]

$$D_{k,i}^e = \frac{d_p}{3} \sqrt{\frac{8RT}{\pi M_i}} \quad (19)$$

where M_i is the molecular mass of nitrogen and oxygen [kg/mol], R is the ideal gas constant [$J.K^{-1}.mol^{-1}$], T is the column temperature [K].

Table 4.1 shows the physical properties of the zeolite, desiccant and adsorption column. The bed voidage and particle voidage are estimated from the voidage variation study and single point BET adsorption total pore volume, respectively. The adsorption constants for zeolite column are fitted with the experimental data based on the single particle adsorption isotherms of LiX zeolite. The PVSA system operates between 1.79 barg for adsorption and -0.82 barg

for desorption under a compressor flow. The time for different steps of the column test is summarized to maintain a stable oxygen flow and achieve a complete regeneration of column in each cycle.

Table 4.1 Characteristics of adsorbent, desiccant and adsorption column [2,13-16]

Adsorbent	**Zeolite LiX**	**Unit**
Average zeolite particle size	600	μm
Average microparticle size	5.75	μm
Zeolite bulk density	790	kg/m^3
Particle voidage, ε_p	0.38	1
Surface excess of N_2, $q^e_{N_2}$	3.42	mol/kg
Surface excess of O_2, $q^e_{O_2}$	6.06	mol/kg
Adsorption constant, b_{N_2}	0.09	1/bar
Adsorption constant, b_{O_2}	0.02	1/bar
Pore tortuosity, τ_P	3	-
BET Surface Area	574.77	m^2/g
Micropore Volume	0.24	cm^3/g
Adsorption Average Pore Diameter	21.26	A
Desiccant Type	Activated Alumina	
Particle density	765	kg/m^3
Average desiccant particle size	600	μm
Adsorption Column		
Length	10	cm
Inside radius	1.5	cm
Column voidage, ε_c	0.36	1

Material	aluminum	-

Table 4.2 shows the characteristics parameters of nitrogen and oxygen for the model equations.

Table 4.2 Characteristics Parameters of Nitrogen and Oxygen [17-19]

Adsorbent	**Zeolite LiX**	**Unit**	**Reference**
Dynamic viscosity of the fluid, μ	1.837×10^{-5}	Pa·s	Smits et al., 2006
Dimensionless Henry's law constant of N_2, K_{N_2}	1.5×10^{-2}	-	Sander, 2015
Dimensionless Henry's law constant of O_2, K_{O_2}	3.2×10^{-2}	-	
Average collision diameter of N_2, σ_{N_2}	3.667	10^{-10} m	
Average collision diameter of O_2, σ_{O_2}	6.056	10^{-10} m	
Characteristic energy of N_2, $\varepsilon_{N_2}/k_{b,N_2}$	99.8	K	Bird et al., 2007
Characteristic energy of O_2, $\varepsilon_{N_2}/k_{b,N_2}$	113	K	
Molecular Weight, M_{N2}	28.013	10^{-3} kg/mol	
Molecular Weight, M_{O2}	31.999	10^{-3} kg/mol	
Gas constant, R	8.314	J/(K·mol)	

4.2.3 Heat transfer in the fluid and solid

The gas and zeolite temperature are solved in the dynamic heat transfer interfaces of COMSOL Multiphysics.

The gas phase heat balance is given by

$$\rho_g \varepsilon_t C_g \frac{\partial T_g}{\partial t} + \varepsilon_p \rho_g C_g \frac{\partial (T_g \boldsymbol{u})}{\partial z} = \varepsilon_p K_g \frac{\partial^2 T_g}{\partial z^2} + \left(1 - \varepsilon_p\right) \frac{6 h_f}{d_p} \left(T_s - T_g\right) - \frac{4 h_w}{d_{in}} \left(T_g - T_w\right) \quad (20)$$

where ε_t is the total column voidage $\varepsilon_t = \varepsilon_c + (1 - \varepsilon_c)\varepsilon_p$, C_g is the gas heat capacity [J/(kg·K)], T_g is the gas temperature [K], T_s is the zeolite temperature [K], K_g is the gas thermal dispersion coefficient [W/(m·K)], h_f is the gas–solid heat transfer coefficient [W/(m^2 ·K)], h_w is the gas-wall convective heat transfer coefficient [W/(m^2 ·K)], d_{in} is the inner diameter of the column [m][20].

The zeolite energy balance is given by

$$\rho_p (1 - \varepsilon_t) C_S \frac{\partial T_s}{\partial t} = (1 - \varepsilon_p) K_s \frac{\partial^2 T_s}{\partial z^2} + \left(1 - \varepsilon_p\right) \frac{6 h_f}{d_p} \left(T_g - T_s\right) + \rho_p (1 - \varepsilon_p) \sum_{i=1}^{2} (\Delta H_i \frac{\partial q_i}{\partial t})$$

(21)

where C_S is the zeolite heat capacity [J/(kg·K)], K_s is the zeolite thermal dispersion coefficient [W/(m·K)], ΔH_i is the heat of adsorption [J/mol].

The column wall energy balance is given by

$$\rho_w C_w \frac{\partial T_w}{\partial t} = K_w \frac{\partial^2 T_w}{\partial z^2} + \frac{4 h_w}{d_{in}} \left(T_g - T_w\right) - \frac{4 h_{out}}{d_{out}} \left(T_w - T_a\right) \quad (22)$$

where ρ_w is the density of column wall [kg/m^3], C_w is the wall heat capacity [J/(kg·K)], T_w is the temperature of wall [K], K_w is the column wall thermal conductivity [W/(m·K)], T_a is the ambient temperature [K], d_{out} is the external diameter [m], h_{out} is the external convective heat transfer coefficient [W/(m^2 ·K)][4].

Table 4.3 shows the physical parameters used to solve the energy balance of the gas/zeolite in the heat transfer interface.

Table 4.3 Physical parameters used for heat transfer simulation

Parameters	**Value**	**Unit**	**Reference**
Heat capacity of gas, C_g	968.46	J/(kg·K)	[4]
Heat capacity of zeolite, C_s	715.9	J/(kg·K)	
Heat capacity of column wall-aluminum, C_{w1}	900	J/(kg·K)	[21]
Heat capacity of column wall-glass, C_{w2}	840	J/(kg·K)	
Effective thermal conductivity of gas, K_g	0.09	W/(m·K)	[4]
Thermal conductivity of zeolite, K_s	0.12	W/(m·K)	[22]
Thermal conductivity of column wall-aluminum, K_{w1}	205	W/(m·K)	[21]
Thermal conductivity of column wall-glass, K_{w2}	0.8	W/(m·K)	
Adsorption heat of N_2, ΔH_{N2}	25451.65	J/mol	[20]
Adsorption heat of O_2, ΔH_{O2}	14661.44	J/mol	
Gas–solid heat transfer coefficient, h_f	15.2	W/(m^2 ·K)	
Internal gas-wall convective heat transfer coefficient, h_w	136	W/(m^2 ·K)	[23]
External gas-wall convective heat transfer Coefficient-aluminum, h_{out1}	30.13	W/(m^2 ·K)	Calculated
External gas-wall convective heat transfer Coefficient-glass, h_{out2}	13.48	W/(m^2 ·K)	

Initial condition of adsorption step:

At t=0, the initial pressure (gauge) = - 0.82 [barg], the inflow is set at p = 1.79 [barg], ω_{N_2} = 0.79, T=293.15 K;

The initial adsorbed nitrogen concentration = 0.3172 [mol/kg], initial adsorbed oxygen concentration = 0.02564 [mol/kg];

Initial condition of desorption step:

At t = 0, the initial pressure = 1.79 [barg], the inflow is set at p (gauge) = -0.82 [barg], ω_{N_2} = 0.79, T=294.98 K;

The initial adsorbed nitrogen concentration = 1.333 [mol/kg], the initial adsorbed oxygen concentration = 0.1329 [mol/kg];

4.2.4 Geometry and meshing

The geometry of the column used for the model simulation was a cylinder with a height of 20 cm and a diameter of 3 cm. The gas source entered at the bottom of the column and enriched oxygen stream exited at the top of the column shown in Figure 4.2(a).

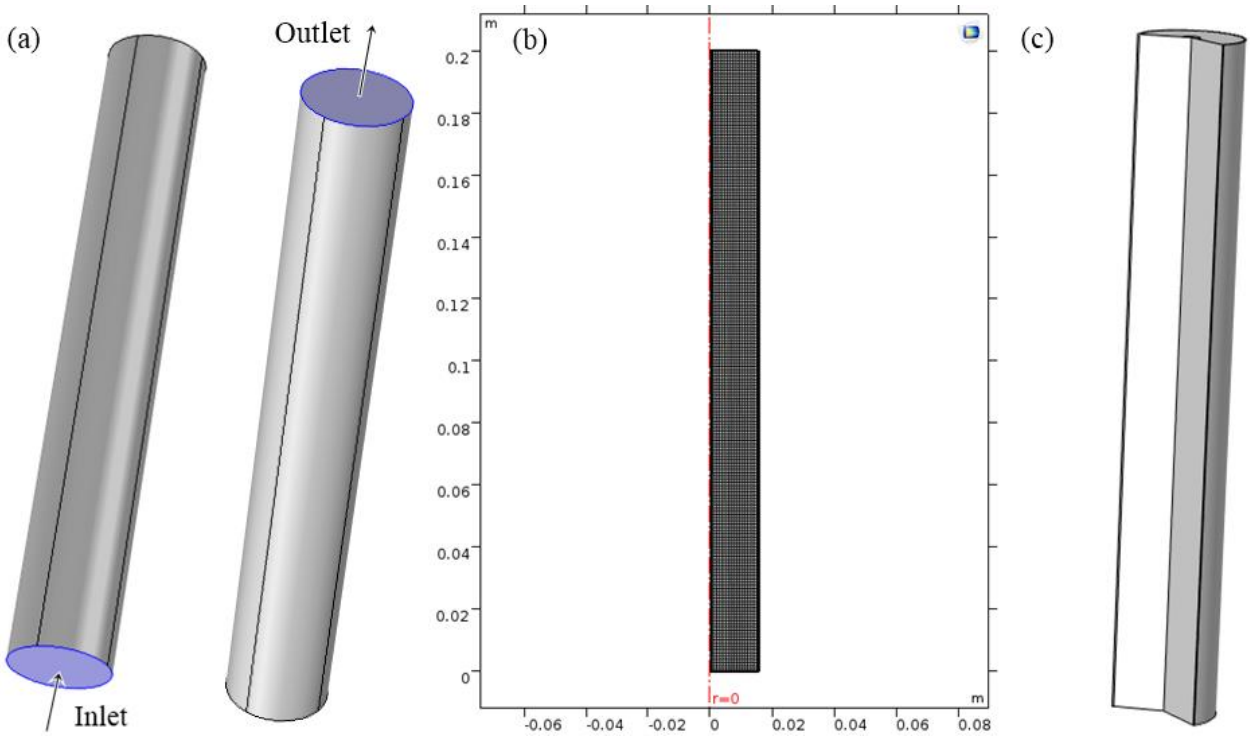

Figure 4.2 (a) Schematics of adsorption column; (b) refined mesh with axis of symmetry; (c) full model geometry

The computational mesh was a swept rectangular mesh. The shape of the rectangular mesh fits both the shape of the axial gas dispersion pattern (plug flow) and the boundary layer condition. In order to find an appropriate mesh size, a mesh refinement study was undertaken with the difference function:

$$\%Difference = \frac{|\omega_{O_2}(mesh_x) - \omega_{O_2}(mesh_{finest})|}{\omega_{O_2}(mesh_{finest})} \times 100\%$$

Where $\omega_{O_2}(mesh_x)$ is the oxygen vol.% of outflow at the mesh size x [mm] and $\omega_{O_2}(mesh_{finest})$ is the oxygen vol.% of outflow at the finest mesh size [mm].

Figure 4.3 shows the results of the mesh refinement study. The relative tolerance was set to 10^{-6} and largest % Difference of all the time points for each mesh size was evaluated. All the

mesh sizes below 1mm were fine enough using the criterion of less than 1% difference. The mesh size = 1mm was selected and used for all the simulations. The refined mesh and geometry are shown in Fig.4.2(b) and (c).

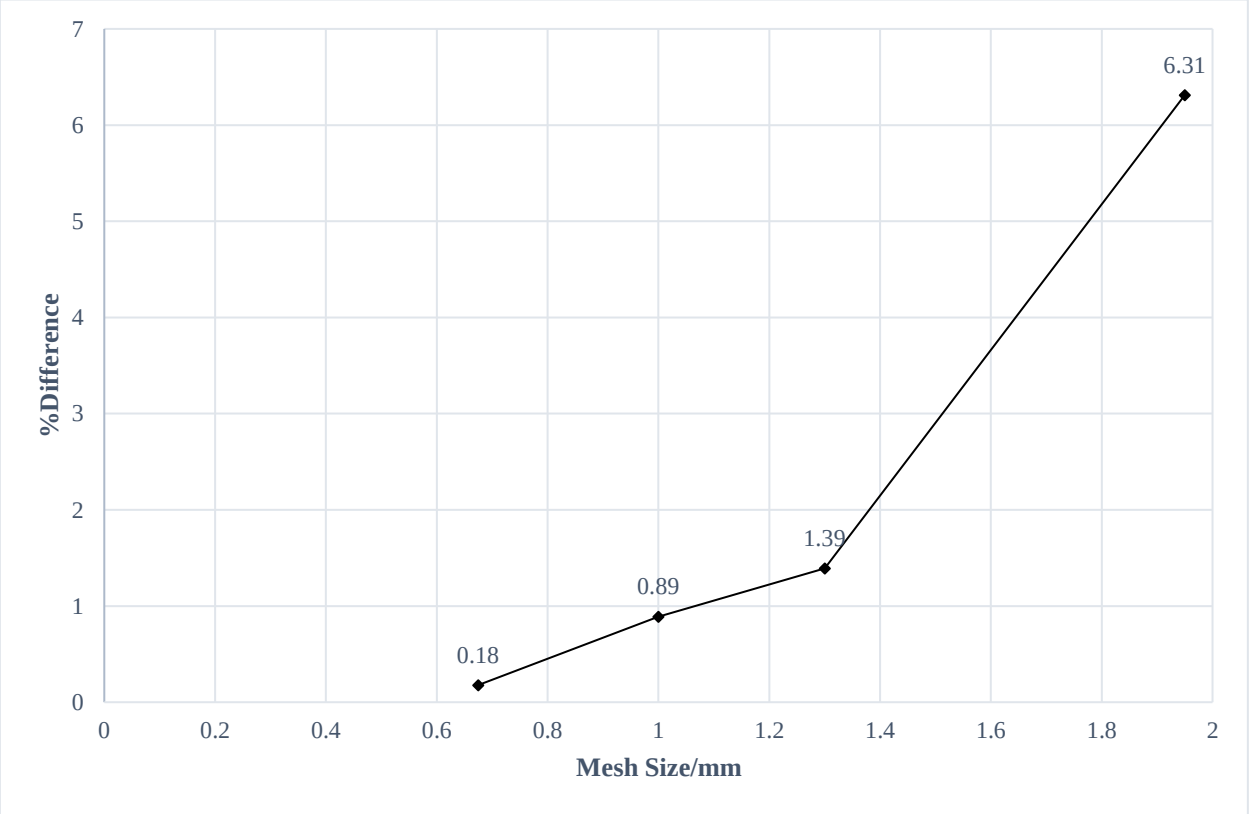

Figure 4.3 Mesh refinement study results

Reference

[1] COMSOL, 2016. COMSOL Documentation. www.comsol.com.

[2] Rao, V. Rama, S. Farooq, and W. B. Krantz. "Design of a two- step pulsed pressure-swing adsorption- based oxygen concentrator." AIChE journal 56.2 (2010): 354-370.

[3] Rao, Vemula Rama, Mayuresh V. Kothare, and Shivaji Sircar. "Numerical simulation of rapid pressurization and depressurization of a zeolite column using nitrogen." Adsorption 20.1 (2014): 53-60.

[4] Hosseinzadeh Hejazi, Sayed Alireza, et al. "Dynamic Column Breakthrough and Process Studies of High-Purity Oxygen Production Using Silver-Exchanged Titanosilicates." Industrial & Engineering Chemistry Research 55.20 (2016): 5993-6005.

[5] Rege, Salil U., and Ralph T. Yang. "Limits for air separation by adsorption with LiX zeolite." Industrial & engineering chemistry research 36.12 (1997): 5358-5365.

[6] Chapman, Sydney, and Thomas George Cowling. The mathematical theory of non-uniform gases: an account of the kinetic theory of viscosity, thermal conduction and diffusion in gases. Cambridge university press, 1970.

[7] Omar, Hecham M., and Sohrab Rohani. "Removal of CO2 from landfill gas with landfill leachate using absorption process." International Journal of Greenhouse Gas Control 58 (2017): 159-168.

[8] Ö. Akgiray and A. M. Saatçı, Water Science and Technology: Water Supply, Vol:1, Issue:2, pp. 65–72, 2001.

[9] Satterfield, Charles N. Mass transfer in heterogeneous catalysis. The MIT Press, 1970.

[10] Kumar, R., and S. Sircar. "Skin resistance for adsorbate mass transfer into extruded adsorbent pellets." Chemical engineering science 41.9 (1986): 2215-2223.

[11] Reid, R. C., J. M. Prausnitz, and T. K. Sherwood. "The Properties of Gases and Liquids ((3rd Edn).) McGraw-Hill." New York (1977): 548.

[12] Cunningham, Roberto E., and R. J. J. Williams. Diffusion in gases and porous media. Vol. 1. New York: Plenum Press, 1980.

[13] Santos, J. C., F. D. Magalhaes, and A. Mendes. "Contamination of zeolites used in oxygen production by PSA: effects of water and carbon dioxide." Industrial & Engineering Chemistry Research 47.16 (2008): 6197-6203.

[14] Santos, J. C., et al. "High-purity oxygen production by pressure swing adsorption." Industrial & engineering chemistry research 46.2 (2007): 591-599.

[15] Activated Alumina. (2011). Micromeritics Instrument Corporation, Norcross, GA 30093, USA.

[16] Farooq, S., D. M. Ruthven, and H. A. Boniface. "Numerical simulation of a pressure swing adsorption oxygen unit." Chemical Engineering Science 44.12 (1989): 2809-2816.

[17] Smits, Alexander J., and Jean-Paul Dussauge. Turbulent shear layers in supersonic flow. Springer Science & Business Media, 2006.

[18] Sander, R. "Compilation of Henry's law constants (version 4.0) for water as solvent." Atmospheric Chemistry & Physics 15.8 (2015).

[19] Bird, R. Byron, Warren E. Stewart, and Edwin N. Lightfoot. Transport phenomena. John Wiley & Sons, 2007.

[20] Zhu, Xianqiang, et al. "Study of a novel rapid vacuum pressure swing adsorption process with intermediate gas pressurization for producing oxygen." Adsorption 23.1 (2017): 175-184.

[21] Lopes, Filipe VS, Carlos A. Grande, and Alírio E. Rodrigues. "Activated carbon for hydrogen purification by pressure swing adsorption: Multicomponent breakthrough curves and PSA performance." Chemical Engineering Science 66.3 (2011): 303-317.

[22] Sears, Zemansky,Young and Freedman, University Physics, 10th Ed., Addison-Wesley, 2000.

[23] Murashov, Vladimir V., and Mary Anne White. "Thermal properties of zeolites: effective thermal conductivity of dehydrated powdered zeolite 4A." Materials Chemistry and Physics 75.1 (2002): 178-180.

Chapter 5

5. Result and discussion of adsorption column oxygen output

The experimental data of flowrate, oxygen concentration and outlet pressure at the column end during the adsorption/desorption cycle tests is presented in this chapter. The simulation outcomes from the model discussed in chapter 4 was also validated with the experimental results. The dynamic model is also used to simulate the inlet gas flow pattern for the inlet gas distributor design and adsorption performance of different evacuation pressure at desorption stage for the selection of pressure swing range. With the optimization of oxygen concentration process, the operational parameters for air compressor and solenoid valves are obtained for the continuous oxygen production.

5.1 Experimental results and model validation

5.1.1 Velocity profile

Figure 5.1 compares the experimental flow rate with the simulation results. The experimental and model output flowrates are 1.226 L/min and 1.24 L/min, respectively. The difference of the experimental data and simulation results is 1.1% which means the modified Free and Porous Media Flow Interface is able to represent the outlet flow condition. Before 21s, the adsorption column is in the pressurization stage without any gas flowing out through the outlet. The flow rate of the outlet is maintained at 1.226 L/min at the production stage which means the same amount of mass flow entering and exiting the adsorption column to maintain the adsorption pressure after t = 21s.

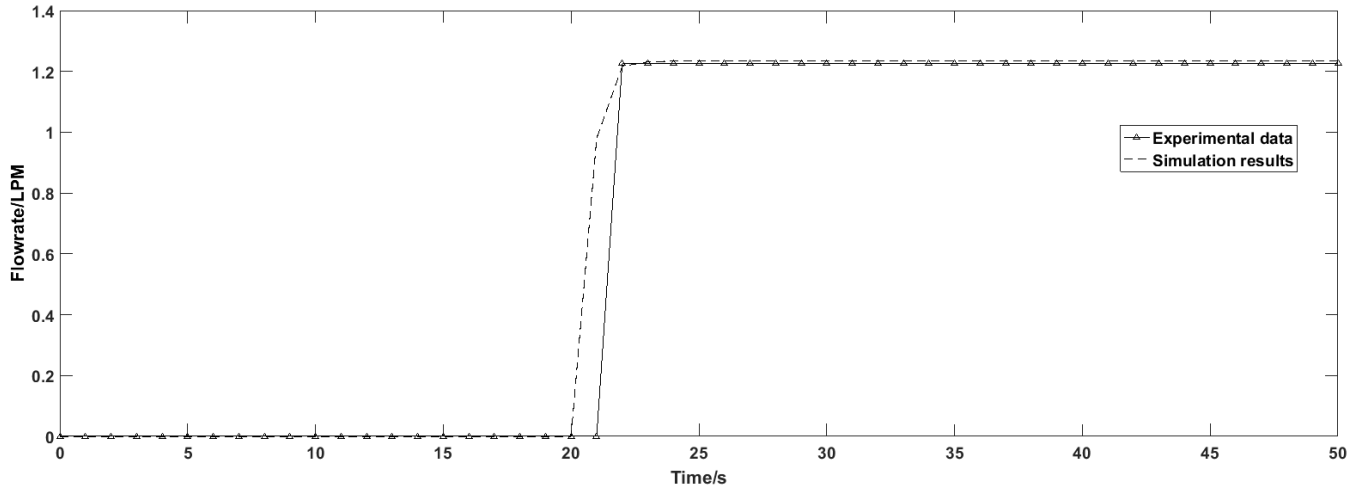

Figure 5.1 Comparison of the experimental and simulation results of the column outlet flow rate

Figure 5.2 shows the internal gas velocity profile at different times during the adsorption step. The 'arrow' surface represents the direction of velocity vector. When the bed is being pressurized, the velocity decreases from the inlet to the outlet due to the closed outlet boundary condition (Figure 5.2(a) and (b)). The velocity distribution at the production stage (Figure 5.2(c)) is uniform which means the column is saturated and concentrated gas is transported out from the outlet of the column at a constant pressure.

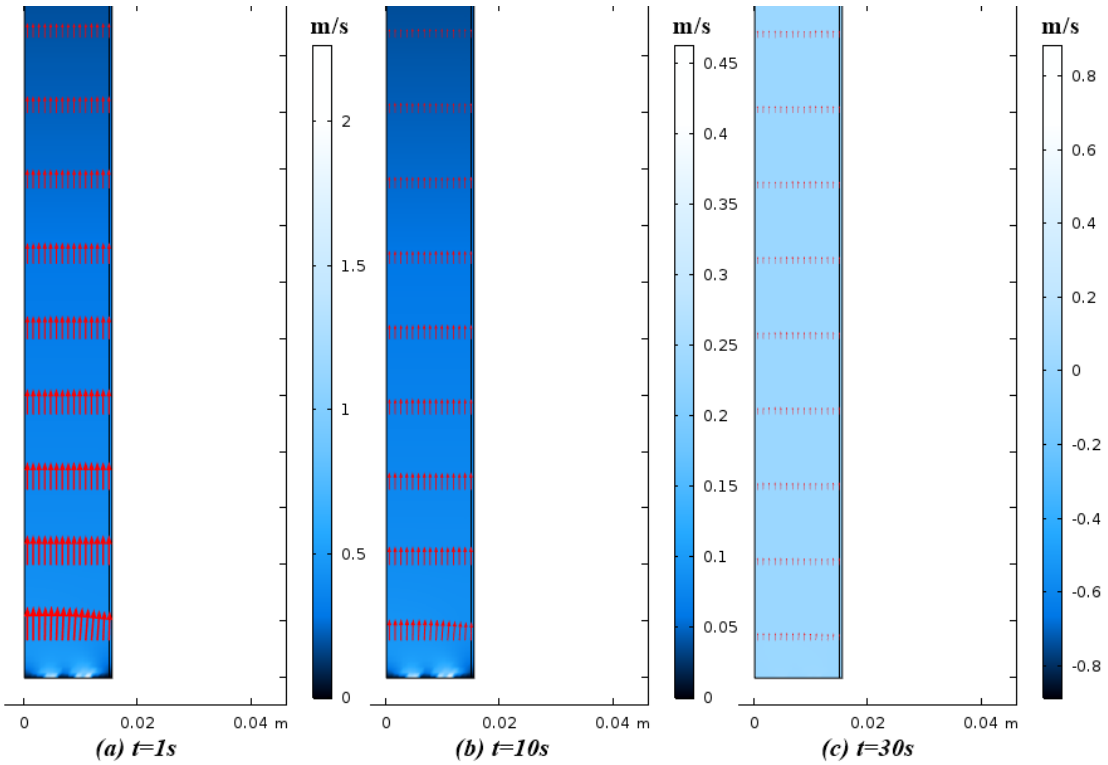

Figure 5.2 Internal velocity profile of simulation at time=1s, 10s and 30s

5.1.2 Pressure profile

Figure 5.3 shows the outlet pressure profile at different times during the adsorption step in the Free and Porous Media Flow Interface. The difference of the simulation results and the experimental data is negligible which is significant to the adsorption function in the Transport of Diluted Species in Porous Media Interface. According to the outlet pressure and flowrate profile in Fig.5.1 and Fig.5.3, the model is able to represent the pressurization step flow condition of a portable oxygen concentrator with an air compressor instead of a constant flowrate simulation.

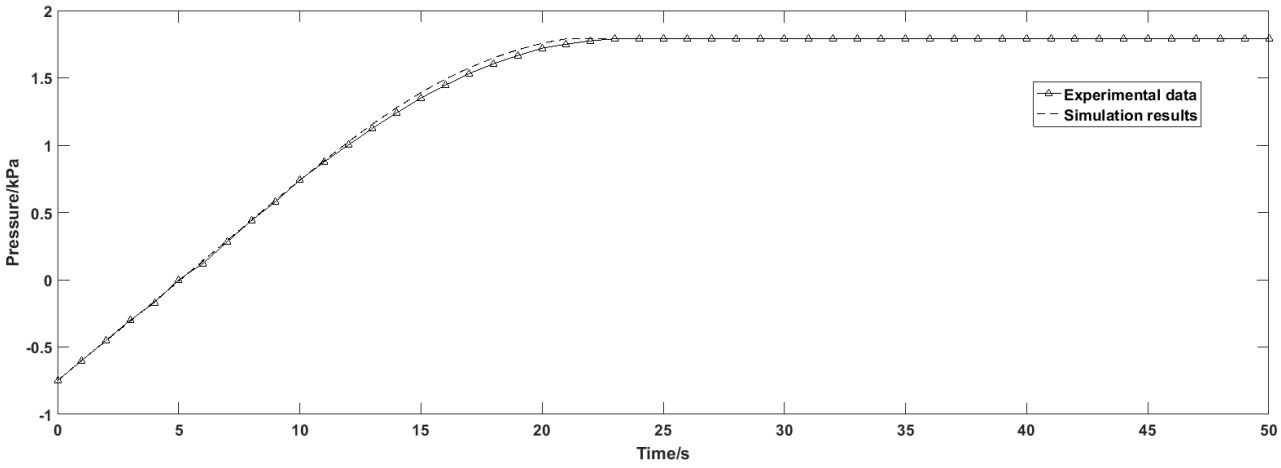

Figure 5.3 Comparison of the experimental and simulation results of the column outlet pressure

5.1.3 Oxygen concentration profile

Figure 5.4 shows the experimental and the simulation results of the outlet oxygen concentration at adsorption pressure =1.79 barg and desorption pressure = -0.82 barg. The enriched oxygen product starts to flow out of the column at t = 21s and the outlet oxygen concentration in the product flow reaches the peak at t = 35s. The experimental data shows the same enriched tendency of oxygen in the outflow as the simulation output. Compared to the simulation results, a slight difference of the oxygen breakthrough curve is observed from the experimental oxygen sensor data. This could be explained by the inaccuracy of the multicomponent Sips adsorption equations due to the complexity of the heterogeneous zeolite porous surface.

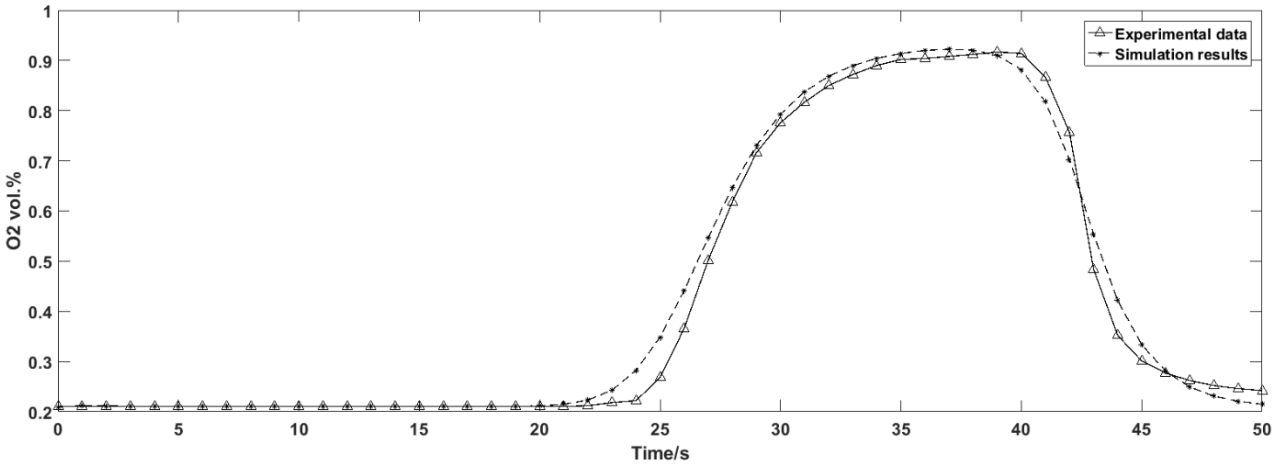

Figure 5.4 Experimental outflow oxygen concentration with simulation results

5.1.4 Adsorbed component (N_2/O_2) profile

Figure 5.5 shows the average surface excess of the zeolite surface at the adsorption and desorption stage. The amount of N_2 and O_2 adsorbed to the zeolite particle gradually decreases when the adsorption column is connected to the suction port of the air compressor to create vacuum desorption condition inside the column. The adsorbed N_2 and O_2 are released from the zeolite at blowdown and purge stages which generates a clean bed for the next adsorption cycle.

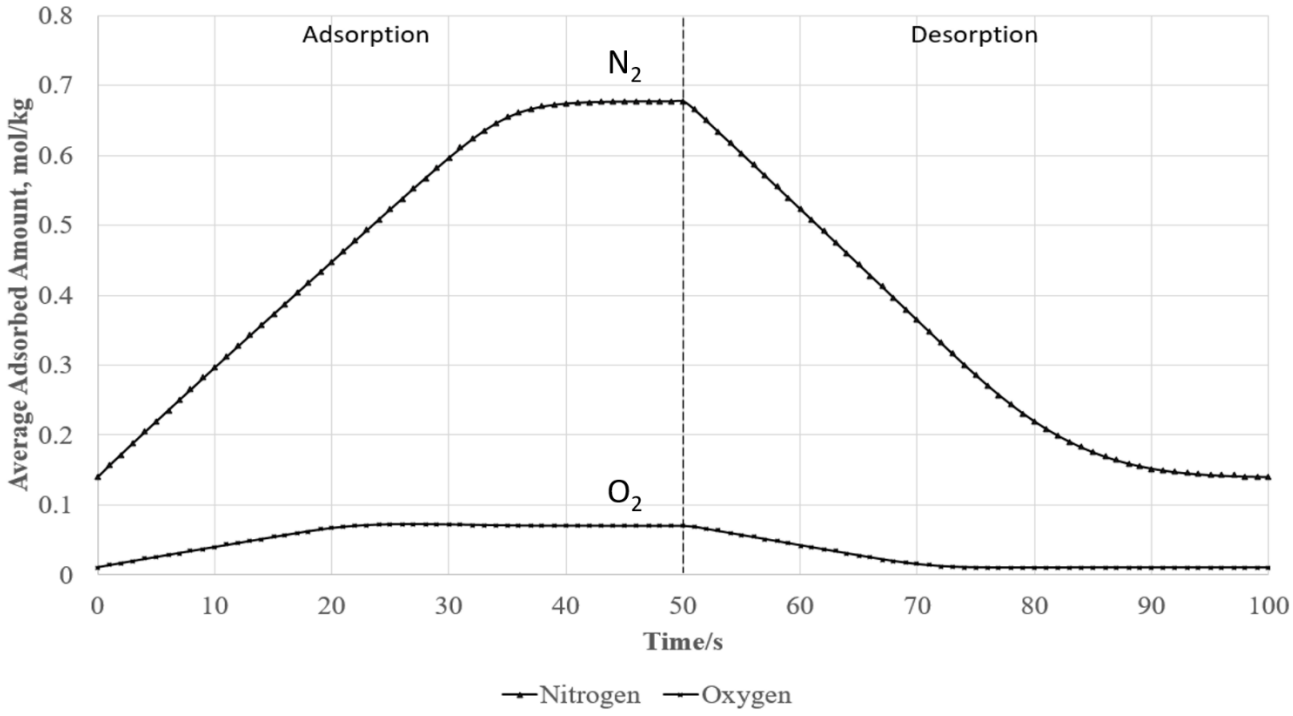

Figure 5.5 Simulation results of average adsorbed nitrogen and oxygen amount to the zeolite particles

Figure 5.6, Figure 5.7 and Figure 5.8 shows the adsorbed N_2 and O_2 concentration profiles at t=1s, 10s and 30s during the adsorption step. The high-pressure flow is introduced from the inlet to pressurize the column at t=1s and adsorbed by the zeolite layers around the column inlet. The mass transfer zone is moving forward from the inlet to outlet of the column at t=10s and 30s which means the adsorption column is getting saturated with time. The mass transfer zone of the oxygen moves faster than that of the nitrogen at t=10s and 30s due to its lower surface excess onto the zeolite microporous area.

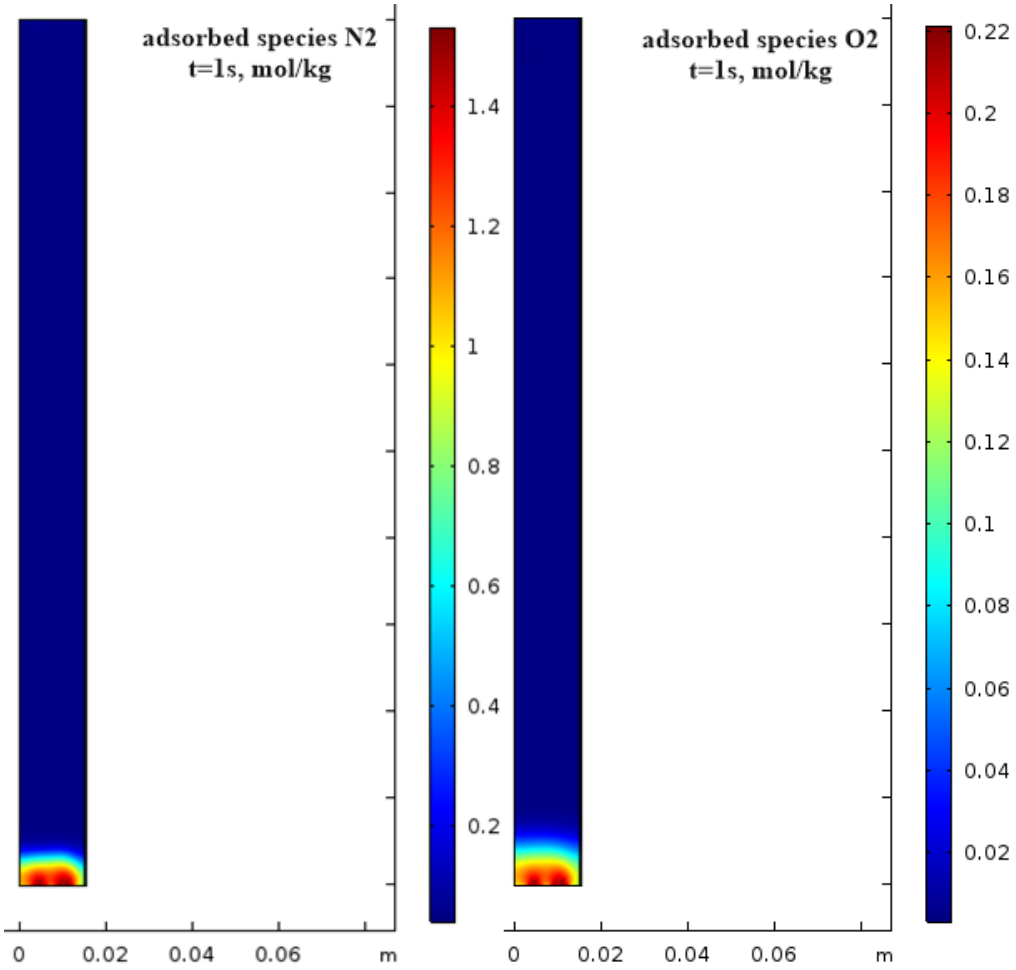

Figure 5.6 Adsorbed N_2 and O_2 concentration profiles at t=1s

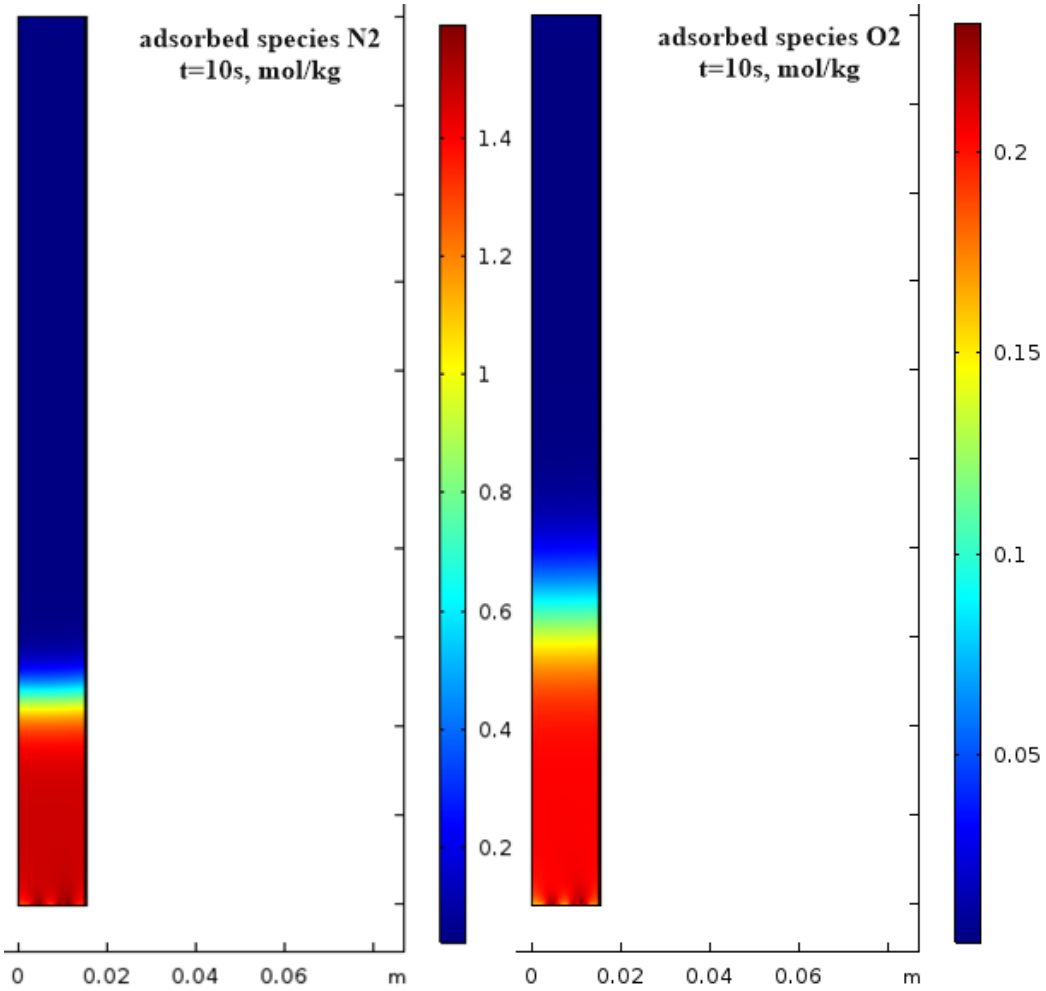

Figure 5.7 Adsorbed N_2 and O_2 concentration profiles at t=10s

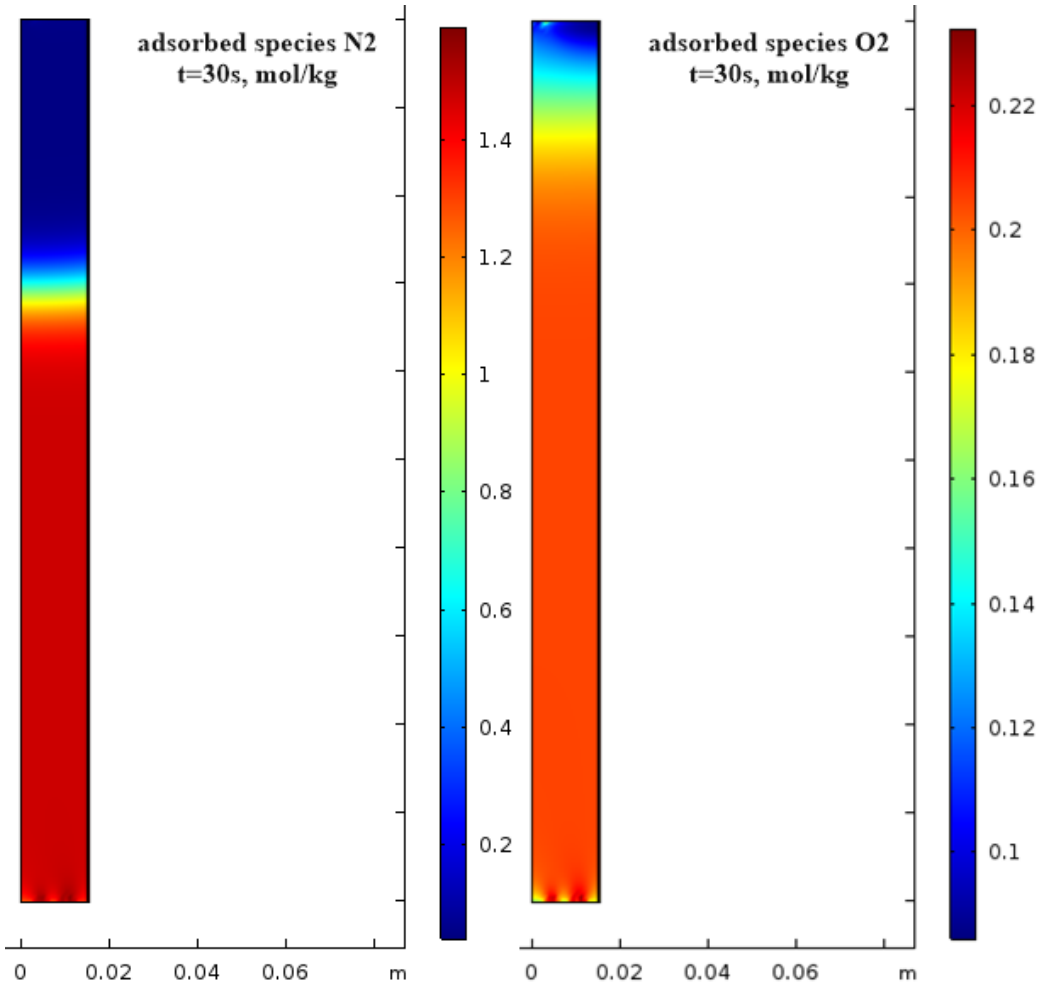

Figure 5.8 Adsorbed N_2 and O_2 concentration profiles at t=30s

5.1.5 Zeolite temperature profile

Figure 5.9 shows the mid column temperature simulation results of the zeolite particles at the adsorption and desorption stage with different column wall materials (glass and aluminum). The aluminum wall provides a higher boundary gas-wall thermal conductivity which benefits the cooling of the zeolite particles during the desorption stage. Considering the isosteric heat during the separation process, a material with relatively high thermal conductivity should be selected for the column manufacturing to maintain the nitrogen capacity of the zeolite during the adsorption step.

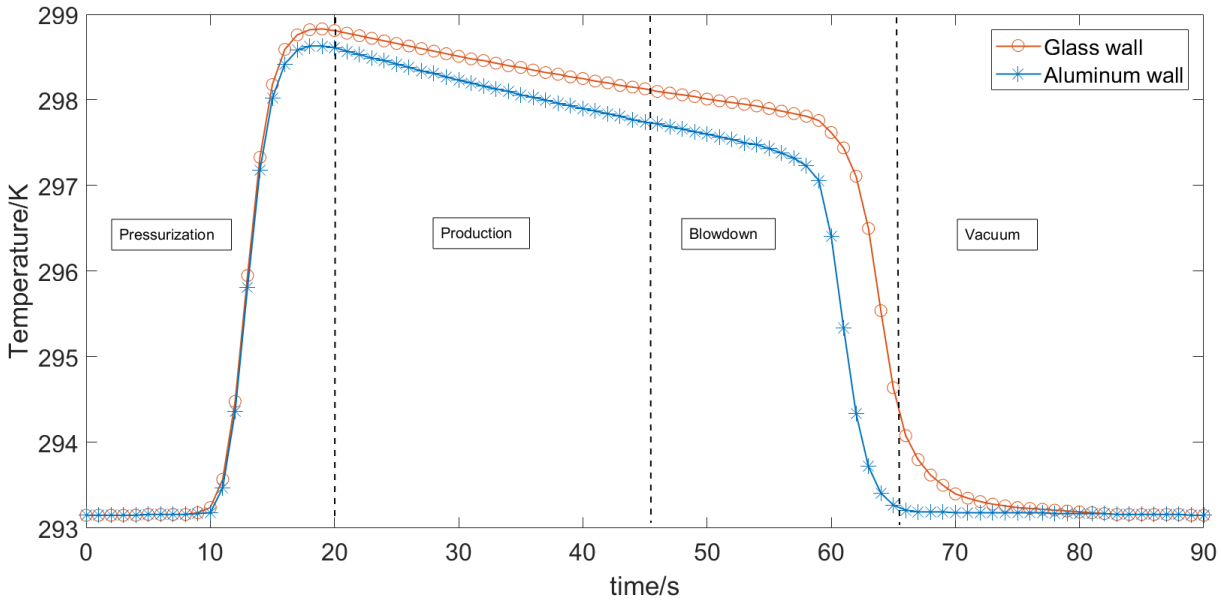

Figure 5.9 Mid-column temperature profile at adsorption and desorption stage with two column wall materials

5.2 Miniaturization and Optimization of PSA oxygen concentration apparatus

5.2.1 Design of Inlet and outlet distribution column using COMSOL CFD module

Two types of inlet flow distribution were investigated for the column adsorption test. Figure 5.10(a) illustrates the common central flow from a tubing to the column inlet without inlet distributor and Figure 5.10(b) illustrates the distributed inflow with an inlet gas distributor. Figure 5.11 shows the N_2 concentration profiles of two different inflow type at different times during the pressurization step. The distribution of the central flow is not uniform with a radial

dispersion from column axis to the boundary while the distributed flow is closed to an ideal plug flow with negligible radial dispersion. Figure 5.12 compares the outflow concentration for distributed inflow and central flow. The results are in accord with the experimental data that pressurization time of the column with central inflow is 1.6s longer than that of the column with the distributed flow. The inlet gas distributor is significant for the inflow air and decreases the pressurization time for the adsorption cycle.

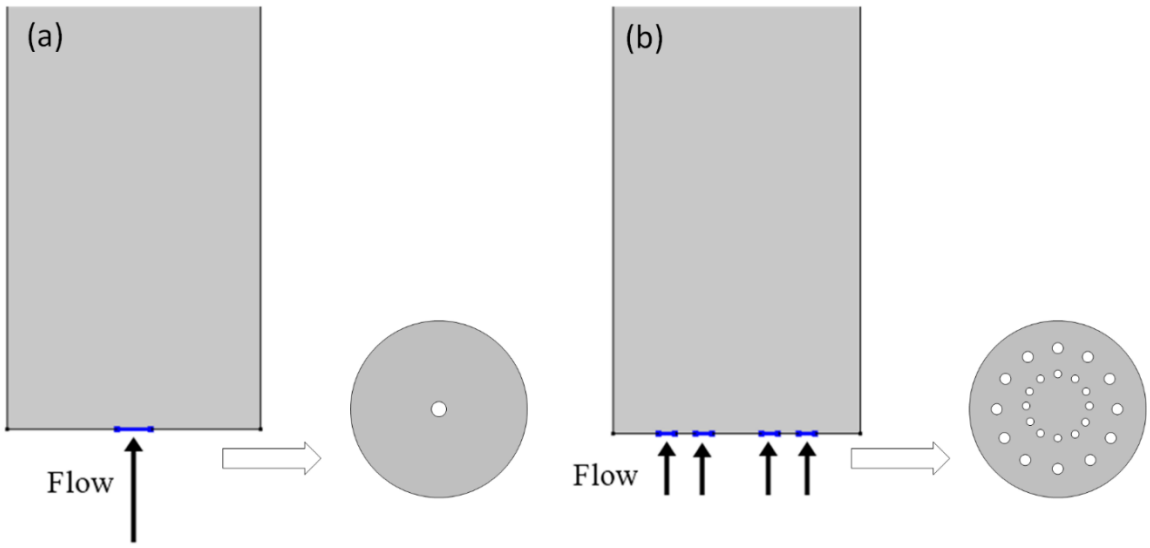

Figure 5.10 Schematics of inflow type at the inlet of the adsorption column (a) central flow without inlet distributor (b) distributed flow with inlet distributor

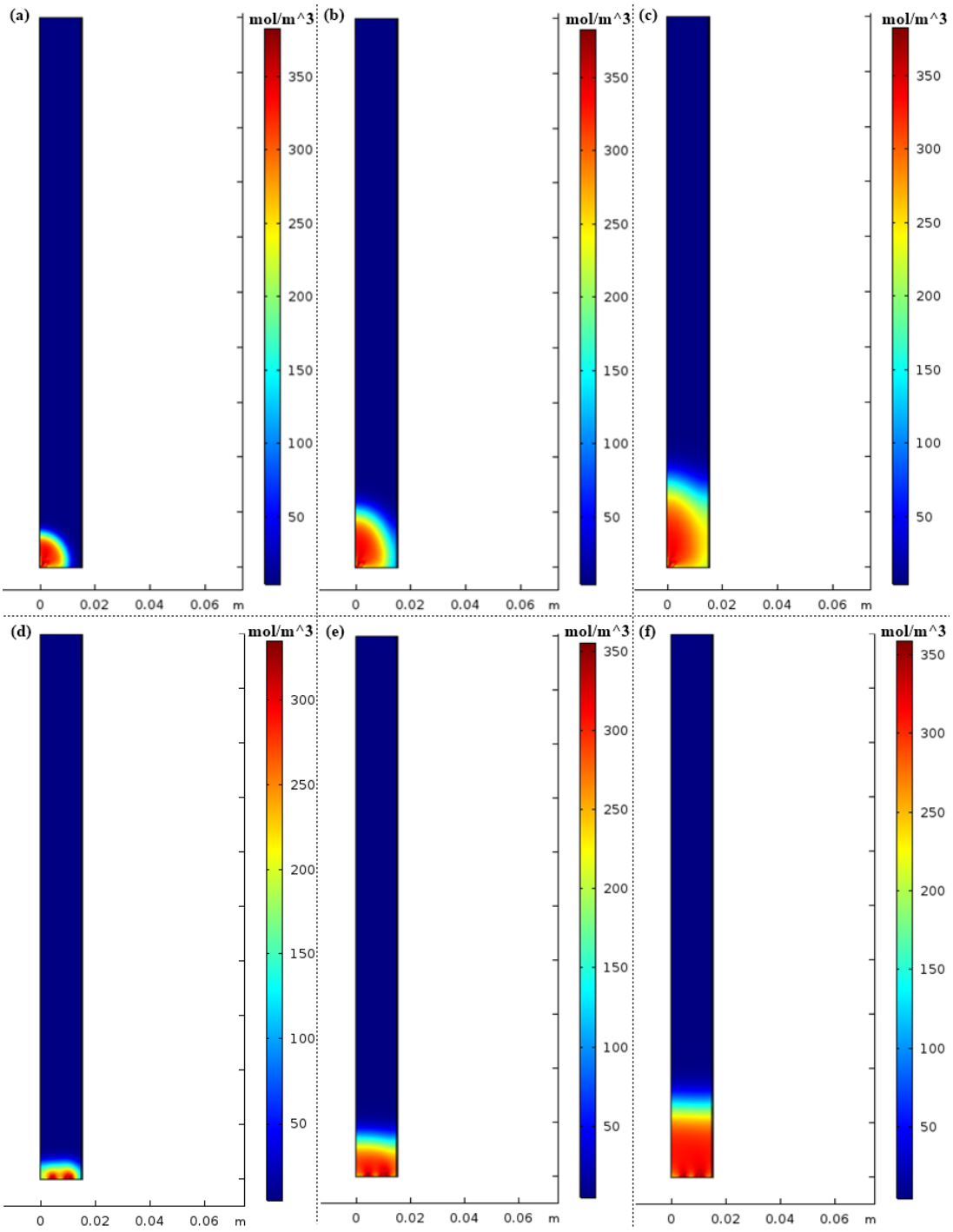

Figure 5.11 (a) N_2 concentration profile without inlet distributor at t=1s; (b) N_2 concentration profile without inlet distributor at t=3s; (c) N_2 concentration profile without inlet distributor at t=6s; (d) N_2 concentration profile with inlet distributor at t=1s; (e) N_2 concentration profile with inlet distributor at t=3s; (f) N_2 concentration profile with inlet distributor at t=6s

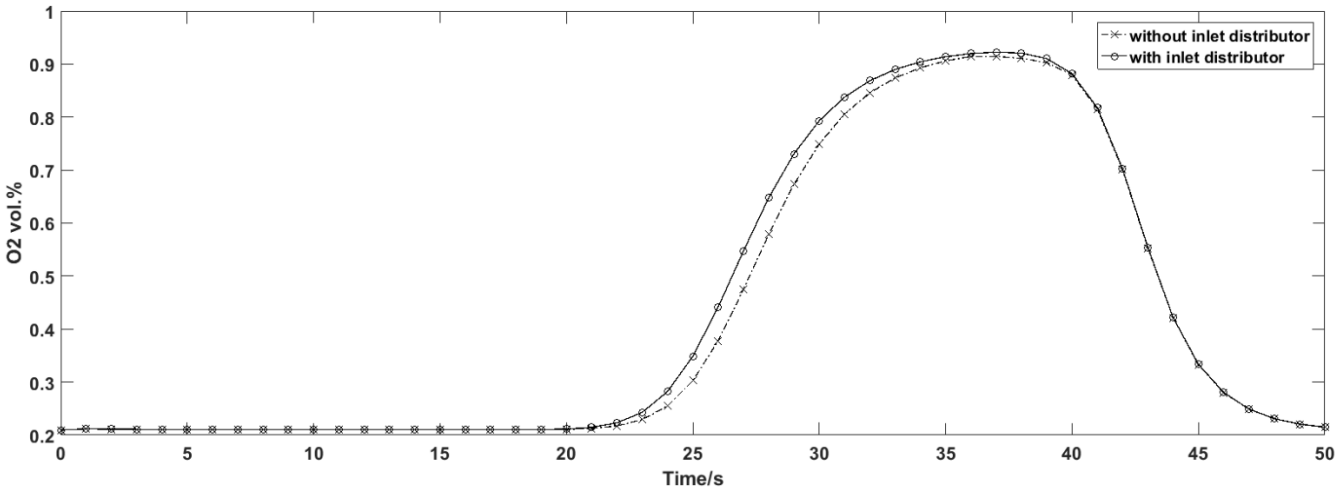

Figure 5.12 Simulation results of outflow oxygen concentration for different inflow type

5.2.2 Pressure swing range test

Figure 5.13 shows the concentration peak of the oxygen output breakthrough curve under different vacuum swing ranges. The nitrogen capacity of the zeolite decreases drastically when the pressure of vacuum port increases from 18 kPa (abs) to 34 kPa (abs). The deep vacuum desorption step is able to increase the productivity of the adsorption column. The simulation results also exhibit a good fitting precision of the experimental data with the maximum difference 0.67%.

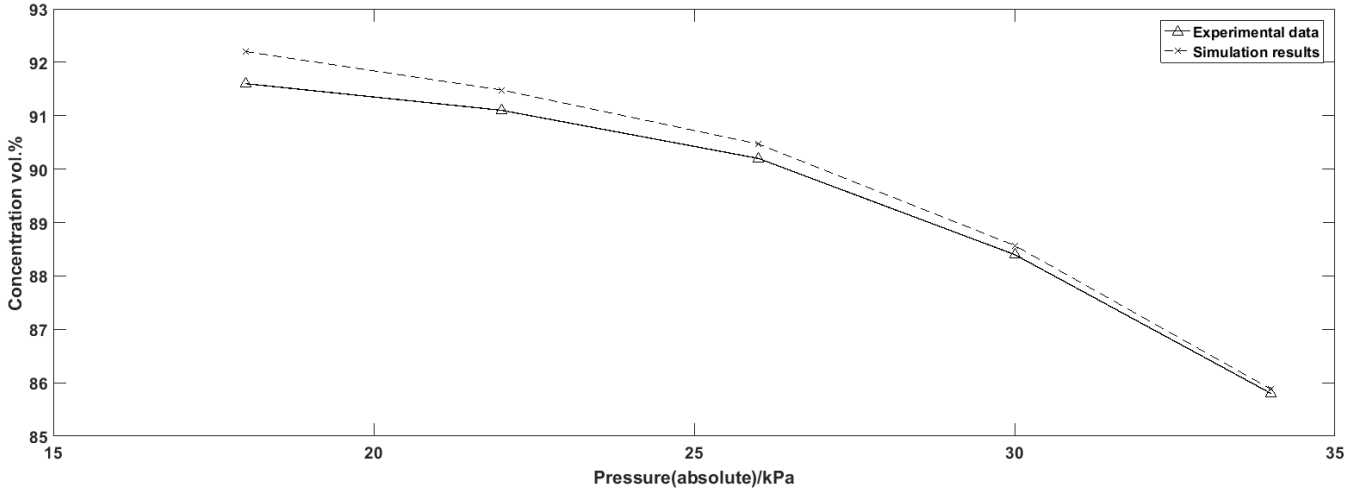

Figure 5.13 Output oxygen concentration peak from different vacuum swing range to 1.79 bar gauge pressure

5.2.3 Flowrate switch strategy

According to the previous column test, the productivity of the adsorption process is limited by the pressurization process without any enriched oxygen flowing out. For the portable oxygen concentrator, the gas flow is generated by the air compressor and could be controlled by the input power. The most mature power control technique for miniature appliance is the pulse width modulation (PWM). The input voltage is controlled by a high frequency square wave switching between on and off shown in Fig.5.14. The on/off pattern could simulate the voltages between full on (5 Volts) and off (0 Volts) by changing the portion of the time the signal spends on versus the time that the signal spends off. The primary goal for the flowrate of the enriched oxygen product is 2 L/min so for the adsorption step the inflow should be set at 2 L/min. However, the pressurization step could be accelerated by increasing the input flowrate. The relation of input flowrate and pressurizing time is illustrated in Fig.5.15. The flowrate at pressurization step is set at 6 L/min which is maximum output of the air

compressor while the flowrate at adsorption step is set at 2 L/min to generate a stable enriched output oxygen product flow.

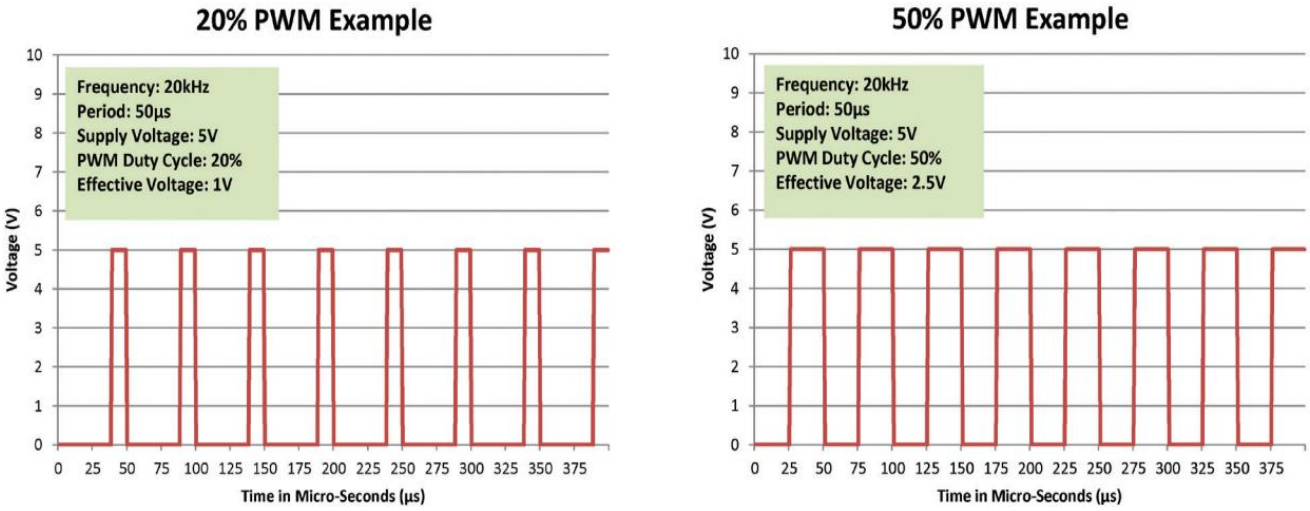

Figure 5.14 Examples of pulse width modulation (PWM) of a voltage control

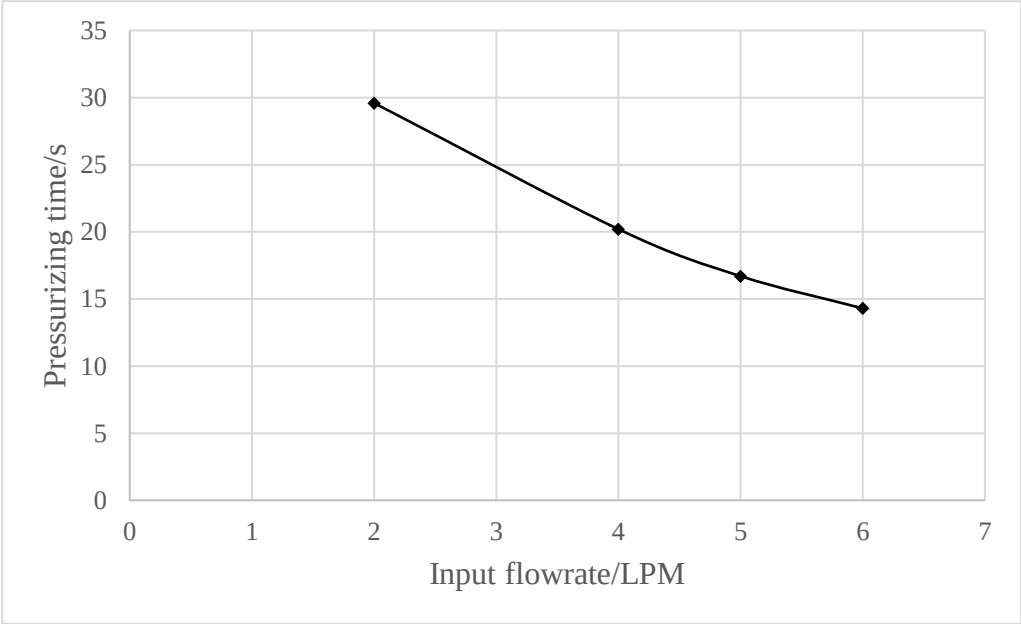

Figure 5.15 *Pressurizing time versus input flowrate*

5.2.4 Desiccant layer design

Based on the previous zeolite characterization, the nitrogen capacity of zeolite decreases gradually with the vapor in the air during the pressure swing adsorption process. Although the zeolite is renewable with the thermal regeneration steps. The lifespan of the zeolite column could be shrinking in a moist environment. In order to protect the zeolite, desiccant layer before the zeolite layer inside column is significant to remove most of the vapor flowing into the zeolite column. The performance of the desiccant (activated alumina) was tested in a column of 3 cm in diameter and 5 cm in length. The desiccant test was performed under the same PVSA cycle with the zeolite swing from -0.82 barg to 1.79 barg. The relative humidity (RH) is measured by the digital temperature/humidity sensor DHT22 with a microcontroller program to collect the data [1]. The microcontroller is named NodeMCU which is an open source programmable hardware. The results of humidity are shown in Fig.5.16. The relative humidity was decreased to 1 RH% from room humidity in the adsorption steps while the adsorbed vapor could be regenerated in the vacuum desorption steps. The performance of the air drying is outstanding with only 1 RH% vapor remained in the gas flow and the results is relatively stable.

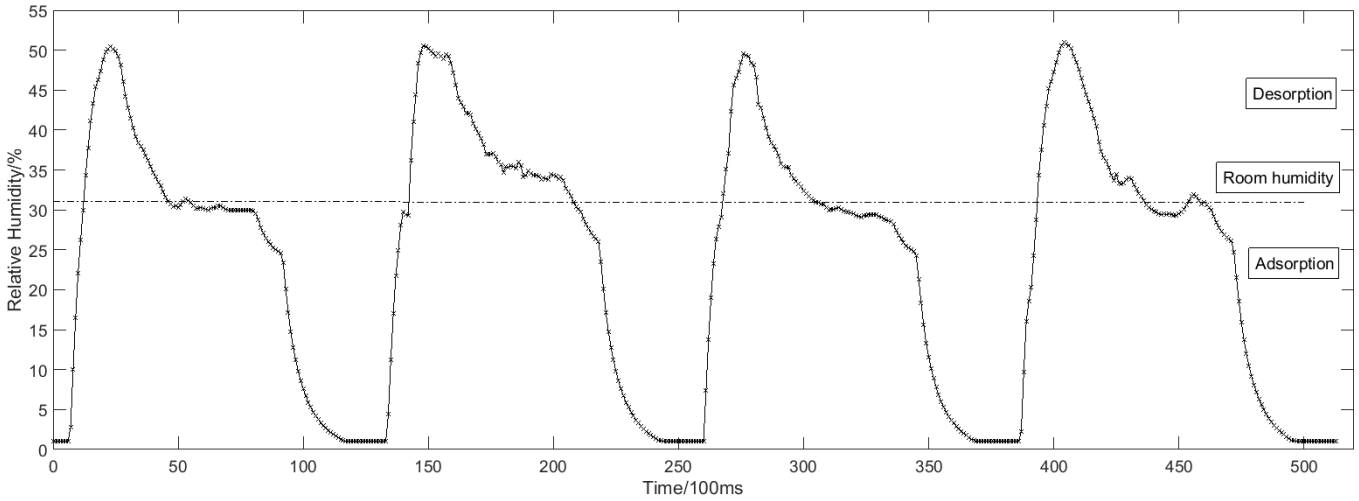

Figure 5.16 Output relative humidity of the desiccant tower under PVSA cycle

Reference

[1] DHT22 digital temperature and humidity sensor. (2016). Sparkfun, Boulder, Colorado

Chapter 6

6. Continuous oxygen production

6.1 Concentrator prototype with two adsorption columns

Figure 6.1 shows the schematic of the oxygen concentrator using a two-column PVSA cycle. The concentrator consists of two adsorption zeolite columns, a dual-head air compressor (Parker Hannifin Corp., TTC IIS Miniature Diaphragm Pump, Hollis, NH), five 3-way solenoid valves (Parker Hannifin Corp., X-Valve, Hollis, NH), a back-pressure regulator, an oxygen sensor (Teledyne GB300 Oxygen analyzer, Thousand Oaks, California), a surge tank, a pressure sensor (Freescale Semiconductor, MPXV7002DPT1CTND, Austin, Texas) and a cooling fan [1-4]. The valve sequence is shown in Table 6.1. The concentrator operation consists of four different steps. In step 1, column 1 is pressurized by the compressor while column 2 is connected to ambient air to decrease the pressure. In step 2, the pressure inside column 1 reaches the working pressure (1.79 barg) with enriched oxygen flowing out through the backpressure regulator (set at 1.79 barg) to the surge tank. Meanwhile the pressure in column 2 decreases to vacuum via the air compressor to regenerate the zeolite. In step 3 and step 4, the adsorption and desorption positions of column 1 and 2 are reversed to regenerate the saturated column 1 and pressurize the regenerated column 2. By switching the valve sequence (step 1→4→1), a continuous enriched oxygen stream can be obtained from the surge tank. The flow directions of the two different types of valves (normally open and distributor 3-way solenoid valves) are shown in Fig.6.2 with two different roles in the pressure swing operations. Valve 1 and 2 are normally open 3-way valves directing the pressurizing flow and countercurrent blowdown flow while valve 3 and 4 are distributor 3-way valves for pressurizing and depressurizing port control at the column end. In order to reduce the compressor size, a dual-head air compressor is considered to perform pressurization and vacuum operation simultaneously. By sharing the central motor, two diaphragms can separately provide pressurized gas and evacuation pressure. Compared to the size and total power consumption of two diaphragm compressors, a dual-compressor is less bulky (25% size reduction) and more efficient (12% input power saving) which benefits the miniaturization of

the prototype. Summarizing the system design, the PVSA process which uses vacuum for desorption and pressurization for adsorption can achieve relatively high capacity allowing more nitrogen adsorption while using a smaller compressor for gas supply.

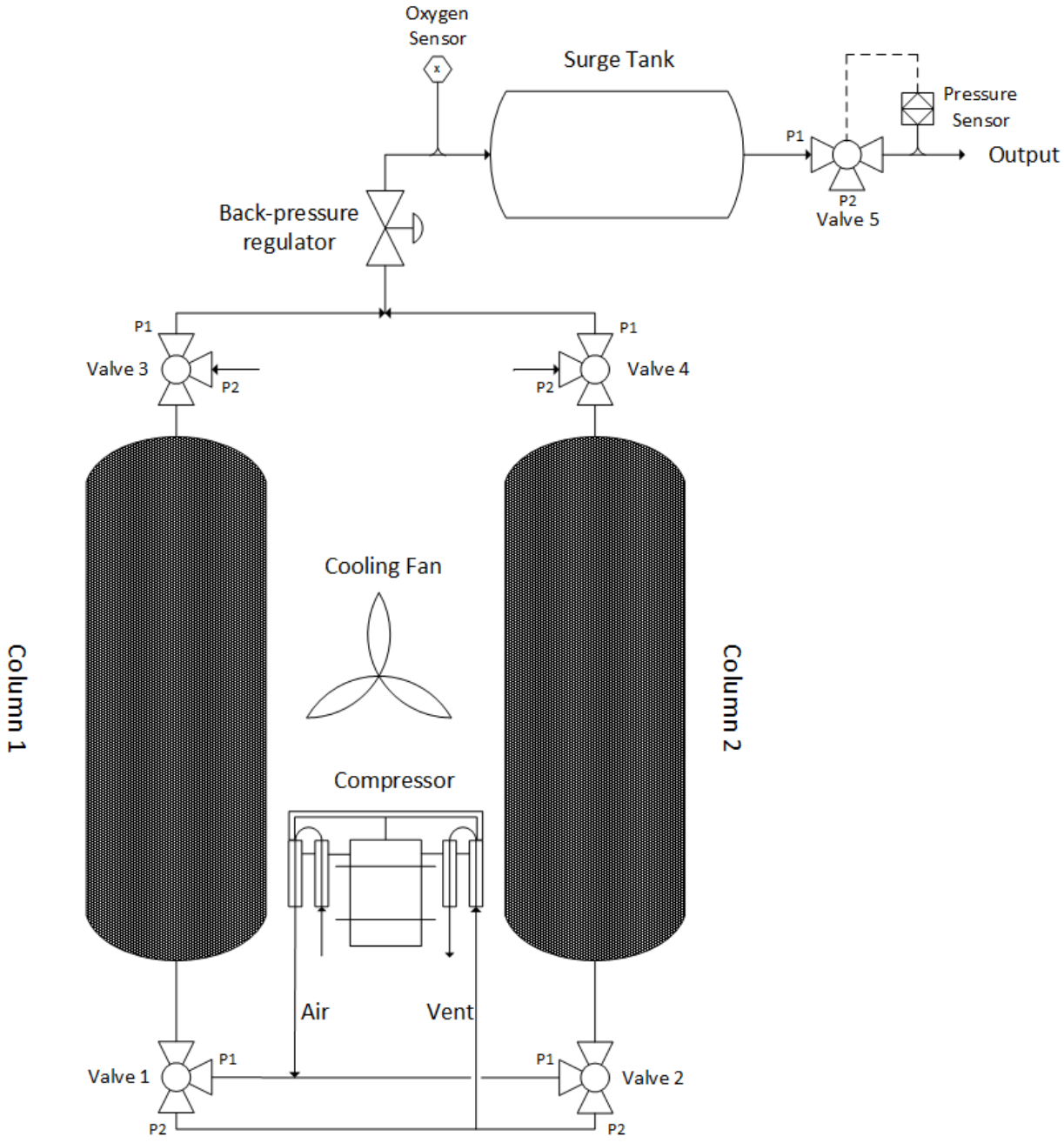

Figure 6.1 Schematics of the PSA oxygen concentrator design

Table 6.1 The valve operation sequence for the PVSA cycle

Step	Stage	Column 1		Stage	Column 2	
		Valve 1	Valve 3		Valve 2	Valve 4
1	**Pressurization**	P1	P1	**Blowdown**	P2	P2
2	**Production**	P1	P1	**Vacuum**	P2	P1
3	**Blowdown**	P2	P2	**Pressurization**	P1	P1
4	**Vacuum**	P2	P1	**Production**	P1	P1

P1, P2 represents valve position 1 and 2.

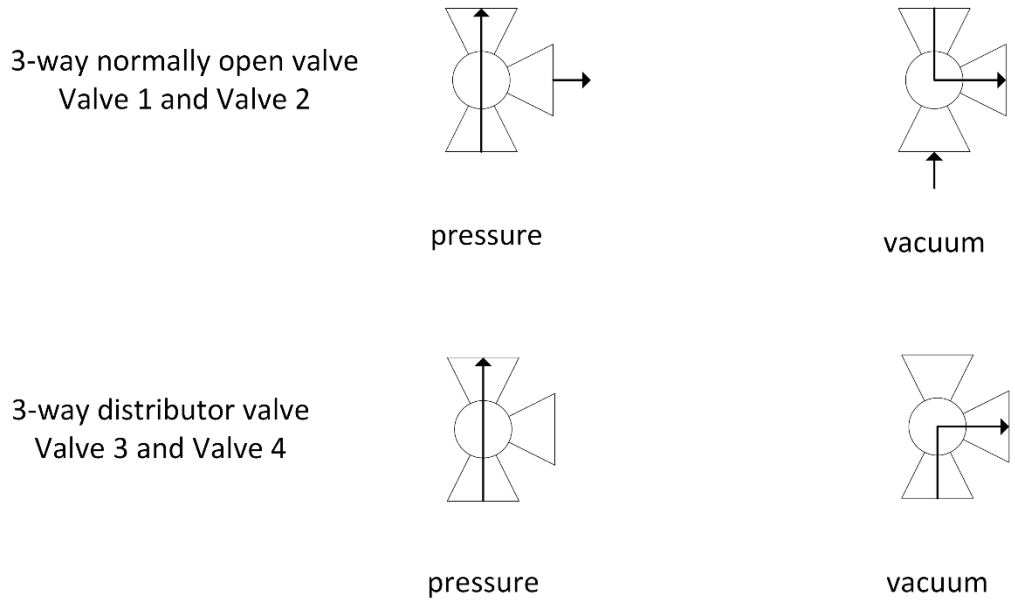

Figure 6.2 Flow directions Schematics of the normally open and distributor 3-way valve under pressure and vacuum conditions

Figure 6.3 illustrates the prototype of the oxygen concentrator with automated hardware system. The details of the solenoid valves, oxygen analyzer, microcontroller and MOSFET amplifier circuit are illustrated in Appendix A with photographs.

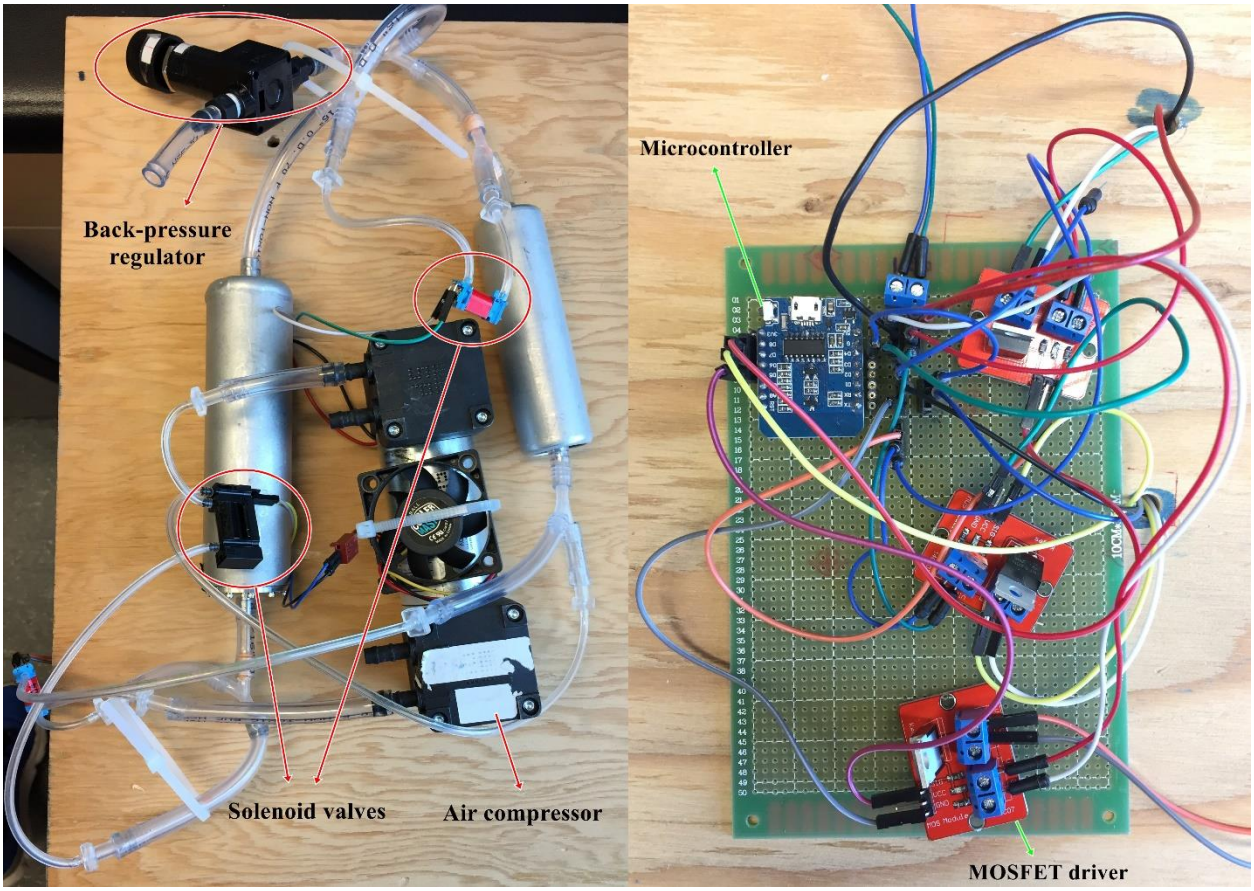

Figure 6.3 Photograph of the PVSA oxygen concentrator prototype

6.2 Microcontroller programming for valve/compressor operations

For the oxygen concentrator prototype, the air compressor and solenoid valves are all controlled by the digital signals from the controller. The first version of the controlling system is established in the visual programming platform—LabVIEW [5]. The merit of the LabVIEW programs for the concentrator design is that the software is able to generate a control panel

for the adjustment of the operational parameters during the performance test shown in Fig.6.4. Unlike the modification of the microcontroller script that requires reprogramming to the chip, the control panel from LabVIEW provides a convenient man-machine interaction platform through the data acquisition (DAQ) system which benefits the process for the parameters optimization. The valve opening, compressor flowrate and the time for each step could be revised directly through the control panel and execute in the next adsorption cycle.

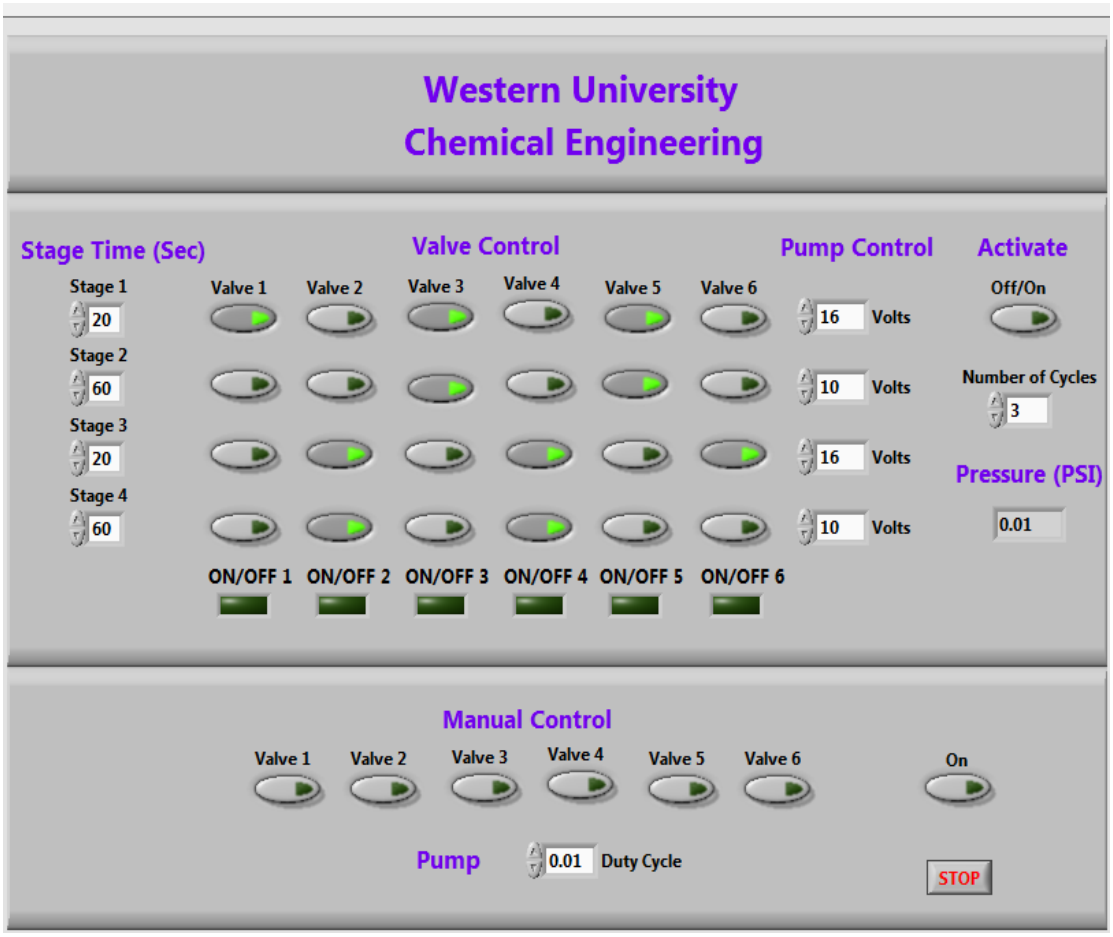

Figure 6.4 Control panel for the concentrator performance test generated by LabVIEW 2014

After the concentrator performance test, the operational parameters for the portable oxygen concentrator is summarized and the LabVIEW program is rewritten from the graphic

programming to the real microcontroller program. The control circuit design for the oxygen concentrator is shown in Fig.6.5 with microcontroller and amplifier circuit. The microcontroller NodeMCU is programmed by a powerful and embeddable scripting language—Lua [6]. The main program is presented in Appendix C.

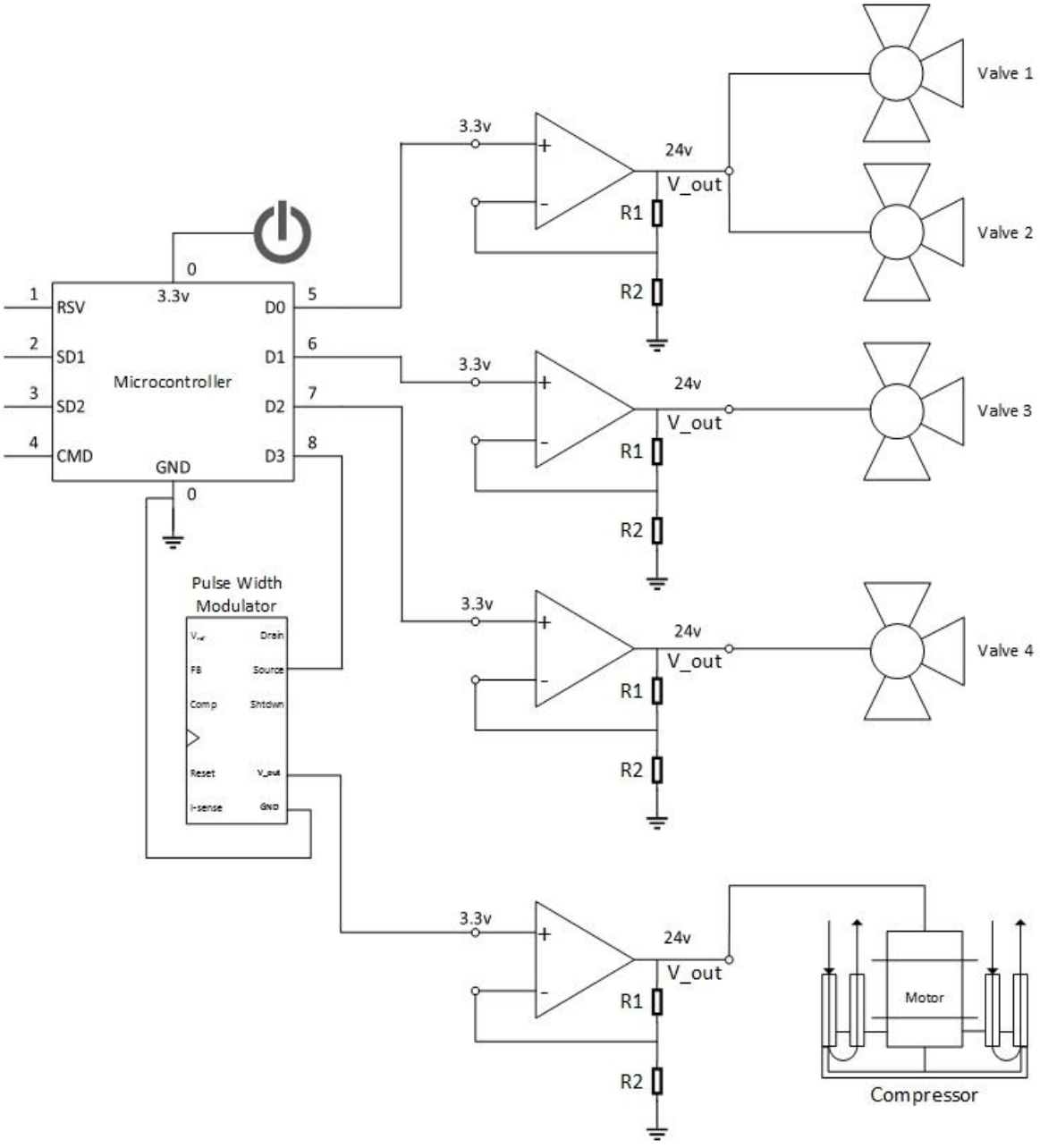

Figure 6.5 Control circuit for the portable oxygen concentrator

6.3 Prototype performance test

The concentrator is tested with a vacuum/pressure swing cycle between -0.82 barg and 1.79 barg. The flowrate of output stream is 1.128 L/min and the average oxygen concentration peak is 72.35 vol.%. The results of the output oxygen concentration are illustrated in Fig.6.6. The output oxygen concentration is almost stable at 1.79 barg which means the desorption under vacuum is effective and desorption time is long enough to regenerate the zeolite. The enriched continuous oxygen stream can be conserved in a storage tank to produce a steady enriched air stream. The adsorption column designed for the prototype is a cylinder of 3cm in diameter and 10 cm in length. Higher concentration could be achieved by increasing the length for a longer mass transfer area. A medical grade oxygen product flow (O_2 concentration > 88 vol.%) was achieved with the column length over 20 cm.

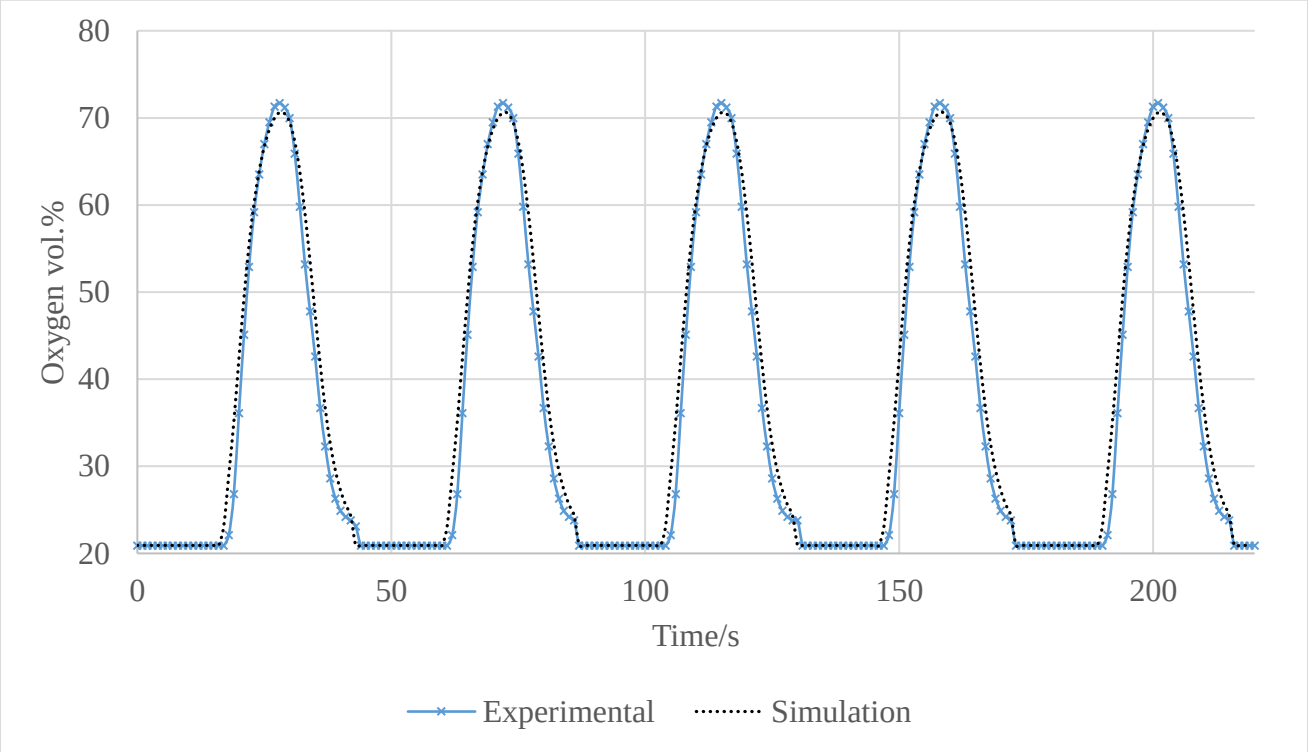

Figure 6.6 Experimental output in a continuous mode with simulation results

6.4 Product conservation and transportation to the patient by flow sensor

The portable oxygen concentrators are usually designed for the patients suffered from obstructive sleep apnea (OSA) and chronic obstructive pulmonary disease (COPD). The most effective therapy for these kinds of patents is continuous positive airway pressure (CPAP) which works by providing a positive air pressure to keep the airways continuously open for a patient who is unable to breathe spontaneously on their own. The therapy is usually performed by a CPAP flow generator with a mask delivering the gas to the patients. The schematics of a conventional CPAP device is illustrated in Fig.6.7.

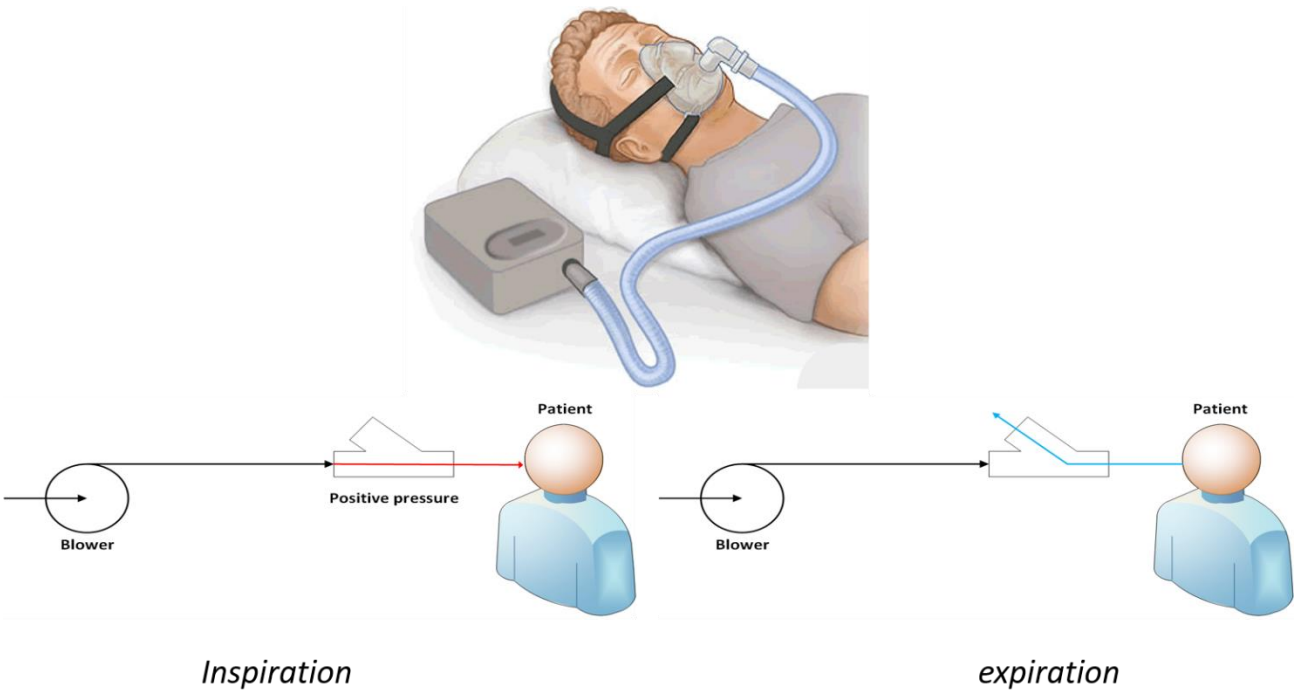

Figure 6.7 Schematics of a CPAP device with its different functions at inspiration and expiration stages

However, the conventional CPAP machines have several drawbacks. The super-atmospheric pressure is generated all the time which means the flow at the expiration is wasted along with the wasted power. In additions, the super-atmospheric pressure at expiration would make it difficult for patients to exhale. In order to shutoff the continuous pressure supply at expiration stage, methods of breath monitoring are required to distinguish the inspiration and expiration stages automatically. Compared to the complicated flow direction detection methods that usually bring additional resistance to the normal respiration flow, a simplified breath monitoring methods are presented in this work using the differential pressure transducer. The schematics of the monitor design is illustrated in Fig.6.8 with the signal recorded from the transducer. The pressure sensor port is connected to the nasal tube and the signal in compared to the other senor port detecting the atmospheric pressure. At inspiration stage, a negative differential pressure is monitored which is recorded as a sign of inhale motion while at inspiration stage, a positive differential pressure is monitored which is recorded as a sign of exhale motion.

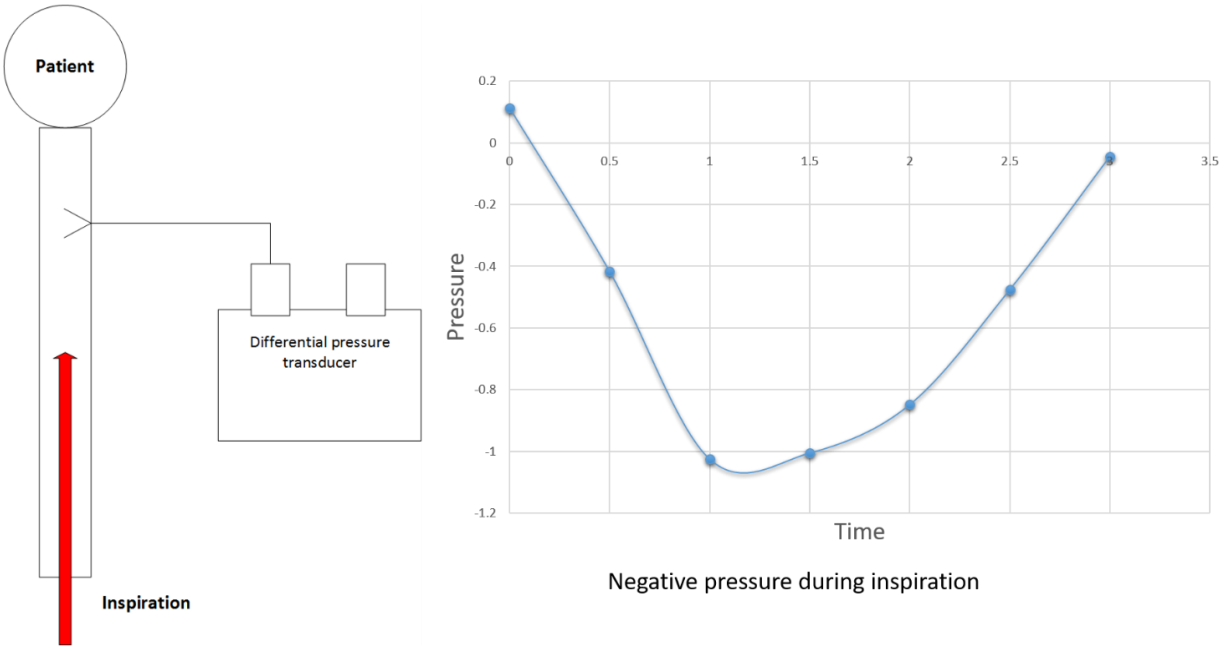

Figure 6.8(a) The schematics of breath monitor design using differential pressure transducer at inspiration stage

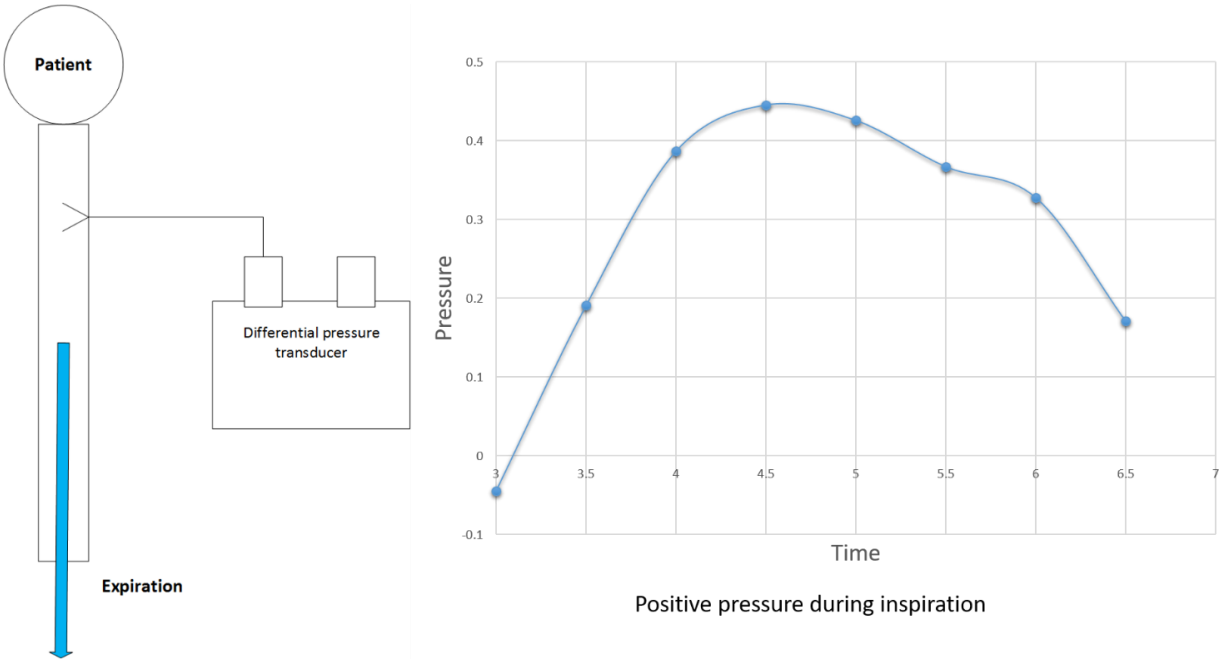

Figure 6.9(b) The schematics of breath monitor design using differential pressure transducer at expiration stage

Based on the results from the breath monitor tests, the goal for the novel CPAP machine design is set as:

(a) Add breath monitoring to the mask function and distinguish the inspiration and expiration stage

(b) Supply positive pressure only at inspiration stage to save the oxygen product gas

(c) Provide additional enriched oxygen flow instead of just additional gas flow to improve the blood oxygen content

The schematics of the novel CPAP machine design are shown in Fig.6.9 with a solenoid valve to control the enriched oxygen flow in the surge tank. The oxygen flow would only be delivered to the patients at inspiration stage. The results of the breath tests in a continuous mode are illustrated in Fig.6.10 after signal calibration. The monitor is able to provide an accurate detection of respiration status.

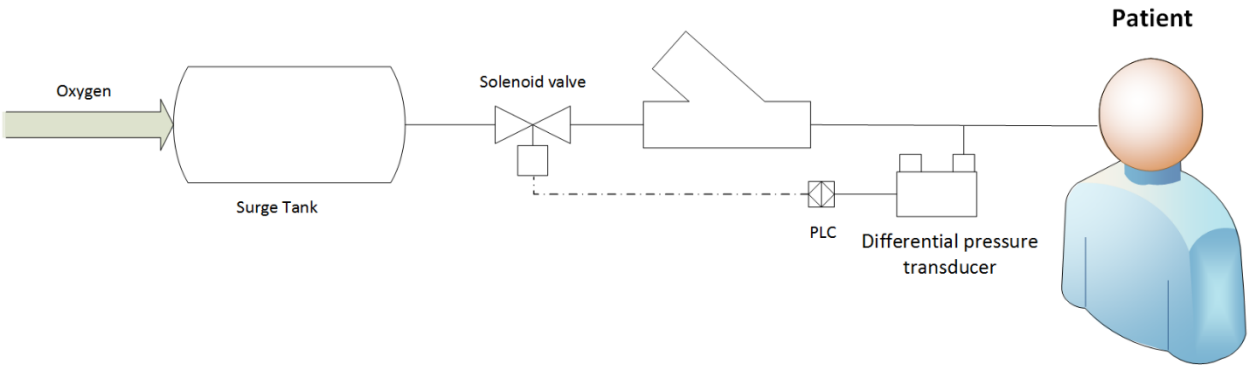

Figure 6.10 Schematics of the novel CPAP machine design

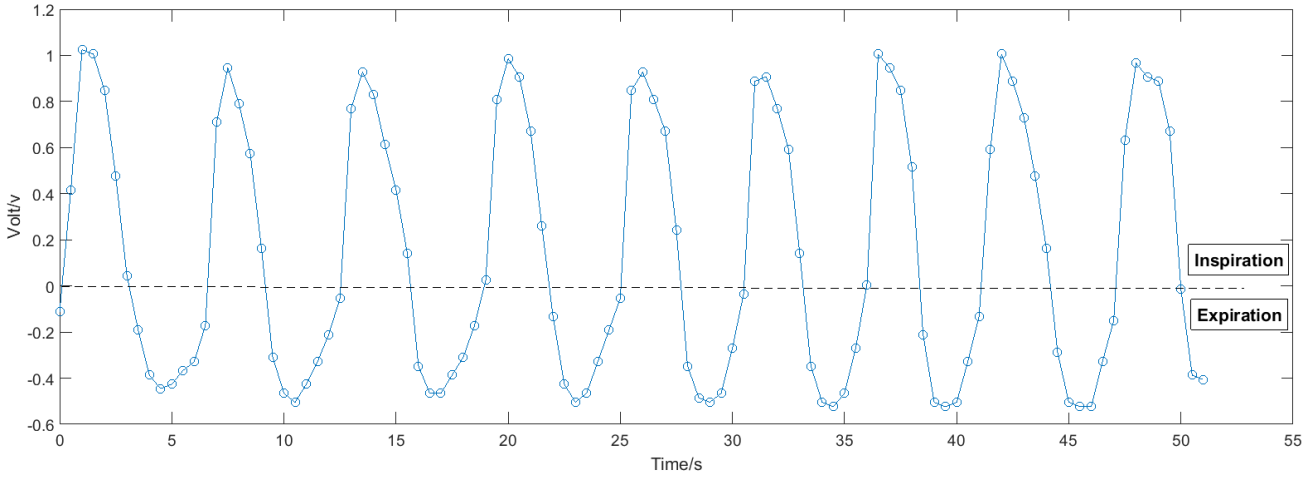

Figure 6.11 Results of breath monitoring in a continuous mode, signal calibrated by volts

For the COPD patients, continuous oxygen supply is important for the relief of chronic bronchitis or emphysema. The algorithm for COPD patients: provide oxygen supply during the inspiration while stop oxygen supply during expiration. The flowchart for treatment COPD patients is shown in Fig.6.11 (V is the signal after calibration).

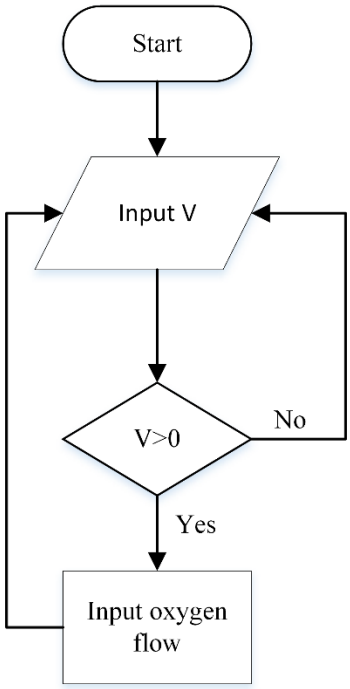

Figure 6.12 Flowchart for treatment COPD patients

Obstructive sleep apnea (OSA) is mainly caused by intermittently relax of the throat muscles. Lower inspiration pressure during snoring could be detected by the breath monitoring apparatus. The algorithm for OSA patients: summarize the maximum inspiration pressure in each breath cycle and compared to the normal inspiration pressure of the patients. If the inspiration pressure is low, execute additional positive pressure therapy in the next breath cycle. The flowchart for the treatment of OSA patients is illustrated in Fig.6.12 (V-limit is the pre-set normal inspiration pressure). Figure 6.13 shows the appearance of snoring from the pressure signals with the additional oxygen flow treatment in the next cycle.

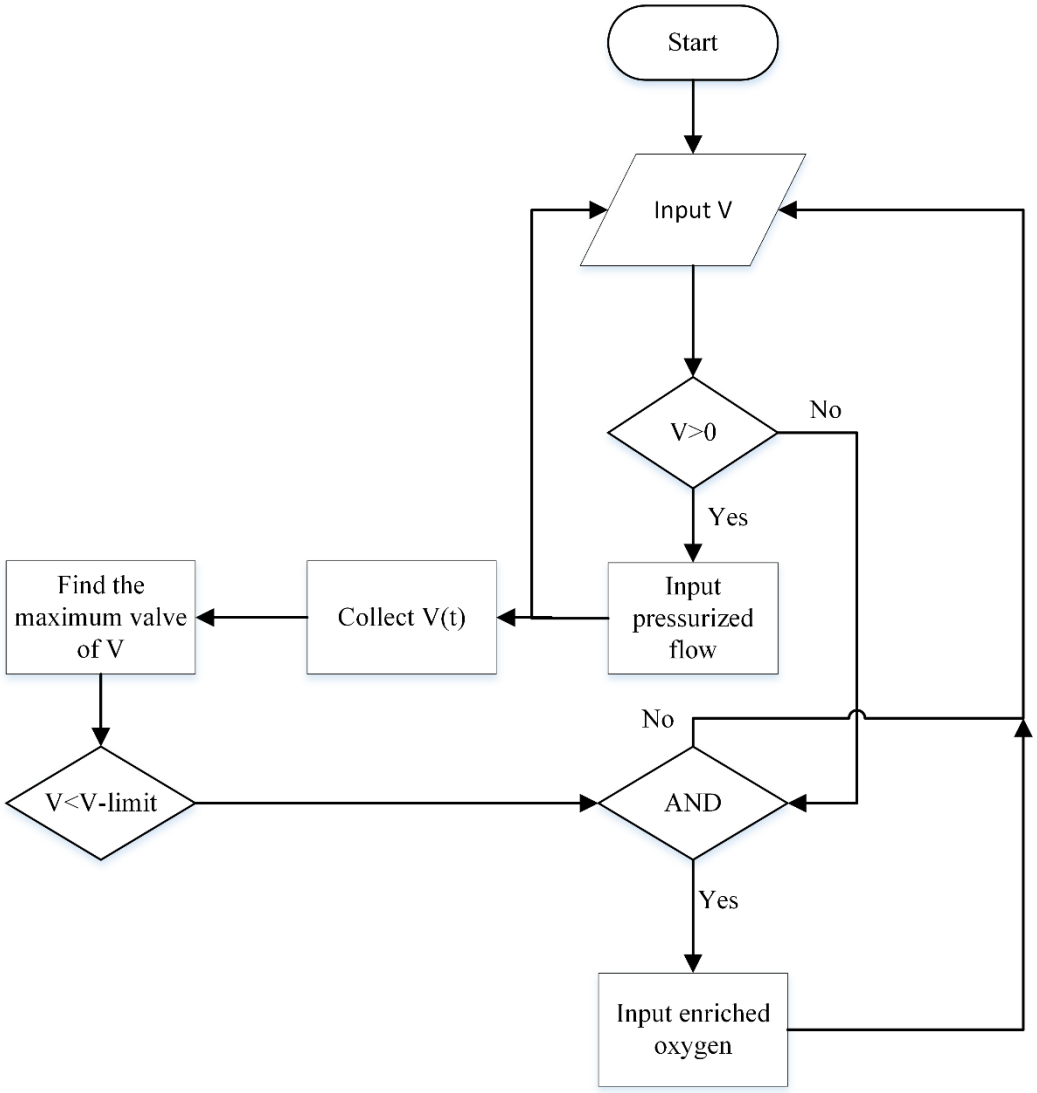

Figure 6.13 Flowchart for the treatment of OSA patients

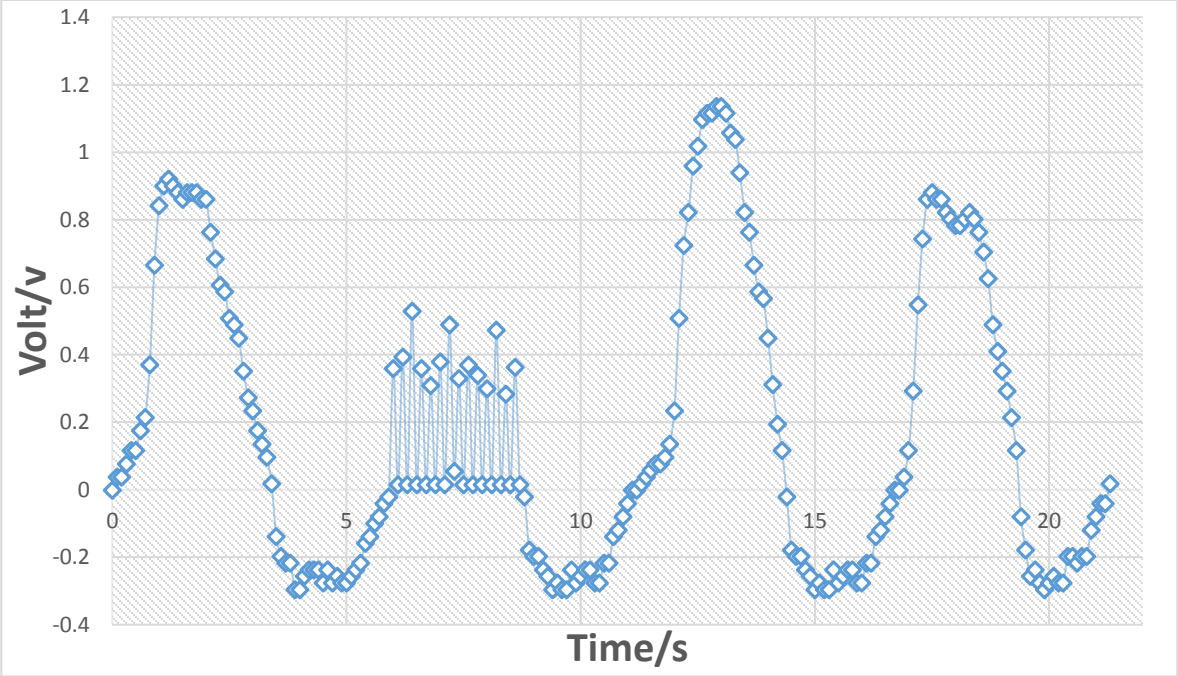

Figure 6.14 Monitor signals showing the appearance of snoring

For the patients with poor autonomous breathing capacity, both inspiration and expiration assistance is required to help with the breath. The basic treatment of this type of patients is: providing positive pressure during inspiration while providing negative pressure during expiration. Additional air compressor is necessary to generate pressure/vacuum condition for the device. The modified CPAP machine with inspiration and expiration assistance is shown in Fig.6.14. The inlet and outlet of the air compressor is used separately to provide pressure and vacuum improve breath flow.

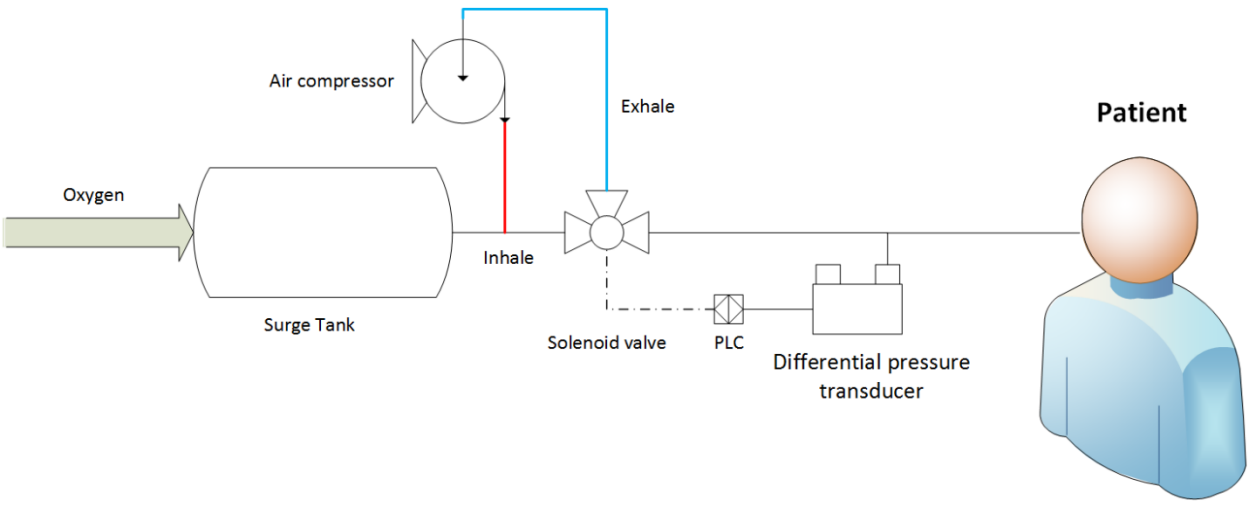

Figure 6.15 CPAP machine design with inspiration and expiration assistance

Reference

[1] TTC-IIS Series Miniature Diaphragm Pumps. (2013). Precision Fluidics Division. Parker Hannifin Corporation, Hollis, NH.

[2] X-Valve. (2015). Precision Fluidics Division. Parker Hannifin Corporation, Hollis, NH.

[3] Model GB300 Percent Portable Oxygen Analyzer. (2011). TELEDYNE ANALYTICAL INSTRUMENTS. A Teledyne Technologies Company, California, USA.

[4] MPXV7002 Series Integrated Silicon Pressure Sensor. (2009). Freescale Semiconductor, Inc.

[5] LabVIEW, 2016. National Instruments documentation. http://www.ni.com/en-us/shop/labview.html

[6] NodeMCU, 2016. NodeMCU Documentation. http://nodemcu.com/index_en.html

Chapter 7

7. Conclusion and future work

7.1 Conclusion

A portable two-column pressure vacuum swing adsorption (PVSA) oxygen concentrator was built in our laboratory and its performance was modeled by solving the continuity equations and the momentum equation in COMSOL Multiphysics. The concentration system uses a Li^+ exchanged 13X zeolite (LiX) as the adsorbent to selectively adsorb nitrogen generating an enriched oxygen product flow. The output concentration of the oxygen is 50 vol.%-70 vol.% at a flowrate of 1.2 L/min in a pulsed cycling production mode. The output concentration level could be adjusted by the column length with the maximum concentration varying from 70 vol.% to 90 vol.% with the column length from 10 cm to 20 cm. The model was able to simulate the microporous adsorption of nitrogen under a dry and CO_2 free compressor flow. The velocity and oxygen concentration profiles were investigated at every time step ($\Delta t = 0.1s$) during the four operation stages: pressurization, production, blowdown and desorption. With the process optimization, it was possible to get better operational parameters and design characteristics to improve the performance of the concentrator units and meet the terminal requirements of oxygen supply. The valves and the compressor of the prototype are controlled by a microcontroller program for continuous oxygen production. The concentrator is a lightweight and miniature unit to carry on and suitable for outside oxygen supplement applications.

Table 7.1 compares the productivity of the lab-made PVSA oxygen concentrator to the previous PSA oxygen concentration process reported in the literatures. The PVSA oxygen concentrator exhibits the lowest BSF (lbs of adsorbent/ tons of oxygen in product one day) which means the highest productivity. The application of large pressure swing range (deep vacuum pressure for desorption) increases the adsorption selectivity of N_2 to O_2 which benefits the nitrogen capacity of the adsorbent in each adsorption cycle. With the novel CPAP

mask design, the PVSA oxygen concentrator could be adjustable to various patients providing a sufficient oxygen supply as a portable appratus.

Table 7.1 Productivity of different PSA process

Process	Adsorbent (zeolite)	Particle size (μm)	PA:PD (atm)	O_2 purity (%)	Total cycle time (s)	Adsorption time (s)	BSF(lbs/ TPDc O_2)
Huang and Chou et al.1995	5A	125	1.85:1	89.2	5.5	1	1588
Santos et al.2006	Oxysiv 5	580	3:01	~95	18	9	528
Santos et al.2006	Oxysiv 7	610	3:01	~95	16	7	455
Santos et al.2007	Ag-Li-X	1010	3.5:1	99.5	17.7	6.6	594
PVSA prototype	LiX	600	15.2:1	92	90	43	369

PA and PD represents the pressure of adsorption and desorption, respectively.

7.2 Future work

Future development could be focused on the additional temperature swing for the adsorption process. By combining pressure swing with temperature swing, the capacity of the adsorbent would increase with a faster regeneration rate due to the heating during the desorption steps. A potential heating/cooling method is the application of semiconductor chiller which is widely used as a cooling device for small appliance. The semiconductor chilling plate is made with thermoelectric materials based on the Peltier–Seebeck effect that temperature gradients could be generated by electricity shown in Fig.7.2. The semiconductor chiller has the advantage of fast response and reasonable power/size ratio compared to the conventional refrigeration cycle. However, it might require customize design for a cylinder cooling jacket because only cooling plate available on the market. Sufficient heat exchange area is required

to design the chiller for the fast cycling adsorption process. The design of adsorption column with semiconductor chilling and heating jacket to conduct pressure and temperature swing adsorption cycle is illustrated in Fig.7.3.

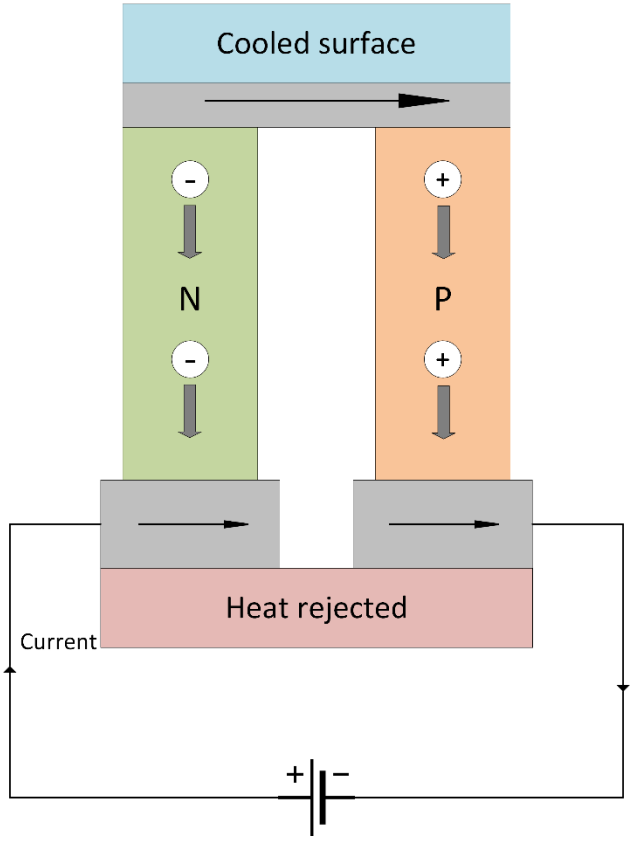

Figure 7.1 Schematics of semiconductor chilling plate

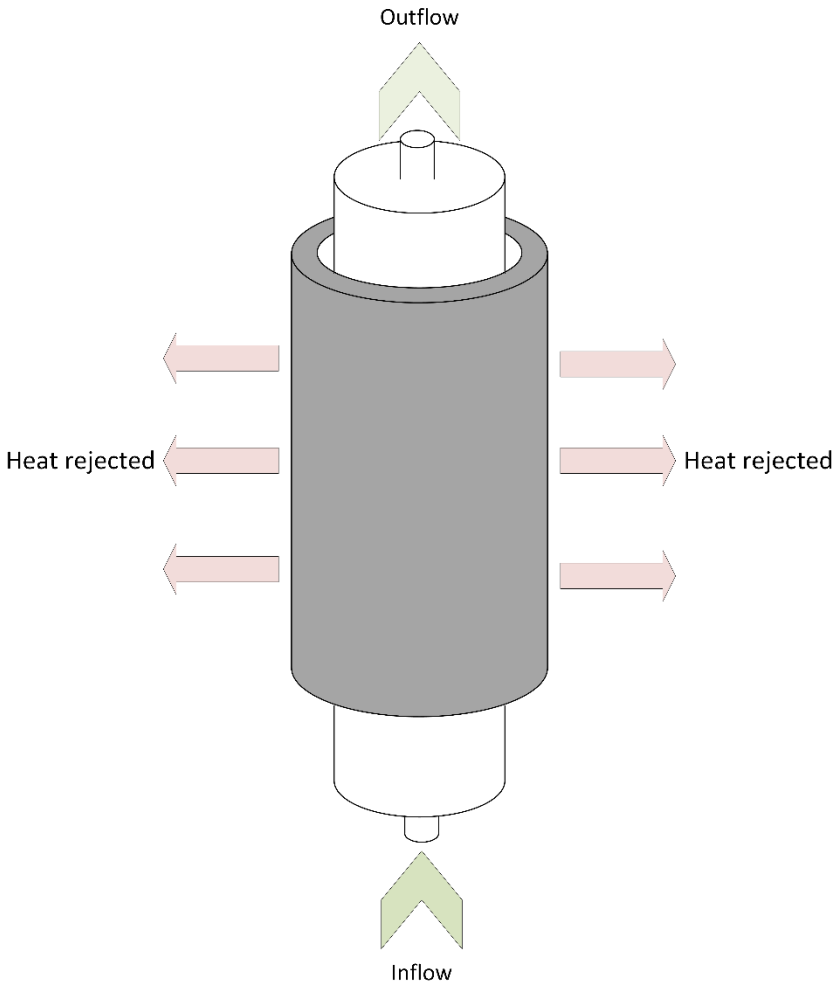

Figure 7.2 Adsorption column with semiconductor chilling jacket

Appendices

Appendix A

Details of the oxygen concentrator prototype:

Figure A.1 shows the microcontroller and MOSFET drive circuit of the concentrator

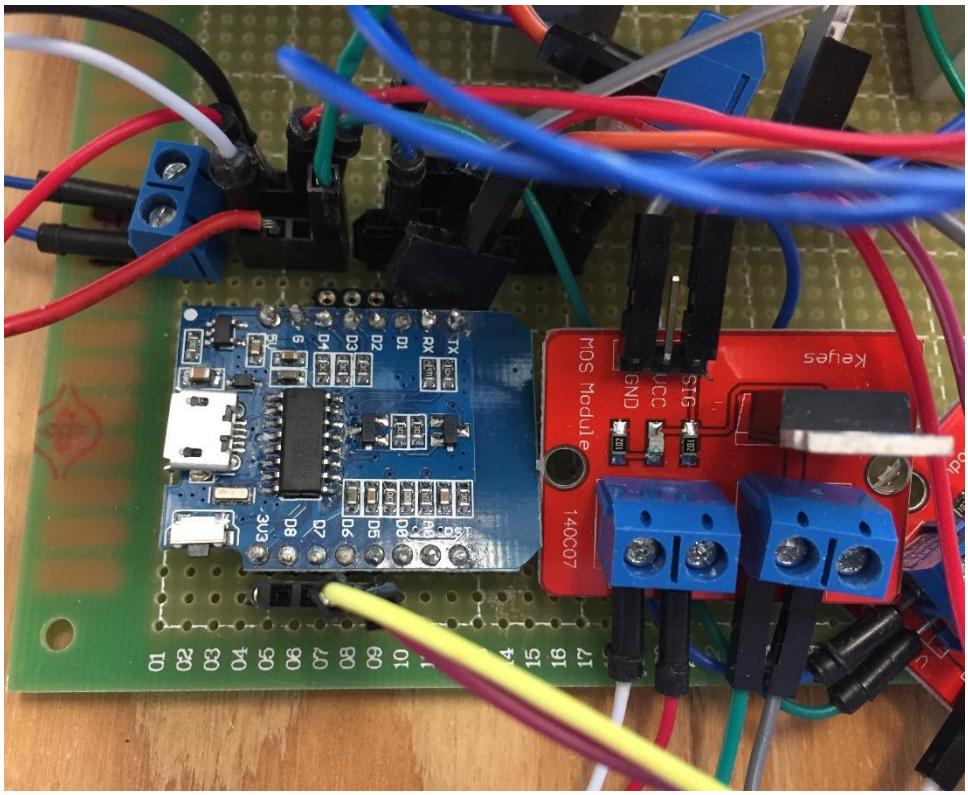

Figure A.1 Photograph of microcontroller and MOSFET amplifier circuit

Figure A.2 and Figure A.3 shows the 3-way solenoid valve and oxygen analyzer respectively.

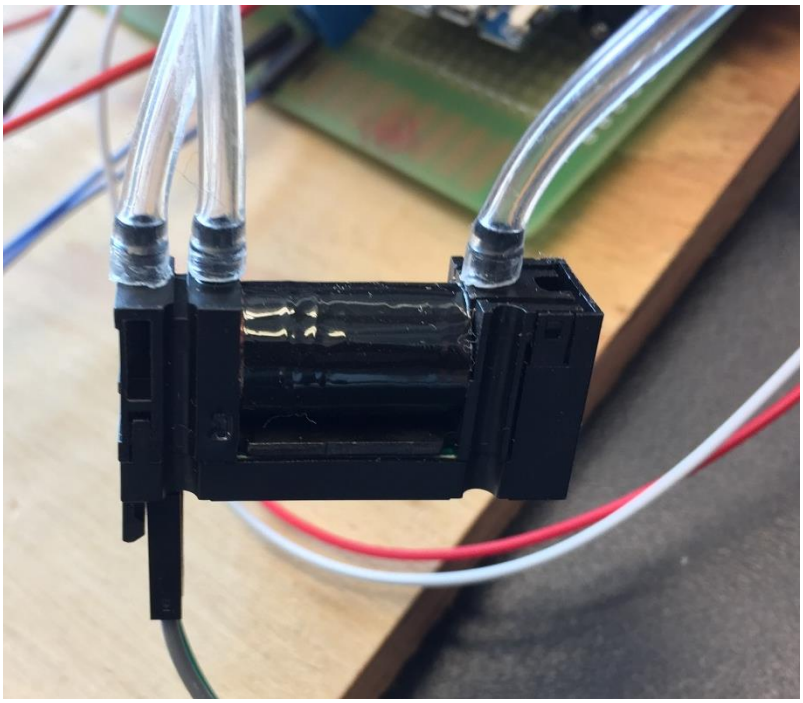

Figure A.2 Photograph of the 3-way solenoid valve

Figure A.3 Photograph of oxygen analyzer

Appendix B

Microcontroller program for the temperature and humidity reading:

```
pin = 3

id=0

function stage1()

  status, temp, humi, temp_dec, humi_dec = dht.read(pin)

  if status==dht.OK then

    print("DHT Temperature:"..temp..";".."Humidity:"..humi)
```

```
  elseif status == dht.ERROR_CHECKSUM then
    print( "DHT Checksum error." )
  elseif status == dht.ERROR_TIMEOUT then
    print( "DHT timed out." )
  end
tmr.delay(1000000)
end
```

Appendix C

Microcontroller program for the PSA cycle:

```
valveX1 = 1;
valveX2 = 5;
valveX3 = 6;
valveX4 = 8;
gpio.mode(valveX1,gpio.OUTPUT)
gpio.mode(valveX2,gpio.OUTPUT)
gpio.mode(valveX3,gpio.OUTPUT)
gpio.mode(valveX4,gpio.OUTPUT)
id=0
```

```
function stage1()
  print "enter stage 1"
  gpio.write(valveX1,gpio.LOW)
  gpio.write(valveX2,gpio.HIGH)
  gpio.write(valveX3,gpio.LOW)
  gpio.write(valveX4,gpio.LOW)
  tmr.alarm(0,10000,tmr.ALARM_SINGLE,stage2);
  print "exit stage 1"
end
  function stage2()
    print "enter stage 2"
    gpio.write(valveX1,gpio.HIGH)
    gpio.write(valveX2,gpio.LOW)
    gpio.write(valveX3,gpio.LOW)
    gpio.write(valveX4,gpio.HIGH)
    tmr.alarm(0,15000,tmr.ALARM_SINGLE,stage3);
    print "exit stage 2"
 end
function stage3()
   print "enter stage 3"
```

```
 gpio.write(valveX1,gpio.HIGH)
 gpio.write(valveX2,gpio.LOW)
 gpio.write(valveX3,gpio.LOW)
 gpio.write(valveX4,gpio.LOW)
 tmr.alarm(0,40000,tmr.ALARM_SINGLE,stage4);
 print "exit stage 3"
end
 function stage4()
   print "enter stage 4"
   gpio.write(valveX1,gpio.LOW)
   gpio.write(valveX2,gpio.HIGH)
   gpio.write(valveX3,gpio.HIGH)
   gpio.write(valveX4,gpio.LOW)
   tmr.alarm(0,15000,tmr.ALARM_SINGLE,stage5);
   print "exit stage 4"
 end
 function stage5()
   print "enter stage 5"
   gpio.write(valveX1,gpio.LOW)
   gpio.write(valveX2,gpio.HIGH)
```

```
    gpio.write(valveX3,gpio.LOW)
    gpio.write(valveX4,gpio.LOW)
    tmr.alarm(0,60000,tmr.ALARM_SINGLE,stage2);
    print "exit stage 5"
 end
stage1();
```

Curriculum Vitae

Name:	Mingfei Pan
Post-secondary Education and Degrees:	East China University of Science and Technology, Shanghai, China 2011-2015 B.E.Sc
Related Work Experience:	Teaching Assistant The University of Western Ontario 2016-2017

Publications:

Mingfei Pan, Hecham M. Omar, and Sohrab Rohani. "Application of Nanosize Zeolite Molecular Sieves for Medical Oxygen Concentration." Nanomaterials 7.8 (2017): 195.